Aalto-yliopisto
Insinööritieteiden
korkeakoulu

NTNU
Norwegian University of
Science and Technology

Aaron Tam

A systematic analysis of test-based model-scale icebreaking patterns

Master's Thesis submitted in partial fulfillment of the requirements for the degree of Master of Science in Technology

Espoo 31.08.2019
Supervisor: Professor Pentti Kujala
Director: Professor Pentti Kujala

Aalto-yliopisto
Insinööritieteiden
korkeakoulu

Aalto-yliopisto, PL 11000, 00076 AALTO
www.aalto.fi

Diplomityön tiivistelmä

Author Aaron Tam

Title of thesis A systematic analysis of test-based model-scale icebreaking patterns

Master program Cold Climate Engineering **Code** ENG25

Thesis supervisor(s) Professor Pentti Kujala

Thesis advisor(s)
Knut Høyland
Fang Li

Date 31.08.2019 **Number of pages** 143 **Language** English

Abstract

The study of icebreaking patterns has been sparsely studied over the course of the past half century. Various methods have been developed primarily to approximate the size of the resultant cusps and general inferences from the observations of the cusps and relating properties. The objective of this work aims to compile the current state of the art in this field and perform model tests focusing on icebreaking pattern. The resultant cusps of the tests were recorded, measured, compiled, statistically fit, and analyzed in works with comparing to currently available approximation methods as well as revisit any current theories regarding the nature of icebreaking pattern and its scalability. The cusps and patterns formed from model tests from the Azipod-version model of the MT *Uikku* at slow speeds were used for the comparison and analysis. The tests show primarily the confirmation of most current theories with an exception to one criterion regarding elasticity, promoted potential prospects for scaling, and found greater accuracy from theoretical and full-scale based approximation methods as opposed to model scale prediction methods.

Keywords model testing in ice, icebreaking pattern, ice cusps

Acknowledgements

I sent my warm thanks to Aalto University, the Norwegian University of Science and Technology, and the Nordic Master's Cold Climate Engineering Program for allowing me to study and pursue educational and scholarly development in this field.

I would like to thank my supervisor, Pentti Kujala for the opportunity for me to pursue this study and all the corresponding experimental work involved, and Knut Høyland for his guidance and input throughout the course of the study.

I am very thankful for the guidance by my thesis advisor, Fang Li, for assisting me throughout the span of this endeavor in the theoretical, experimental, and analytical work involved.

My gratitude extends also to the Aalto University Ice Tank Manager, Otto Puolakka, and the Aalto Ice Tank Lab Technicians, Teemu Päivärinta and Lasse Turja for all their help in making the model tests possible and converting the data from the instrumentation. Additionally, I send my thanks to all my colleagues at the Aalto University Ice Tank for their assistance and input throughout the course of my work.

Lastly, I would like to express my thanks to all my friends and family for all their love and support throughout the course of my studies.

Espoo, August 2019

Aaron Tam

Table of Contents

Abstract
Acknowledgements
1 Introduction 1
1.1 Introduction of icebreaking patterns 1
1.2 Research Questions 1
2 State of the Art and Theory 3
2.1 Icebreaking pattern definition 3
2.1.1 Scalability of Cusps 4
2.1.2 Icebreaking Pattern 8
2.1.3 Thickness Dependency 13
2.1.4 Speed Dependency 14
2.1.5 Load Length Dependency 16
2.2 Methods of Approximation 18
2.2.1 Statistical – McKindra and Lutton's Bay Class Fit (1981) 18
2.2.2 Statistical – Izumiyama's Cone Circles (1992) 20
2.2.3 Semi-Empirical – Kostras's Semi-Ellipse (1983) 21
2.2.3.1 Applied Numerical Model – Liu et al (2006) 22
2.2.4 Semi-Empirical – Tatinclaux's Shapes (1985) 23
2.2.5 Semi-Empirical – Wang's Circles (2001) 24
2.2.5.1 Applied Numerical Model – Su (2011) 25
2.2.6 Theoretical – Nevel's Elastically Founded Semi-Inf Plate (1958) 25
2.2.6.1 Modified Nevel – Lubbad and Løset's Radial Wedges (2011) 27
2.2.6.2 Modified Nevel – Li's Discretized Wedges (2019) 28
2.2.7 Theoretical – Erceg's Discretized Beams (2015) 31
2.2.8 Numerical – Valanto's 3D Hydrodynamic Solution (2001) 32
2.2.9 Numerical – Sawamura FEM Solution (2008) 33
2.2.10 Numerical – Summary of Methiod 34
2.3 Model Testing in Ice 35
3 Method 38
3.1 Aalto Ice Tank 38
3.2 MT *Uikku* Testing 40
3.2.1 Past MT *Uikku* Tests 41
3.2.2 Experiment Preparations 42
3.2.3 Model Tank Testing 44
3.3 Digital Processing 46
3.3.1 Video Processing 46
3.3.2 Image Processing 47
3.4 Prediction Methods 49
3.4.1 Statistical Prediction 50
3.4.2 Analytical Prediction 51
3.4.3 Theoretical Prediction 52
3.4.4 Dimension Conversion 55
4 Results and Discussions 57
4.1 Results and Observations 57
4.2 Single vs Multiple Contact 58
4.3 Prediction Method Comparison 61
4.4 Scalability 69

4.5 Icebreaking Pattern....70
4.6 Distribution Fitting....72
5 Conclusion....75
6 Bibliography....78
7 List of Appendices....81
Appendix A - Cusp Data Table....A-1
Appendix A.1 V=0.162m/s Single Contact Cusp Data....A-2
Appendix A.2 V=0.162m/s Multiple Contact Cusp Data....A-10
Appendix A.3 V=0.270m/s Single Contact Cusp Data....A-14
Appendix A.4 V=0.270m/s Multiple Contact Cusp Data....A-22
Appendix B - Icebreaking Pattern Photographs....B-1
Appendix C - Distributions and Histograms....C-1
Appendix C.1 V=0.162m/s Histograms....C-2
Appendix C.2 V=0.162m/s Distributions....C-6
Appendix C.3 V=0.270m/s Histograms....C-10
Appendix C.4 V=0.270m/s Distributions....C-14
Appendix C.5 Prediction Method Histogram Comparison....C-18

Table of Figures

Figure 1. Cusp dimension definition....3
Figure 2. Model and full-scale ice breaking cusp pattern for Icebreaker *Moskva* (Enkvist 1972)....5
Figure 3. Model and full-scale ice breaking cusp pattern for icebreaking tug *Jelparri* (Enkvist 1972)....6
Figure 4. Model and full-scale cusp width comparison for Polar Class icebreakers (Ettema et al '87)....7
Figure 5. Polar Class Icebreaker Icebreaking Pattern (at h_i=30mm, σ_f=25kPa) (Ettema et al 1987)....9
Figure 6. Polar Class Icebreaker Underwater Ice Floe Flow (Ettema et al 1987)....9
Figure 7. Yamaguchi et al's crack analysis method (Yamaguchi et al 1997)....10
Figure 8. Bow forms and corresponding icebreaking patterns (Yamaguchi et al 1997)....11
Figure 9. Non-dimensional icebreaking resistance and velocity relation for the Yamaguchi's tested bows (Yamaguchi et al 1997)....12
Figure 10. Icebreaking pattern and floe size based on bow shape (Myland and Ehlers 2014)....12
Figure 11. Demonstration of thickness effects on icebreaking pattern and cusps where the left is thin ice and the right is thick ice (Valanto 1995, image taken from Myland and Ehlers 2014)....13
Figure 12. Cusp width as a function of ice thickness and velocity (Ettema et al 1987)....14
Figure 13. Cusp width as a function of velocity from Finncarrier and Jelppari (Enkvist 1972)....15
Figure 14. Non-dimensional cusp width as function of velocity in full scale for landing craft bow (Varsta 1980)....15
Figure 15. Distribution of ice cusp lengths for tests for MT *Uikku* (von Bock und Polach 2011)....16
Figure 16. Full-scale icebreaking pattern of MS Kemira (Daley 1992)....17
Figure 17. Cusp loading rate/contact geometry dependency (Daley 1992)....17
Figure 18. Bay Class Log-Normal Cumulative Distribution for 33cm thick freshwater ice at 9 knots (McKindra and Lutton 1981)....19
Figure 19. Cusp crack size distribution (Su, Skjetne, and Berg 2014)....20
Figure 20. Kostras et al's cusp approximation and dimensional definitions (Kostras et al 1983)....21
Figure 21. Simulated model-scale CCGS *Terry Fox* pure yaw channel from (Liu et al 2006)....23
Figure 22. Ice breaking pattern as per Su (2010)'s simulation in the case without shoulder crushing (1) and with shoulder crushing (2) (Su 2010)....25
Figure 23. Nevel crack pattern on an ice sheet and a narrow free infinite wedge on an elastic foundation (Nevel 1958)....26
Figure 24. Lubbad and Løset equivalent loading system for semi-infinite ice sheet under external load over a half circular area....27
Figure 25. Lubbad and Løset generated cracking pattern on free edge based on contact points (Lubbad and Løset 2011)....28
Figure 26. Icebreaking pattern from Li et al's discretized wedges model for South African icebreaker, S.A. *Agulhas II* (Li et al 2019)....30
Figure 27. Erceg's interaction process illustration and radial ice beams (Erceg et al 2015)....31

Figure 28. Icebreaking pattern for MT *Uikku* in 0.5m FS level ice using Erceg's discretized beam model (Erceg et al 2015) 31
Figure 29. Computational grid domain in Valanto '01 Model (Valanto 2001) 32
Figure 30. Cusp formation in Valanto '01 Model (Valanto 2001) 33
Figure 31. Schematic diagram and FE mesh of the Sawamura FEM model (Sawamura '12) 34
Figure 32. Aalto Ice Tank 38
Figure 33. General Arrangements of MT *Uikku* (Garvin 2003) 40
Figure 34. Diagram of the field of vision from the cameras in reference to the model 42
Figure 35. Depiction of camera locations on the hull in reference with the ice sheet 43
Figure 36. MT *Uikku* in the Ice Tank 44
Figure 37. MT *Uikku* attached to the ice tank main carriage 45
Figure 38. Pre-visual adjustment overlapped video example frame 46
Figure 39. Post-visual and marker additions video example frame 47
Figure 40. Example of single point contact cusp sketching 48
Figure 41. Example of multiple point contact sketching 49
Figure 42. McKindra and Lutton Scaled Cusp Fit 50
Figure 43. Database inputs and outputs 53
Figure 44. Diagram of ice wedge relevant dimensional parameters 53
Figure 45. Cusp Radius to Cusp Length/Width Diagram 55
Figure 46. Cusp Radius to Cusp Length/Width Diagram 56
Figure 47. Single Contact Length Edge/Center Comparison for V=0.162m/s 67
Figure 48. Single Contact Length Edge/Center Comparison for V=0.270m/s 67
Figure 49. MT *Uikku* model scale icebreaking pattern for 0.162m/s speed 71
Figure 50. MT *Uikku* model scale icebreaking pattern for 0.270m/s speed 71
Figure 51. Single contact cusp length histogram and distribution for V=0.162m/s 72
Figure 52. Multiple contact cusp length histogram and distribution for V=0.162m/s 73

Table of Tables

Table 1. Set of Log-Normal Cumulative Distribution for Bay-Class Tugs in 33cm thick freshwater ice (McKindra and Lutton 1981) 19
Table 2. Summary of Cusp Methods of Approximation 35
Table 3. Summary of scaling laws based on Froude, Cauchy, and geometric similarity (Timco 1984) 36
Table 4. General characteristics of MT *Uikku* 40
Table 5. MT *Uikku* test results and parameters from Garvin's tests in 2003 41
Table 6. MT *Uikku* test results and parameters from von Bock und Polach tests in 2010 41
Table 7. Location and settings of the GoPro cameras 43
Table 8. Test and Original Garvin Ice Property Values 57
Table 9. Cusp Geometry Results 58
Table 10. Length/Width Ratio for different contact types 59
Table 11. Cusp count and area for v=0.162m/s 60
Table 12. Cusp count and area for v=0.270m/s 60
Table 13. Cusp Geometrical Comparison – V=0.162m/s – Single Contact 61
Table 14. Cusp Geometrical Comparison – V=0.162m/s – Multiple Contact 62
Table 15. Cusp Geometrical Comparison – V=0.162m/s – All Contact 62
Table 16. Cusp Geometrical Comparison – V=0.270m/s – Single Contact 63
Table 17. Cusp Geometrical Comparison – V=0.270m/s – Multiple Contact 63
Table 18. Cusp Geometrical Comparison – V=0.270m/s – All Contact 64
Table 19. Dimension/Thickness Ratios 70
Table 20. Lognormal distribution values for the cusp geometric properties 73

List of Symbols

A	[m^2]	Ice cusp area
A_{nev}	[-]	Boundary condition coefficient for Nevel's solution
B	[m]	Beam
B_e	[-]	Constant for Wang's Equation
B_{nev}	[-]	Boundary condition coefficient for Nevel's solution
Cn	[-]	Cauchy number
C_{it}	[-]	Factor for dimensional effects on Wang's Radius
C_l	[-]	Constant for Wang's Equation
C_v	[-]	Factor for angle effects on Wang's radius
d_c	[m]	Crushing center location
D_c	[m]	Kostras cusp depth (Same as Cusp Width)
D_w	[m]	Kostras wedge depth
du_0	[-]	Function based on χ used in Nevel's solution
du_1	[-]	Function based on χ used in Nevel's solution
du_2	[-]	Function based on χ used in Nevel's solution
du_3	[-]	Function based on χ used in Nevel's solution
E	[kPa]	Modulus of elasticity of ice
E_{ref}	[kPa]	Reference modulus of elasticity of ice
f(θ)	[-]	Crushing only based deflection field
Fn	[-]	Froude number
g	[m/s^2]	Acceleration due to gravity
g(θ)	[-]	Interaction only based deflection field
h	[m]	Ice thickness (general)
hm	[m]	Ice thickness (model scale)

h_{ref}	[m]	Reference ice thickness
k	[-]	Crushing line inclination
k_b	[N/m^3]	Buoyancy force per unit volume
L	[m]	Cusp length
LBP	[m]	Length between perpendiculars
LOA	[m]	Length overall
l_{br}	[m]	Crack radius length
l_b	[m]	Crack width
l_{bx}	[m]	Crack width in the forward direction
l_c	[m]	Characteristic length of ice
l_{cr}	[m]	Total crack length per unit distance
l_{center}	[m]	Length from crushing point to center limits of the greater wedge
l_{edge1}	[m]	Length from crushing point to 1st side limit of the greater wedge
l_{edge2}	[m]	Length from crushing point to 2nd side limit of the greater wedge
M_{edge}	[Nm]	Moment boundary condition for the greater wedge
mu	[-]	Lognormal distribution mean value
V_{edge}	[Nm	Shear boundary condition for the greater wedge
Pitch	[-]	Cusping pattern pitch
P_{ext}	[N]	Total external force on wedge
R	[N]	Approximated crack cusp radius
R_m	[N]	Mean cusp radius
R_{br}	[N]	Breaking component of ice resistance
R_{ice}	[N]	Resistance from ice (model ice)
R_{ir}	[N]	Rest ice resistance
R_{OW}	[N]	Open water resistance

R_{tot}	[N]	Total resistance from ice and water (model ice)
r_c	[m]	Wedge crushing depth
sigma	[-]	Lognormal distribution standard deviation value
T	[m]	Draft
v	[-]	Poisson's ratio of ice
V	[m/s]	Ship velocity (general)
V_m	[m/s]	Ship velocity (model scale)
V_n	[m/s]	Normal velocity between hull and contact point of ice
$w(\theta)$	[-]	Resultant deflection field
W_c	[m]	Kostras cusp width (Same as Cusp Length)
W_w	[m]	Kostas wedge width
W	[m]	Cusp width
x	[m]	Distance measured along the wedge from the loaded corner
y	[m]	Vertical deflection of wedge
Z_m	[-]	Distributive mean value for Izumiyama's cone circles
α	[deg]	Hull waterline angle at the center of a cusp
β'	[deg]	Normal frame angle at the center of a cusp
β	[deg]	Frame angle at the center of a cusp
γ	[kN/m^3]	Specific weight of water
Δ	[tons]	Displacement
δP_v	[N]	External vertical force on wedge due to loading
η_3	[-]	Average directional cosine of the first 20% of the ship's length
θ	[deg]	Wedge angle, or the angle of cusp at contact
λ	[-]	Scaling factor
ρ	[tons/m^3]	Density of water

σ_c	[kPa]	Compressive strength of the ice
$\sigma_{c,ref}$	[kPa]	Reference compressive strength of the ice
σ_f	[kPa]	Downward lexural strength of the ice
σ_h	[kPa]	Horizontal compression stress on wedge
σ_m	[kPa]	Maximum radial stress on wedge
σ_u	[kPa]	Upward bending strength of the ice
σ_v	[kPa]	Vertical loading deflection induced max stress on wedge
τ_c	[m]	Characteristic wedge crushing depth
φ	[deg]	Hull stem angle
χ	[-]	Non-dimensional distance measured along wedge
χ_m	[-]	Non-dimensional distance measured along wedge of max stress
ψ	[deg]	Hull flare angle

Abbreviations

ARCDEV	**ARC**tic **DE**monstration **V**oyage (Joint EU-Russia Project)
CL	Centerline
CDF	Cumulative Distribution Function
DWL	Design Waterline
DWT	Deadweight tons
EU	European Union
FDM	Finite Difference Method
FPS	Frames per second
FS	Full Scale
LOA	Length overall
LBP	Length between perpendiculars
MS	Motor Ship
MT	Motor Tanker
NSR	Northern Sea Route
RORO	Roll on - Roll off
SAFEWIN	**SAFE**ty of **WIN**ter Navigation in Dynamic Ice (EU Project)
ST	Station
STD	Standard Deviation
USCG	United States Coast Guard
CCGS	Canadian Coast Guard Ship

1 Introduction

1.1 Introduction of icebreaking patterns

At the end of the present decade, the interests of maritime operations in ice-covered waters continue to grow along innovations in shipping and changes in the environment. Amongst the various ice features present in the face of maritime activity, ships are predominantly designed to operate against level ice. The breaking portion during the penetration through level ice field contributes to a significant part of the ice-going resistance in ships. With various hull forms and design features that serve to effectively break the ice, model tests are a common method to test designs in ice using scaled models, ice properties, and loads.

A historically linked method of analyzing and understanding icebreaking resistance has been trying to understand the icebreaking pattern. The patterns are linked with different hull forms and the continuous failure mechanisms of the ice as the ship moves across a field. Many ice tanks in model scale have capacities for underwater observation, to examine the patterns and ice flow from underneath the tank, while full scale observations are limited to the cusping observations from above the vessel.

However, at the Aalto ice tank, icebreaking pattern observations can only be performed from above the water line. Nevertheless, developing a methodology in observing and analyzing the cusp formations at the bow of the hull could provide benefits to future developments in modeling and scaling ship-ice interactions. Ever-growing technology allows for better analysis in icebreaking patterns compared to the previous century, providing an updated view on the study of broken ice cusps, patterns, and prediction methods.

1.2 Research Questions

The aim of the thesis is to further develop the current understanding of icebreaking patterns. A detailed analysis of the processes in model scale is to be implemented to closely study the

interactions and test the reality of the current state of the art approximation methods. Using high frame rate/high-resolution cameras to capture the icebreaking process in conjunction with developing an image analysis code and methodology, a relatively modern method could be set up to analyze and compare icebreaking patterns for future tests. Attempts are to be made to consider previous methods of analysis to assess the range of the current state of the art icebreaking pattern analysis. The goal was to also set up a methodology to record, compile, process, and analyze cusp data. Lastly, it was to verify and validate the effectiveness of pre-existing cusp approximation methods and assess the general scalability of model-scale icebreaking cusps and icebreaking patterns.

2 State of the Art and Theory

2.1 Icebreaking pattern definition

Icebreaking resistance for ships in terms of looking at the icebreaking pattern has been studied and observed by various researchers in the past half century, stretching from activity from the 1950s to the 2010s. With modern technology shifting more towards numerical modelling, an accurate representation of the icebreaking pattern and cusps become ever more important in the understanding of icebreaking. Where icebreaking cusps are defined as, the pieces of the broken ice pieces that are typically semi elliptical that form from the interaction of the ship and the ice sheet; and icebreaking pattern is the series of cusp formations, representing the pattern of the cusps that the vessel creates in its interaction with the ice sheet. The definition of cusp width and length as per this paper is displayed in figure 1, where the width is the measurement normal to the ship hull to the outer extent of the cusp and the length is the measurement approximately parallel to the ship hull of the end extents of the cusp.

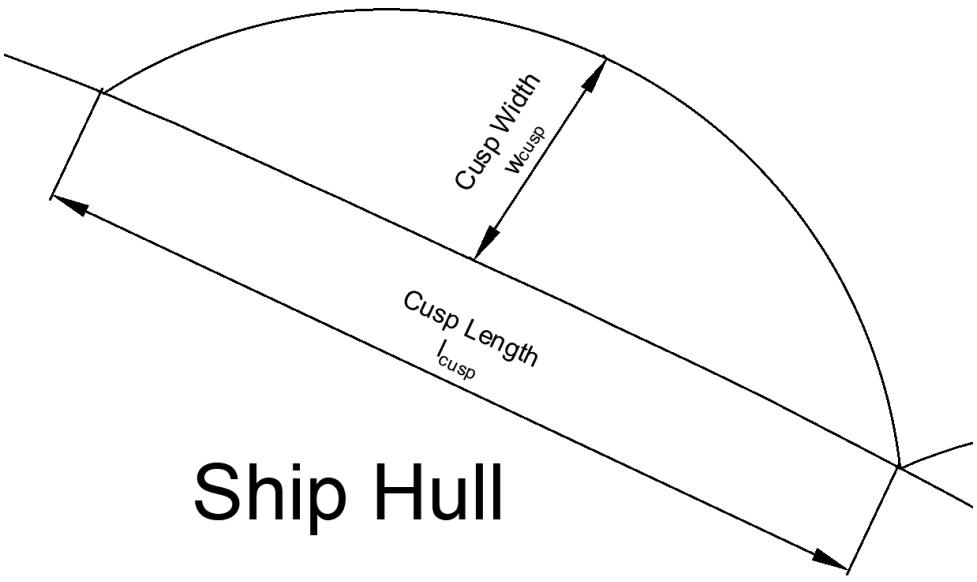

Figure 1. Cusp dimension definition

Historically, one of the major first topics that were addressed was the general scalability of ice between model-scale and full-scale. Beyond scalability issues, research was further continued studying what influences icebreaking cusps and pattern such as bow form, speed, and thickness in such a manner that affected of the total ice-going resistance of ships. Throughout this period, various methods were also developed to approximate the geometrical properties of the cusps for the understanding of resultant broken ice channels and in developing numerical models.

2.1.1 Scalability of Cusps

The visual observations of icebreaking patterns in model scale was observed extensively early on by Ernst Enkvist (1972) who used cameras to analyze breaking patterns from three icebreaking models. Tests were performed at various speeds and ice thicknesses and the results were compared to full-scale tests. This was the first major work to examine the scalability of ice cusps. The models used were the following vessels: the icebreaker, *Moskva*, the RORO ship, *Finncarrier*, and the icebreaking tug *Jelppari*. An example of the variations between icebreaking cusps in full and in a 1:25 model scale can be seen in Figure 2 for the 112m long icebreaker *Moskva*. It could be seen from the figure that despite some minor differences in scaling, the size of the cusp are completely different scales relative to the length of the ship. This fundamental problem is further exemplified by Keinonen (1983) where he investigated that the size of cusps are typically about 3 to 6 times the ice thickness in model scale, while in full scale the cusps are only 0.5 to 2 times the ice thickness. He explained that the difference is a result of internal defects from size effects that are propagated during crushing.

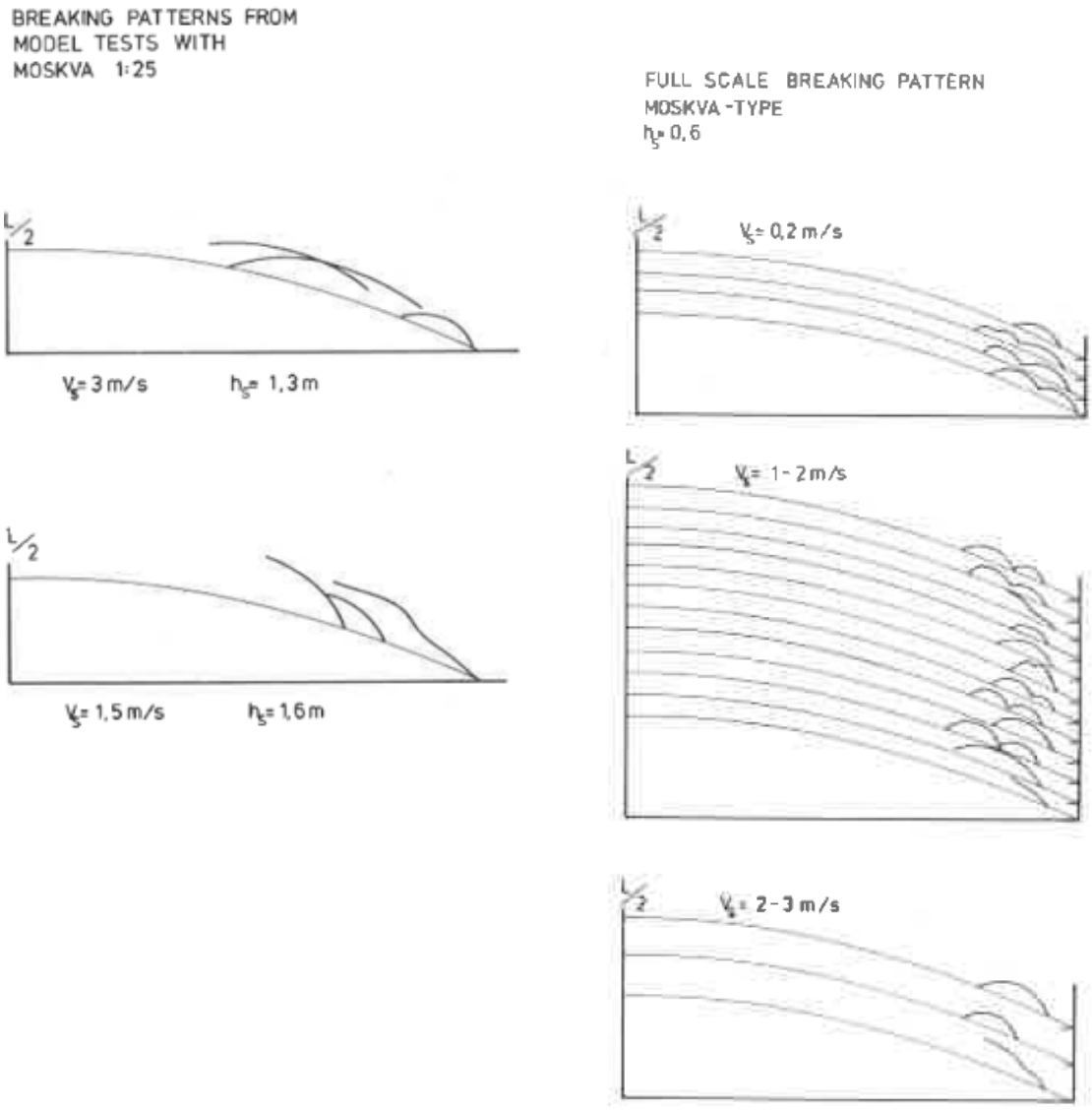

Figure 2. Model and full-scale ice breaking cusp pattern for Icebreaker *Moskva* (Enkvist 1972)

Looking at a small vessel, the icebreaking tug, *Jelparri*, with a magnitude of length less at a length of 15m and its corresponding model scale of ratio 1:5. Here is a much closer similarity in the scale of the ice cusps between the full and model scale. This is supported by Yean et al (1981) in that models larger than 1:20 scale is better at maintaining a similar ice stiffness behavior and thus scale cusp geometries better. Overall, it shows some evidence with size effects being in place in the solid mechanics of working with ice.

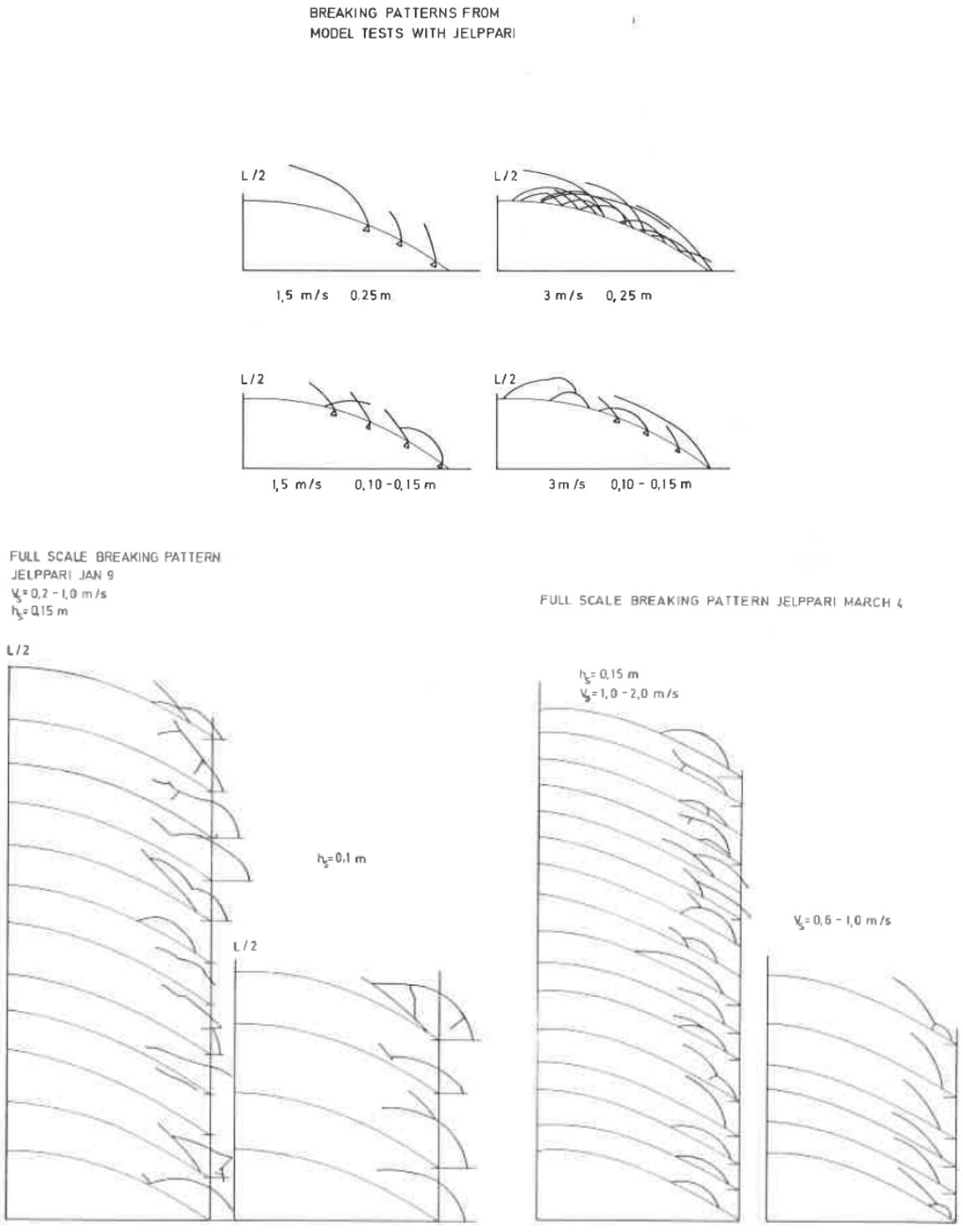

Figure 3. Model and full-scale ice breaking cusp pattern for icebreaking tug *Jelparri* (Enkvist 1972)

In contrast to the size effect conclusions, studies were also performed on the continuous icebreaker pattern of the spoon shaped bow USCG Polar-Class Icebreakers in fixed and free in terms of its freedom of motion as per a study by Ettema et al (1987). A cusp formed by

the model simulated circumferential cracks that arced the length between the bow's stem and its shoulder. An interesting conclusion from Ettema et al (1987)'s paper is that the cusps for the 1:48 model of the icebreaker compared to its full size demonstrated cusps sizes quite close to the full scale. The model scale cusps were only approximately 20% larger than the corresponding scaled down full scale. A chart demonstrating the cusp dimension results are shown in Figure 4.

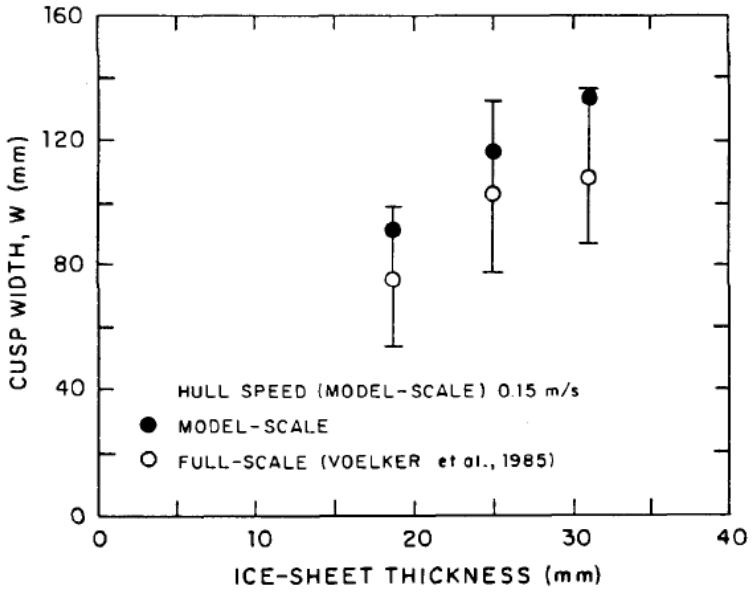

Figure 4. Model and full-scale cusp width comparison for Polar Class icebreakers (Ettema et al '87)

With the completion of the set performed by Ettema et al (1987), not much has been further assessed in the field of the scalability of icebreaking cusps. Despite arguments against it, data has been able to show that the cusps can be appropriately scaled but further data sets are required to gain an accurate understanding. Despite the clashing conclusions regarding cusp size scalability, understandings have evolved involving higher dependencies based on the elastic modulus or the flexural strength as opposed to just the thickness. Yean et al (1981) defined a criterion that the cusp width is related to the elastically based characteristic length, l_c, as defined by equation 1 or otherwise the flexural strength of the ice (Yean et al '81). This

stiffness criterion in which the cusp width is dependent on elasticity is shown in Equation 2 and the corresponding flexural strength criterion is shown on Equation 3. The new variables shown here are E, the modulus of elasticity of the ice, h, the ice thickness, ρ, the density of the water, g, the acceleration due to gravity, σ_f, the flexural strength of the ice, and γ, the specific weight of water. The criterion is based on a semi-infinite floating beam and to summarize this idea, it is that if the stiffness of the ice ($E/\sigma f$) is too low, the width of the cusp is no longer dependent on the elasticity of the ice (Tatinclaux '85). The theory is also influenced by the nature of the interaction of the emersion in failure due to the upward bending of the ice in the original theory.

$$l_c = \left(\frac{Eh^3}{12(1-v^2)\rho g}\right)^{\frac{1}{4}} \tag{1}$$

$$Yean\ et\ al's\ Elastic\ Criterion, \frac{E}{\sigma_f} > 400 * \frac{\sigma_f}{\gamma h}, \qquad W \propto l_c \tag{2}$$

$$Yean\ et\ al's\ Strength\ Criterion, \frac{E}{\sigma_f} < 40 * \frac{\sigma_f}{\gamma h}, \qquad W \propto \left(\frac{\sigma_f}{\gamma h}\right)^{0.5} \tag{3}$$

2.1.2 Icebreaking Pattern

Ettema et al (1987) performed work beyond the scalability of cusps with greater analysis into the nature of icebreaking patterns. One of the first to look at the pattern, the pattern was found to resemble that of a herringbone pattern as shown in Figure 5. It was found that the first cusp formed is longer but the same width as other cusps, mainly as an effect of the entrance into the ice field. It can also be observed that the cusps are dependent on previously broken cusps that influence the contact of the hull and ice. The resulting series of interactions create the pattern. Additional conclusions regarding the pattern and aftereffects are the distancing between the cusps increased with speed and more ice were to remain submerged

under the hull for thinner ice. A depiction of the submerged broken ice pattern is well demonstrated in Figure 6 as well.

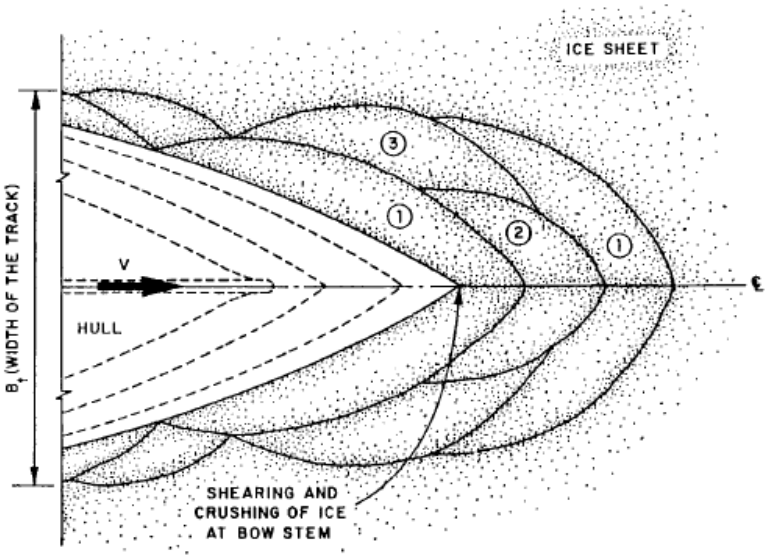

Figure 5. Polar Class Icebreaker Icebreaking Pattern (at h_i=30mm, σ_f=25kPa) (Ettema et al 1987)

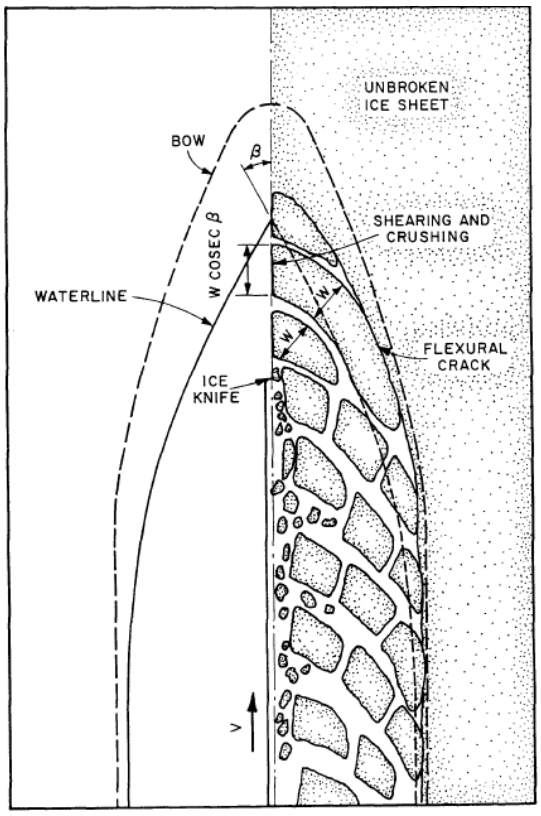

Figure 6. Polar Class Icebreaker Underwater Ice Floe Flow (Ettema et al 1987)

The icebreaker pattern analysis performed by Ettema et al (1987) was only for one hull, research continued with low speed icebreaking pattern dependencies based on bow shape were developed from some tests by Yamaguchi et al (1997). There, three vessels were tested in model-scale level ice, each with a unique bow form type, and he develop unique parameters for his analysis as shown in Figure 7. In this manner, these quantities were introduced in the analysis in the comparison of the hulls. However, regarding all hulls, it was concluded that there is a negative correlation between the total crack length per unit length, l_{cr} and the breaking width, l_b as defined by the figure.

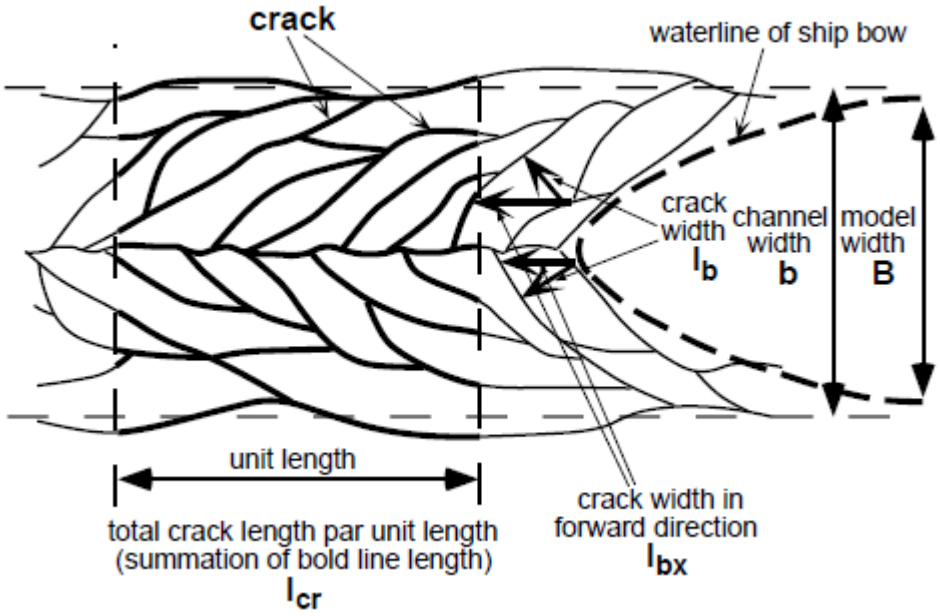

Figure 7. Yamaguchi et al's crack analysis method (Yamaguchi et al 1997)

Three bows were tests: bow A the conventional wedge-shaped bow, bow B the spoon shaped bow, and bow C the concave below the waterline bow. The lines for the three bow forms and the resulting crack patterns are shown in Figure 8. Looking at detailed observations, bow A presents a consistent breaking pattern following the angle of the wedge bow. Bow B has a wide and short breaking pattern throughout as complement to the small stem angle of the

spoon bow. Lastly, Bow C has small cracks in the center and much longer ones on the side, most likely influenced from the concave bow form.

It was also found that with increased speed, the ice-going resistance of A and C increases much more rapidly than does B as shown in Figure 9. However, it was also worth noting that the cusp width, l_b was larger for Bow B than the other bows that correspondingly would reduce the total crack length l_{cr} the vessel forms per a unit distance that ultimately reduces the breaking resistance of the hull. This gave the conclusion that resistance is decreased with hull forms with larger crack widths. The cusp widths were additional correlated negatively with stem angle, further proving the benefit of small stem angles in reducing icebreaking resistance. The physics of this is directly related to the bending failure in the ice from the small stem angle creating bending failures of large widths as opposed to an opposite phenomenon with more crushing. It has also been seen from the test that there is a negative correlation between cusp width and cusp length. Overall, the paper presents the importance of understanding the icebreaking pattern of a vessel as a method to minimize the breaking resistance of ice breaking vessels.

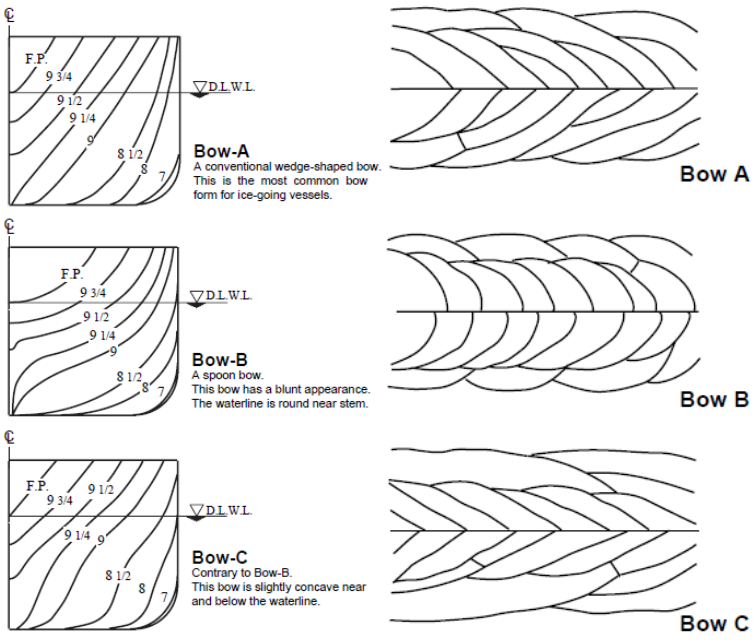

Figure 8. Bow forms and corresponding icebreaking patterns (Yamaguchi et al 1997)

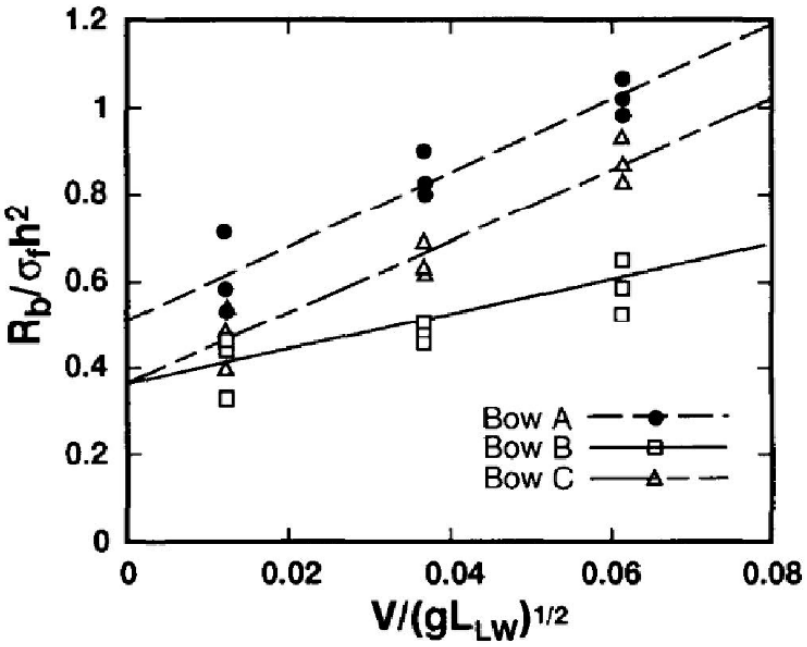

Figure 9. Non-dimensional icebreaking resistance and velocity relation for the Yamaguchi's tested bows (Yamaguchi et al 1997)

Myland and Ehlers (2014) also performed some tests with general qualitative descriptions in relating bow shape to icebreaking pattern. Conclusions were that a rounded bow would create smaller cusps than a wedge bow, and the less convex the bow was at the waterline the more the cusps would appear more bar shaped. A picture showing this comparison is presented in the photographs in Figure 10. The photos were also analyzed for cusp size using a grid for the photographs. The conclusions regarding bow shapes agreed with the observations of Yamaguchi (1997), confirming similar ideas in pattern observations.

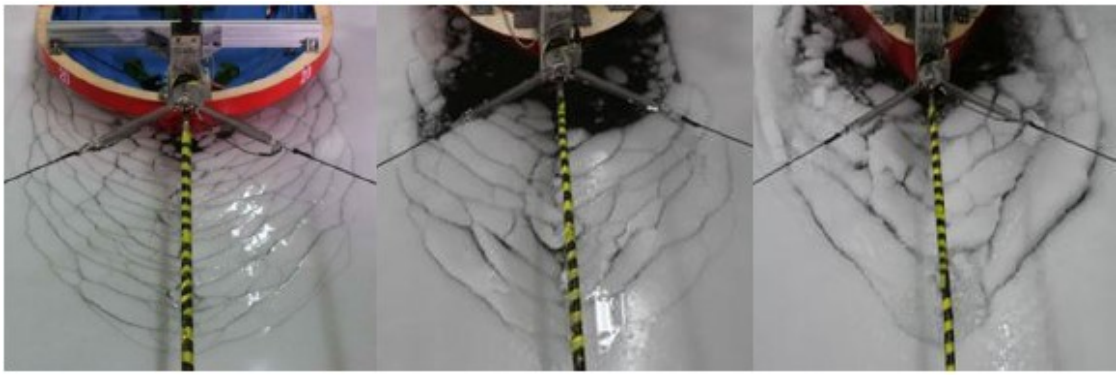

Figure 10. Icebreaking pattern and floe size based on bow shape (Myland and Ehlers 2014)

2.1.3 Thickness Dependency

When looking at the size of cusps, it has been widely accepted that there is a thickness dependency. Based on basic plate/beam theory and the loading of ships onto ice, it can be inferred that there is a natural ice thickness dependency such that the increased thickness would increase the width of the cusps. A good visual representation of this thickness dependency is shown in Figure 11 where the left image shows the breaking pattern in thin ice and the right image shows the breaking pattern in thick ice. As seen on the image, the width of the cusps is much larger in the thicker ice as compared to the thinner ice for the same model.

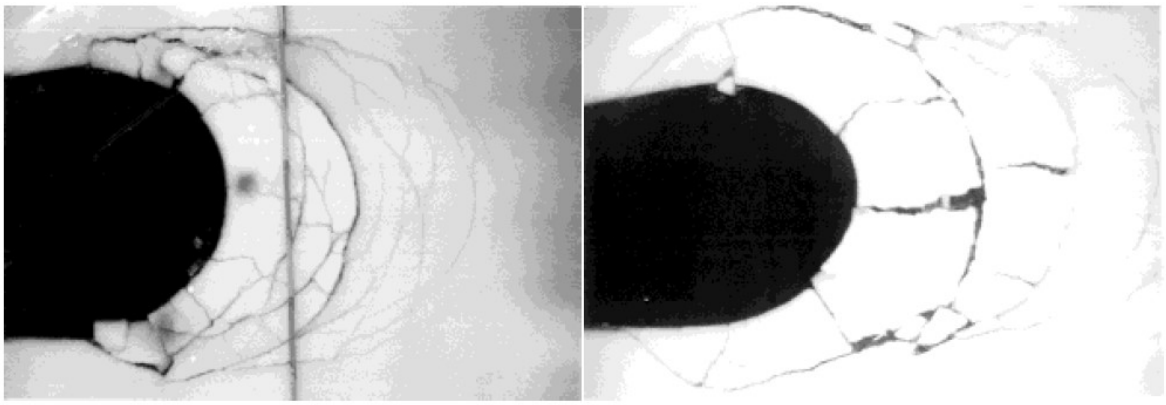

Figure 11. Demonstration of thickness effects on icebreaking pattern and cusps where the left is thin ice and the right is thick ice (Valanto 1995, image taken from Myland and Ehlers 2014)

The thickness dependency was also confirmed with Ettema et al (1987)'s test of the Polar Class icebreaker tests as shown in Figure 12. It could clearly be seen that for the many speeds, that with increased ice thickness there is a corresponding increase in the cusp width of the floes.

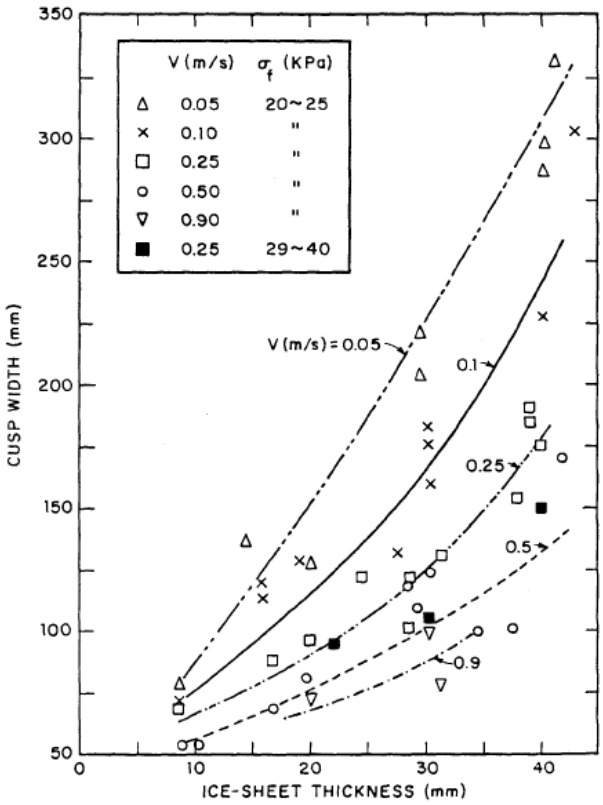

Figure 12. Cusp width as a function of ice thickness and velocity (Ettema et al 1987)

Looking at the Ettema et al (1987)'s figure, it also tells that there is a relation between cusp width and the velocity of the vessel as shown by the curves is discussed in Section 2.1.4.

2.1.4 Speed Dependency

Looking at the speed dependency on the width of cusps, there is wide support regarding the negative correlation between the width of the cusps and the speed of the vessel. As shown previously in Ettema et al (1987)'s plot in Figure 12 in Section 2.1.3, with increased speed the cusp size would be decreased, ranging from the model speed of 0.05m/s to 0.9m/s. The curves show the demonstration that the increased speed greatly reduced the widths of the cusps.

These conclusions, particularly the speed effects in full scale was supported by Enkvist (1972) as shown in Figure 13 for the RORO vessel, *Finncarrier* and the tug, *Jelppari*. Similar results for full scale are also present from Varsta '80 for the full-scale landing craft bow

as shown in Figure 14, where the y-axis is the non-dimensional cusp width, represented by the cusp width divided by the contact length of the landing craft. Various angles of the landing craft were tested, and a similar result was seen for the various angles at changing speeds.

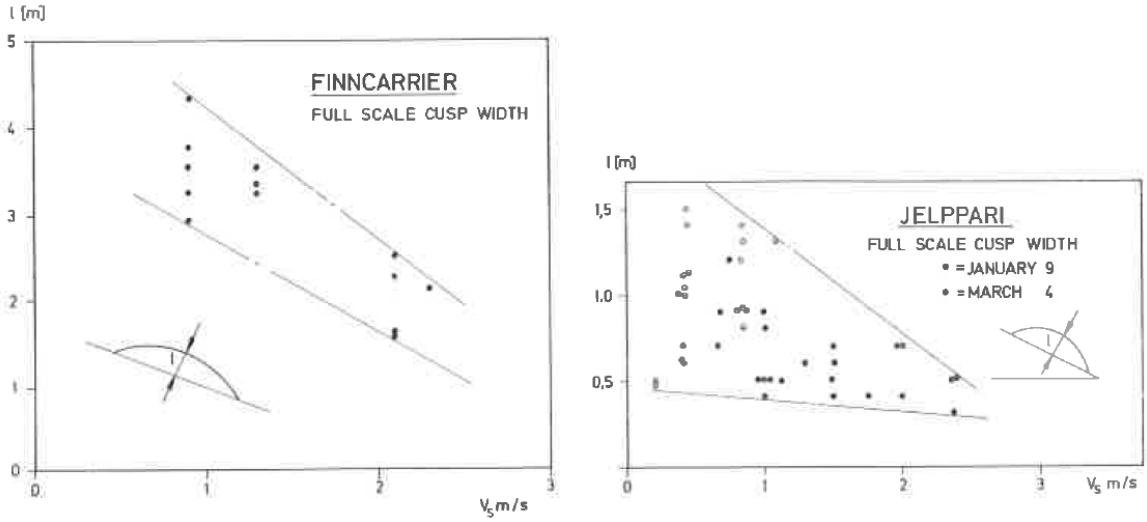

Figure 13. Cusp width as a function of velocity from Finncarrier and Jelppari (Enkvist 1972)

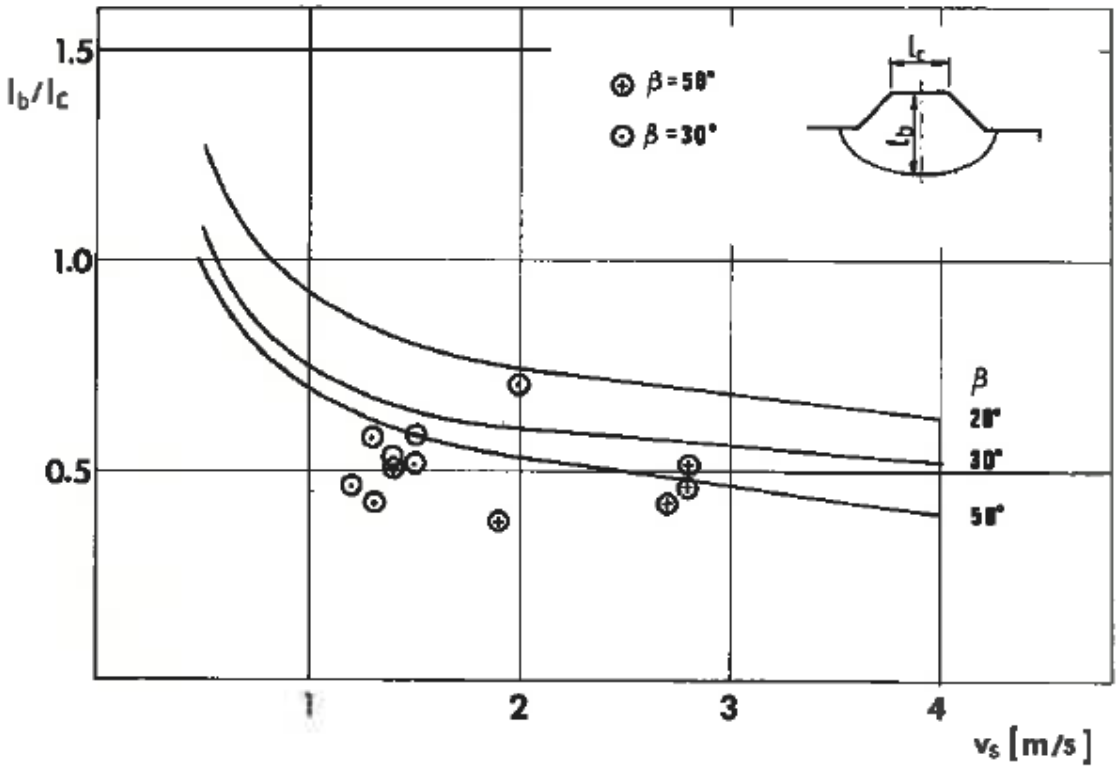

Figure 14. Non-dimensional cusp width as function of velocity in full scale for landing craft bow (Varsta 1980)

Von Bock and Polach and Ehlers (2011) performed tests on the model of the Baltic tanker, MT *Uikku* in a similar fashion as the Ettema et al (1987)'s test regarding free and fixed positions in level ice and some cusping was analyzed. The work here worked more extensively with coordinating the frequencies with cusp dimensions. Nevertheless, von Bock and Polach and Ehlers (2011) in their work used the opposite definitions of the width and length definition of cusps and thus it is important to understand, width in the diagram is the cusp length as per this paper. A distribution of cusp length were approximated for the different sizes in various speeds as shown in Figure 15, and it is also evident that the cusps lengths also decrease with increasing speed.

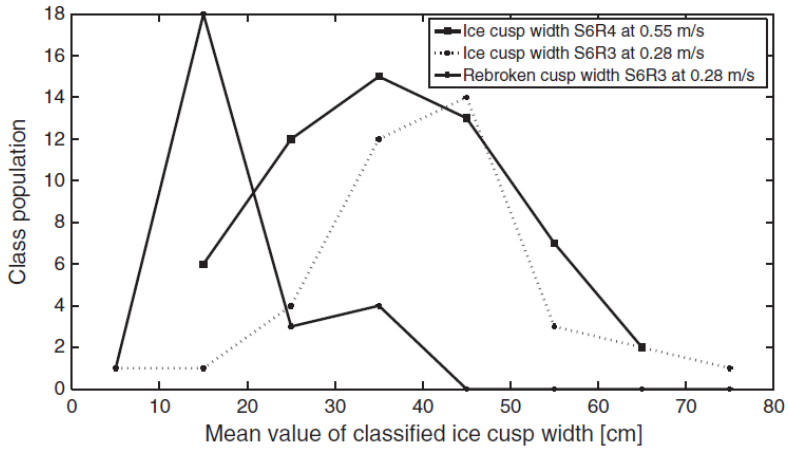

Figure 15. Distribution of ice cusp lengths for tests for MT *Uikku* (von Bock und Polach 2011)
*width in this diagram follows the cusp length as per the definitions from Figure 1

2.1.5 Load Length Dependency

Some work has also been used to look at the load rate dependency on cusps. Daley (1992) presents data from the MS *Kemira* from a full-scale voyage in 1991 where the icebreaking pattern was presented in the report as shown in Figure 16. In his analysis, he categorized the resultant cusps into smaller and larger cusps based on the cusp's loading rate. He claims the dependencies of broken cusps on the formation of future cusps such that the remnant field geometry would affect how the ice sheet would be loaded. A sharp contact between the sheet

and the structure would result in a short loading rate and correspondingly a short wide cusp, and a long flat edge contact between the sheet and the structure result in a longer loading rate and then correspondingly a long thinner cusp. A visualization of this phenomenon is shown in Figure 17.

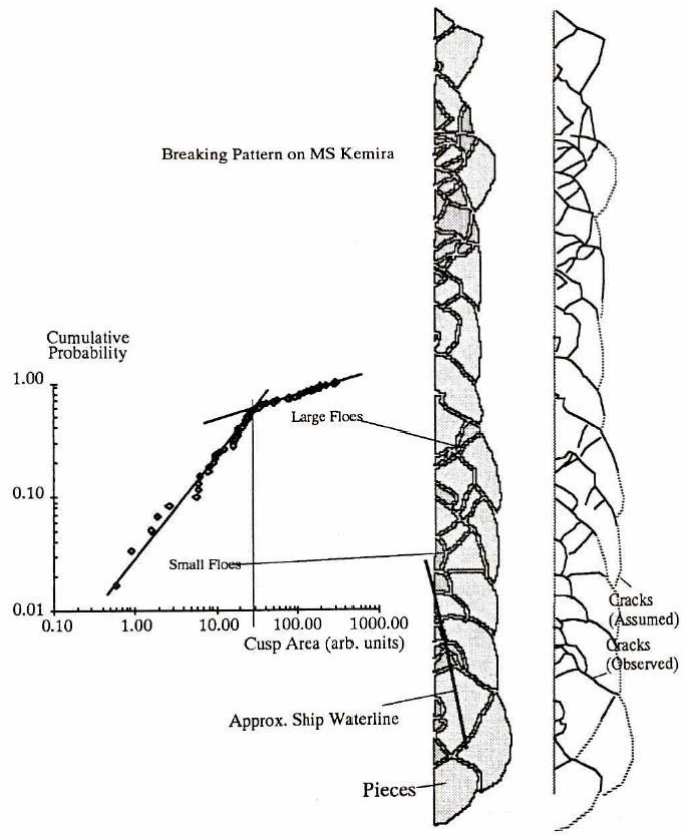

Figure 16. Full-scale icebreaking pattern of MS Kemira (Daley 1992)

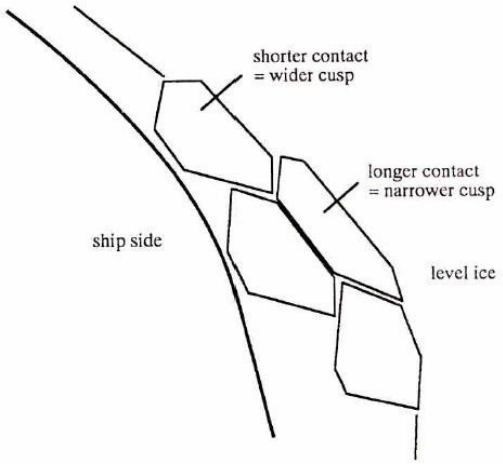

Figure 17. Cusp loading rate/contact geometry dependency (Daley 1992)

2.2 Methods of Approximation

In trying to understand the mechanism of icebreaking throughout the decades, many researchers attempted to develop stronger mathematical approximation methods to estimate the cusps during icebreaking. Multiple types of methods have been proposed to approximate, primarily in the categories of statistical, semi-empirical, theoretical, and numerical. The geometrical assumptions along with the complexity varies between the methods. Typically, these approaches have been implemented in various modern icebreaking simulations following different cusp approaches.

2.2.1 Statistical – McKindra and Lutton's Bay Class Fit (1981)

In 1981, McKindra and Lutton (1981) performed tests on the resulting cusps of the USCG 140' Bay-class tugboats. There, a lognormal distribution regarding the length of the cusps of ice floes from the series tests was fitted to test data and displayed a reasonable fit. The results were for full-scale test in the Great Lake river fresh waters in the St. Mary's River. The fitted data was for the 33cm thick ice. An example resulting CDF of a test at 9 knots with no bubblers is shown in Figure 18. McKindra and Lutton (1981) performed a series of tests at different speeds in the test along with the inclusion of bubblers. A table of the statistically fitted results from the St. Mary's river ice is shown in Table 1. The solution set is limited but the results could be further interpolated for a greater solution set despite being limited to the broken cusp length.

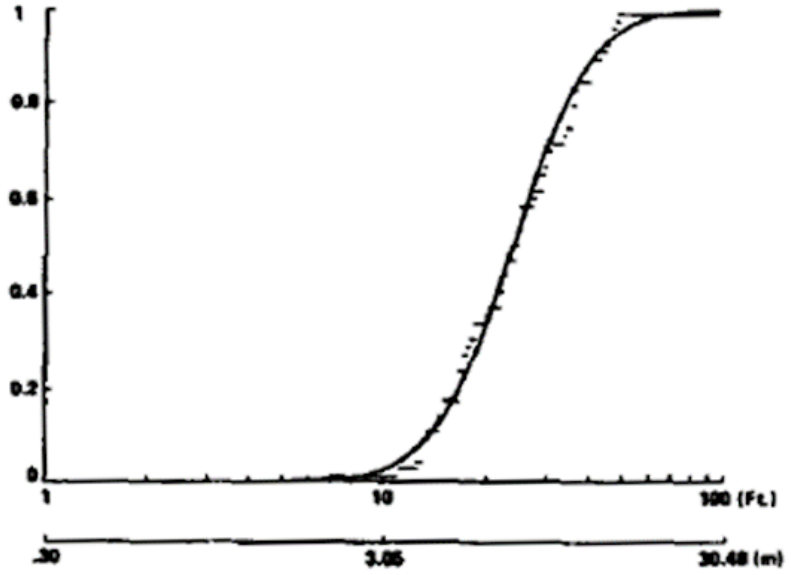

Figure 18. Bay Class Log-Normal Cumulative Distribution for 33cm thick freshwater ice at 9 knots (McKindra and Lutton 1981)

Table 1. Set of Log-Normal Cumulative Distribution for Bay-Class Tugs in 33cm thick freshwater ice (McKindra and Lutton 1981)

Bubblers Off

Ice Length, Meters

Run Number	Speed Ahead (kts)	No. of Pieces	E(X)[a]	Std. Dev.[b]	Minimum	Maximum	Skewness[c]
3600	2.40	36	2.5	1.1	.9	6.4	.43
1100	.98	54	10.4	4.0	4.3	21.3	.20
1300	1.94	54	9.8	4.9	2.9	23.9	.28
1110	5.40	85	7.9	3.6	2.6	20.1	.39
1310	3.64	36	7.7	4.2	2.6	18.6	.35
3430	11.40	20	4.3[e]	2.3[e]	1.4	8.2	.15
3530	11.60	19	3.2[e]	1.2[e]	1.5	4.9	.01
3610	10.80	36	2.9[e]	1.4[e]	1.1	7.2	.39
1120	10.59	91	9.4	5.3	1.8	22.2	.20
1320	5.01	35	7.9	4.7	2.0	17.2	.26
1130	8.99	61	8.0	3.7	2.1	15.1	.15
1330	4.35	24	8.6	3.4	4.3	23.6	.65

a Expected length based on lognormal distribution of lengths
b Square root of variance of length based on lognormal distribution
c Departure from normality (If Skewness is 0, the population is normally distribution)
d Goodness of fit of the lognormal distribution questionable, use of empirical CDF preferred.
e Brash Ice

2.2.2 Statistical – Izumiyama's Cone Circles (1992)

Additional research by Izumiyama (1992) worked further with distribution of cusps but looking at more the development of the cusps as opposed to the resultant cusps. Izumiyama (1992) arrived at a normal distribution from the formations due to structural interaction between model-scale conical structures and ice level ice. Su, Skjetne, and Berg (2014) summarizes some of his data in Figure 10 demonstrating the statistical approach to the problem, as the cusp geometry is approximated with circular radii R.

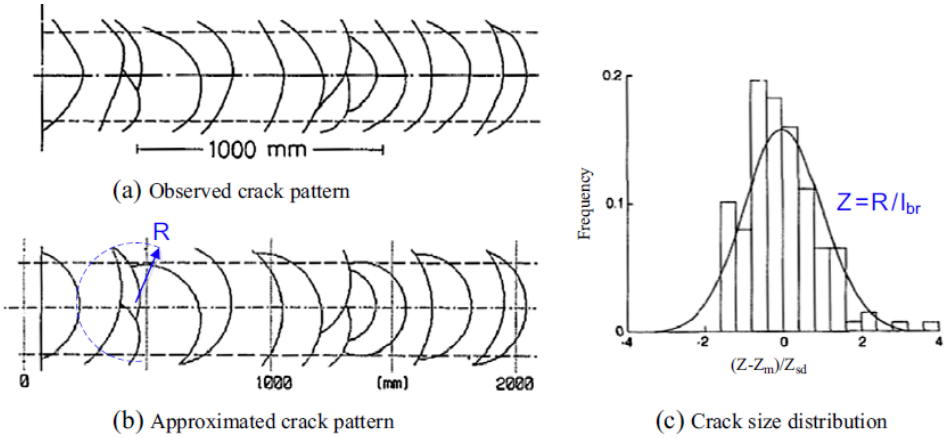

Figure 19. Cusp crack size distribution (Su, Skjetne, and Berg 2014)

Under Izumiyama (1992)'s approximation in the mean cusp case, the mean cusp radius R_m is found by resolving Equation 4 from the distribution mean value Z_m that was found to be 0.937 and a reference crack radius length l_{br}. The definition of the crack radius length used by Izumiyama (1992) is shown in Equation 5. The equation naturally looked at upward bending due to the cone structure and thus the σ_u represents the upward bending strength. Overall, this method concentrates on the flexural strength-based nature of the ice.

$$Z_m = \frac{R_m}{l_{br}} \tag{4}$$

$$l_{br} = \left(\frac{\sigma_u h}{\gamma}\right)^{0.5} \tag{5}$$

2.2.3 Semi-Empirical – Kostras's Semi-Ellipse (1983)

Kostras et al (1983) developed a set of cusp definitions and a corresponding analysis regarding icebreaking pattern (from further developments from (Naegle 1980)). To make the analysis easier, they simplified cusps to semi ellipses along the hull of the ship. With this approximation, dimensions could be defined for the cusps as shown in Figure 20. Variables are displayed in the figure that denote their definitions, with D_c and W_c defining the depth and width of the cusp respectively and D_w and W_w defining the depth and width of the wedges respectively. The definitions of width in the diagram is different of that in the paper, such that Kostras width=cusp length and Kostras depth=cusp width as per Figure 1. A new variable observed from the figure is the *Pitch* and is defined by Equation 7. In these equations, the only new variable is α_c, the hull's waterline angle at the center of the cusp.

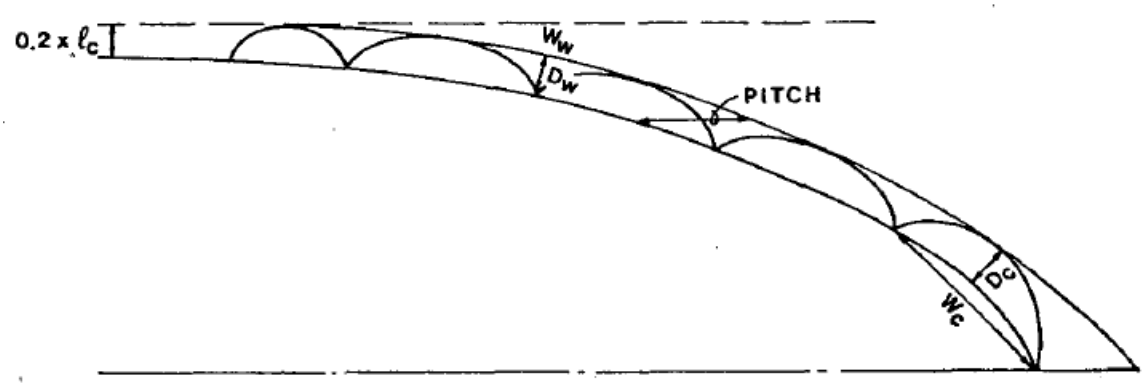

Figure 20. Kostras et al's cusp approximation and dimensional definitions (Kostras et al 1983)
*width in this diagram follows the cusp length, and the depth in this diagram follows cusp width as per the definitions from Figure 1

$$l_c = \left(\frac{Eh^3}{12(1-v^2)\rho g}\right)^{\frac{1}{4}} \tag{6}$$

$$Pitch = \frac{Dc}{\sin(\alpha_c)} \tag{7}$$

Kostras et al (1983) created an analytical approximation method for the expected depths and widths of the cusps as shown in equations 8, 9, and 10. They created two approximation equations in his paper to approximate the cusp size; the first approximation uses the full-scale results of 3 ships: the USCG Wind-class icebreaker-*Staten Island*, the icebreaking tug-

Jelparri, and the icebreaking RORO-*Finncarrier*. A dimensionless linear fitting was used to fit the data and the relation function in equation 8 was generated, where new parameters are *V*, the ship velocity and *β'*, the normal flare angle at the center of the cusp.

$$D_c = l_c(2.42205 + 6.02256(\frac{\sin(\alpha)}{\tan(\beta')})(\frac{V}{\sqrt{gl_c}})^{-1} \quad (8)$$

He provides also a second equation that is fitted more with geometric influences, adding a dependency on the direction cosine on the forward 20 percent of the vessel's length. In this fitting, he modified the coefficients based on five icebreaking ships, the USCG Bay-class icebreaking tug-*Katmal Bay*, USCG Great Lakes Icebreaker-*Mackinaw*, the Canadian Ice-breaker-*Pierre Radisson*, the USCG Wind-class icebreaker-*Staten Island* and the icebreaking oil tanker-SS *Manhattan*. The resulting modified equation is presented in equation 9 where η_3 is the directional cosine of the forward 20 percent of the ship. These equations mainly define the general trends that the size of the cusps depends on, such as smaller cusps with increasing speed.

$$D_c = \eta_3 l_c(1.7153 + 4.2653(\frac{\sin(\alpha)}{\tan(\beta')})(\frac{V}{\sqrt{gl_c}})^{-1} \quad (9)$$

Overall, both equations shown the cusp size's positive correlation with ice thickness and negative correlation with velocity. This confirms with all previous studies, along with the general influences of the hull angles. An additional relation relating the two orthogonal dimensions of ice cusps based on the data fitting is also presented in Equation 10.

$$\frac{W_c}{D_c} = \sqrt{\frac{10.0\ meters}{h}} \quad (10)$$

2.2.3.1 Applied Numerical Model – Liu et al (2006)

The Kostras et al (1983) semi-ellipse model of icebreaking cusps was applied in the ice maneuvering numerical model presented by Liu et al (2006). The numerical models take the

elliptical cusp shape approximations to determine the maneuvering channels that occur during turns. The method was combined with Kashtelyan (1960)'s (referenced from (Kerr 1976)) failure tip bearing capacity pressure load for two 90-degree free floating wedge plates to determine the appropriate force and then applying it to the Sanderson pressure-area curve. The result was able to model with some accuracy the icebreaking channel during maneuvering. An example of a solution is a pure yaw test as per from Liu et al (2006) as shown in Figure 21. The vessel tested in the program is a model scale of the, Canadian Heavy Icebreaker, CCGS *Terry Fox*.

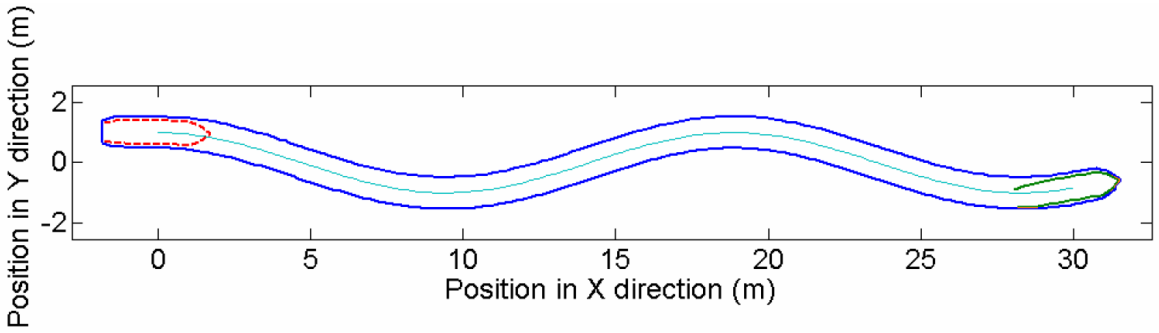

Figure 21. Simulated model-scale CCGS *Terry Fox* pure yaw channel from (Liu et al 2006)

2.2.4 Semi-Empirical – Tatinclaux's Shapes (1985)

A report by Tatinclaux (1985) further exemplifies McKindra and Lutton (1981)'s result of a lognormal distribution with a series of model scale level ice-breaking test with a simple wedge. He performed the test in urea-doped ice and synthetic ice with additional tests performed with a model of the offshore support icebreaker, *Kigoriak*. He claims there was little difference in the results between the icebreaker and the simple wedge. His results confirmed McKindra and Lutton (1981)'s log-normal fit and does further work to define relations of the cusp length and cusp area to the properties of the ice. Using dimensionless linear fitting, he established the two following area and length relations as shown in Equations 11 and 12 for urea ice. For the equations, the only new variable is A, the area of the floe. The assumed

geometry is seven different shape classes that vary in the ultimate determination of the area calculation. The seven shapes used in the classification are rectangle, triangle, trapezoid, diamond, arc, semi-circle, and ellipse.

$$\frac{A}{h^2} = 0.105 * \left(\frac{\sigma_f}{\gamma h}\right) \tag{11}$$

$$\frac{L}{h} = 0.540 * \left(\frac{\sigma_f}{\gamma h}\right)^{\frac{1}{2}} \tag{12}$$

Tatinclaux (1985) generated approximate ratios for relating the bending strength of the ice, the thickness, and the resulting lengths of the flow. The method is only a limited fitting of the data and only analyses length and area of the cusps and not the width. Overall, it is mainly another analytical method to approximate cusp dimensions using simplified geometry. The equations provided is for urea ice, the result for the synthetic ice follow a similar format but with different coefficients are listed in Tatinclaux' paper (1985).

2.2.5 Semi-Empirical – Wang's Circles (2001)

Another approach to the nature of the icebreaking pattern was performed by Wang (2001) who used the full-scale speed dependency plots of Enkvist (1972)'s results of Figure 13 and Varsta (1983)'s results of Figure 14 to generate a linear fit relation between the cusp dimensions and ship speed. The fit was used for Wang (2001)'s model for looking at breaking patterns in conical structures and aimed to look primarily at lower drift ice speeds than ship speeds. A circle radius approximation was used to maintain one dimension. The equation used by Wang is demonstrated in Equation 13. The V_n term is the normal velocity between the hull and the contact point from the ice flow. The C_{it} term represents a combination of empirically derived constant along with values based on the characteristic length of the ice sheet and Cv term is another semi empirical term based on empirics and the nature of the angles of the interaction between the structure and the ice. The C_v term is negative due to the

negative correlation between speed and floe radius. The values of C_{it} and C_v are defined in equations 14 and 15, where C_l and B_e are empirical constants of value 0.320 and -0.144 respectively.

$$R = C_{it} h^{0.75}(1 + C_v V_n) \quad (13)$$

$$C_{it} = \frac{C_l * l_c}{h^{0.75}} \quad (14)$$

$$C_v = B_e \tan\beta \cos\alpha \quad (15)$$

2.2.5.1 Applied Numerical Model – Su (2011)

An application of Wang's circle is in the numerical model by Su (2011). Su(2011) developed a general model of ships in ice and his selected icebreaking cusp method was Wang's model. The idealized circles with a speed dependency made it a simple analytical model to be used in the overarching numerical solution. A diagram showing the application of Wang (2001)'s circle in icebreaking could be seen in Figure 22.

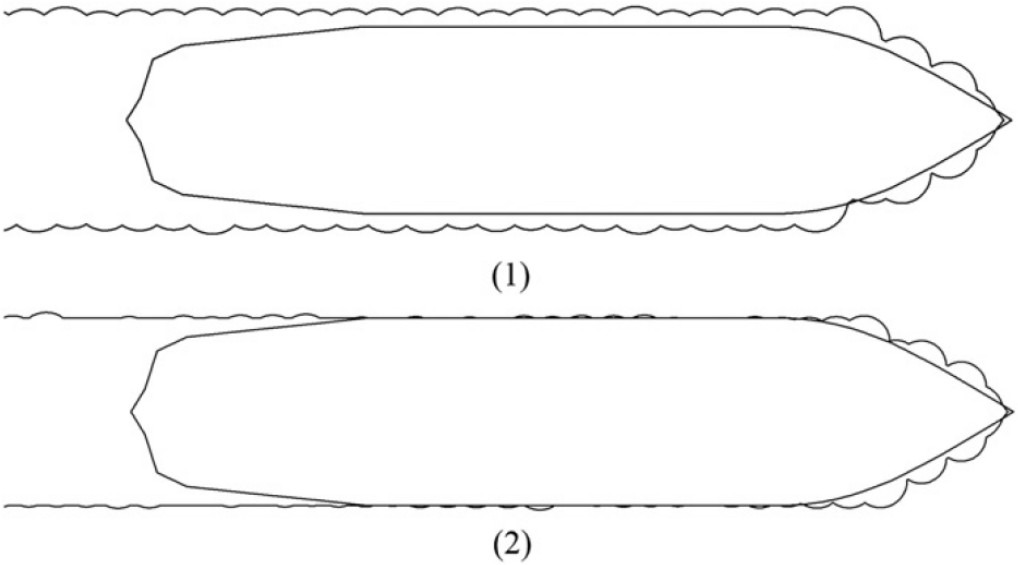

Figure 22. Ice breaking pattern as per Su (2010)'s simulation in the case without shoulder crushing (1) and with shoulder crushing (2) (Su 2010)

2.2.6 Theoretical – Nevel's Elastically Founded Semi-Inf Plate (1958)

A standard solution for broken ice geometry and the source solution that is developed on for further solutions is the Nevel (1958)'s analytical solution for a semi-infinite narrow wedge beam in the elastic foundation of water. The theory was developed for the point load bearing

capacity on an infinite plate of ice that is assumed elastic. In his theory, the ice would first crack radially from the tension on the bottom of the ice and then circumferentially from the tension on top of the ice. The step between the radial cracks to the circumferential is simulated through ice wedge failure. A figure demonstrating this failure mechanism is shown in Figure 23.

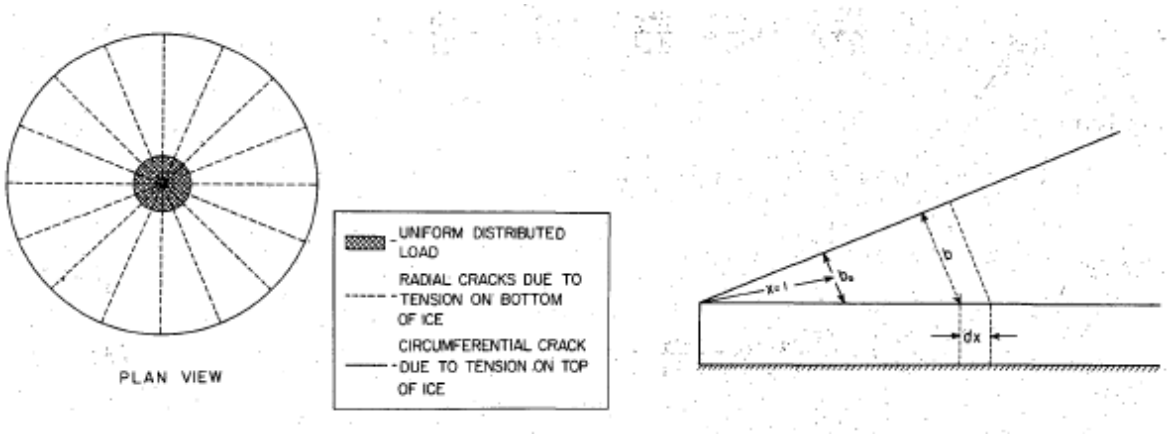

Figure 23. Nevel crack pattern on an ice sheet and a narrow free infinite wedge on an elastic foundation (Nevel 1958)

The initial Nevel (1958)'s association performs the solution along the radial length of the wedge and his solution is presented in Equation 16. In the equation, *y* is the vertical deflection of the wedge, and χ is the non-dimensional distance measured along the wedge. The non-dimensional distance measured along the wedge can be defined by Equation 17 such that *x* is the distance from the loaded corner of the wedge.

$$\frac{d^4y}{d\chi^4} + \frac{2}{\chi}\left(\frac{d^3y}{d\chi^3}\right) + y = 0 \tag{16}$$

$$\chi = \frac{x}{l_c} \tag{17}$$

A solution has been presented for the base scenario regarding the bearing capacity of ice, and his solution can be shown in Equation 18. The variables, A_{nev}, B_{nev}, C_{nev}, D_{nev} are based on boundary conditions and the resultant χ based functions of du_0, du_1, du_2 and du_3 are generated after appropriate Laplace transforms. The du functions are resolved and represented

by a series as per the appendix of the paper by Nevel (1961). The complexity of the equation requires matching numerical solutions for the result.

$$y(\chi) = A_{nev} * du_0(\chi) + B_{nev} * du_1(\chi) + C_{nev} * du_2(\chi) + D_{nev} * du_3(\chi) \qquad (18)$$

2.2.6.1 Modified Nevel – Lubbad and Løset's Radial Wedges (2011)

Lubbad and Løset (2011) takes an approach on icebreaking pattern expanding on the Nevel (1958)'s solution to work primarily on the half circle cusping nature of the interaction of ships with level ice. The Nevel (1958)'s solution looks are primarily at a point load on a sheet, Lubbad and Løset (2011) expanded the solution to a half circle. The two main failure mechanism of Lubbad and Løset (2011)'s approach follows the Nevel (1958) solution description such that the ice fails first in generating radial cracks and then circumferential cracks. Due to the half circle loading nature, the pressure loading was approximated to be a vertical point load at 0.5m from the apex to calculate the max load and the resulting breaking length or radius. A diagram showing this equivalent approximation method to solve the problem is shown in Figure 24.

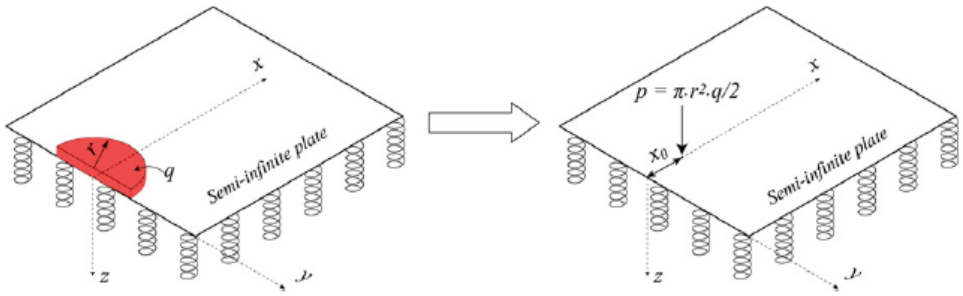

Figure 24. Lubbad and Løset equivalent loading system for semi-infinite ice sheet under external load over a half circular area
Source: Lubbad and Løset '11

The radial crack solution only focuses on the first radial crack length with Nevel (1958)'s solution, and thus Lubbad and Løset (2011) approximates with a random variable, deeming 3 to 5 wedges to form for each semi-circle. The wedges are additionally modeled as triangle for the simplification of the wedge and could not be broken further. Overall, the solution

does not significantly change the bending mechanism and only focuses on simplifying the creation of radial cracks. Based on this interaction, the resultant icebreaking pattern would have an appearance as shown in Figure 25 based on the number of contact points.

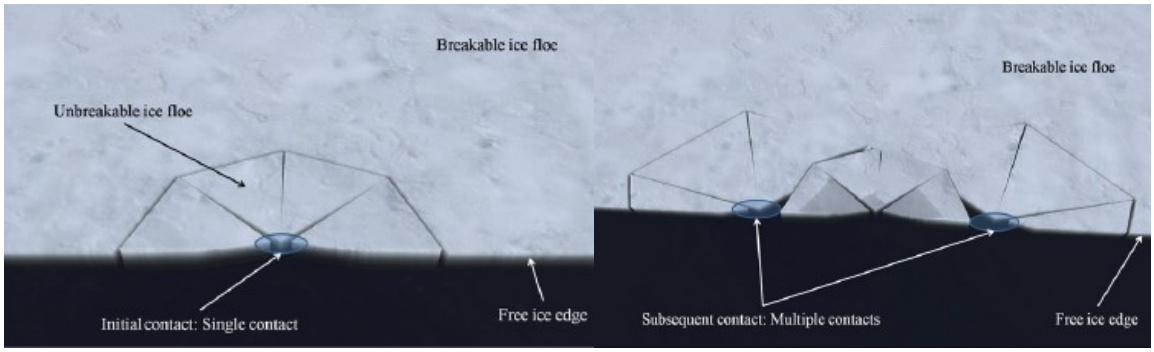

Figure 25. Lubbad and Løset generated cracking pattern on free edge based on contact points (Lubbad and Løset 2011)

2.2.6.2 Modified Nevel – Li's Discretized Wedges (2019)

The nature of ships interacting at angles and imperfect circles require further modification, as large fan shaped wedges are the more prevalent form of geometry in the interaction. To work with this, Li et al (2019) performed further expansions with the Nevel (1958)'s theory to operate on larger wedge where the failure is determined by discretizing to infinitely smaller wedges. Performed in the polar domain, the crushing depth, τ_c, thus varies along the wedge angle, θ, based on the interaction between the ship and the ice, with influences from the crushing inclination. Assuming wedge tip loading, a new deflection field, $f(\theta)$, could be determined as shown in Equation 19 based on modifying the solution from Nevel (1958)'s. However, to account for the interactions between the smaller internal wedges, an additional function, $g(\theta)$, must be included to demonstrate this interaction for the resultant deflection field of $w(\theta)$ as shown in Equation 20. $g(\theta)$ is assumed to be independent of the radial direction variability as the Nevel (1958) original solution represent the larger radial solution and the addition only adjusts for the discretized wedge and angular variabilities in the final balance of forces and moments.

$$f(\theta,\chi) = A\big(\tau_c(\theta)\big) * du_2(\chi) + B\big(\tau_c(\theta)\big) * du_3(\chi) \tag{19}$$

$$w(\theta,\chi) = f(\theta,\chi) * g(\theta) \tag{20}$$

The integral of the internal shear stresses based on Kirchoff-Love plate theory between the wedge plate stress and its differential form was approximated with a first order Taylor Series arriving at Equation 21, and the creation of two coefficients C_1 and C_2. The integral along the radial length provides a result of the shear stress along the length of the wedge as a function of the wedge angle.

$$V_{int} = D\delta\theta\left(\frac{\partial^2 C_1(\theta)g(\theta)}{\partial\theta^2} + \frac{\partial^4 C_2(\theta)g(\theta)}{\partial\theta^4}\right) \tag{21}$$

In a simple fashion, the internal and external forces can be equated along the arc of the wedge. The external forces on the wedge could be summarized by the effects of the vertical load on the ice,δP_v, as defined by 22 based on k_b, the buoyancy force per unit volume. In conjunction with the buoyant reaction force, the external force sums up to the solution on the right side of the Equation 23, while the internal forces are summarized in the left. Additionally, there are the boundary conditions of ensuring zero moments and shear at the ends of the greater wedge is shown in equations 24 and 25.

$$\delta P_v = -k_b \int_{\tau_c}^{+\infty} f(\chi,\theta)(\chi\delta\theta)d\chi \tag{22}$$

$$D\left(\frac{\partial^2 C_1(\theta)g(\theta)}{\partial\theta^2} + \frac{\partial^4 C_2(\theta)g(\theta)}{\partial\theta^4}\right) = (g(\theta)-1)\frac{\delta P_v}{\delta\theta} \tag{23}$$

$$M_{edge} = D\left(C_3(\theta)g(\theta) + \frac{\partial^2 C_4(\theta)g(\theta)}{\partial\theta^2}\right) = 0 \tag{24}$$

$$V_{edge} = D\left(\frac{\partial C_1(\theta)g(\theta)}{\partial\theta} + \frac{\partial^3 C_2(\theta)g(\theta)}{\partial\theta^3}\right) = 0 \tag{25}$$

With all the known theoretical conditions, equation 23 was solved using the Finite Difference Method (FDM) due to the complexity of the problem. The unknown interaction deflection field of g is isolated under matrix form after appropriate discretization, manipulation, and approximations. The operation was performed by Li et al (2019) to build the solution

and database of deflection solutions was created. Furthermore, with the appropriate deflection field $w(\chi, \theta)$, the stress field could be more well understood. First, the location of maximum stresses, χ_m, in the narrow wedges could be pinpointed based on the second radial partial derivative of the crushing based deflection $f(\chi)$ and its corresponding maximum stress. This vertical loading deflection induced maximum stress, σ_v, combined with the horizontal compression stress, σ_h, during interaction summed up provides the maximum radial stress, σ_m. The equations for these three stresses are defined in equations 26, 27, and 28.

$$\sigma_v(\theta) = g(\theta)\frac{Eh}{2(1-v^2)}\frac{d^2 f(\chi,\theta)}{l_c^2 \partial \chi^2} \; where \; \chi = \chi_m(location \; of \; Nevel \; max \; stress) \quad (26)$$

$$\sigma_h(\theta) = -\frac{1}{h\chi_m l_c}\frac{\delta P_h}{\delta \theta}\sin(\theta - \alpha) \quad (27)$$

$$\sigma_m(\theta) = \sigma_v(\theta) + \sigma_h(\theta) \quad (28)$$

With the known stress field, a max stress line could be found along each of the narrow wedges that form the larger wedge. This combined with a known flexural strength of the ice allows the two to match and appropriate propagations of the failure along a matching max stress line across all the narrow wedges when one of the wedges conditions meet the flexural strength of the ice. The targeted solution of this model makes it ideal for the issue at hand; this solution set is thus used as a major theoretical comparison method to the experimental results. This solution methodology works under the elastic regime assumption of the ice. A picture demonstrating the resulting icebreaking pattern using this model for the South African icebreaker, S.A. *Agulhas II*, is shown in Figure 26.

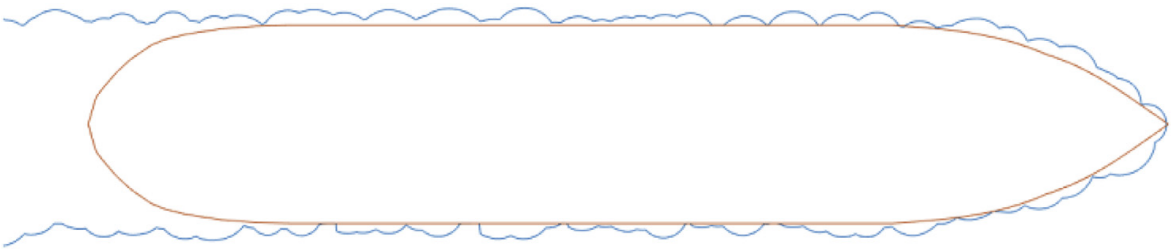

Figure 26. Icebreaking pattern from Li et al's discretized wedges model for South African icebreaker, S.A. *Agulhas II* (Li et al 2019)

2.2.7 Theoretical – Erceg's Discretized Beams (2015)

Expanding on simple beam theory, Erceg et al (2015) discretizing the ice into beams for a range of angles zero to 90 degrees. Due to the nature of the normal beams, a beam interaction factor was introduced to account for the interaction. By applying the crushing and friction force onto the ice into the discretized beams, a solution of the breaking length to cause bending failure was found. A diagram of this solution approach is shown in Figure 27. The completed simulation was only done for 5 cusps for the tanker MT *Uikku* in 0.5m and 500kPa ice and is shown in Figure 28. The measured approximate width and length of the cusp from the diagram is all that is available, and the value is 3.7m and 6.7m correspondingly for the non-first cusp. The geometrical scaled down versions of these values would be used in the comparisons to the tests.

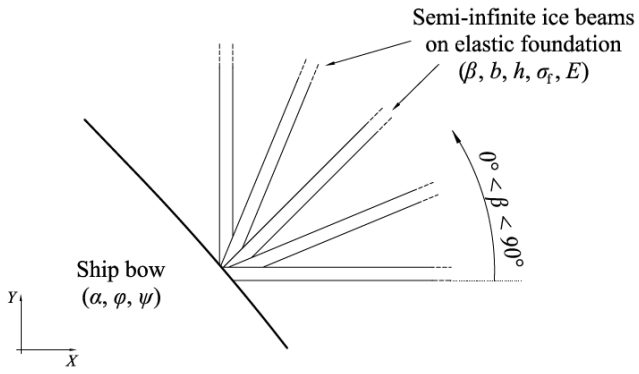

Figure 27. Erceg's interaction process illustration and radial ice beams (Erceg et al 2015)

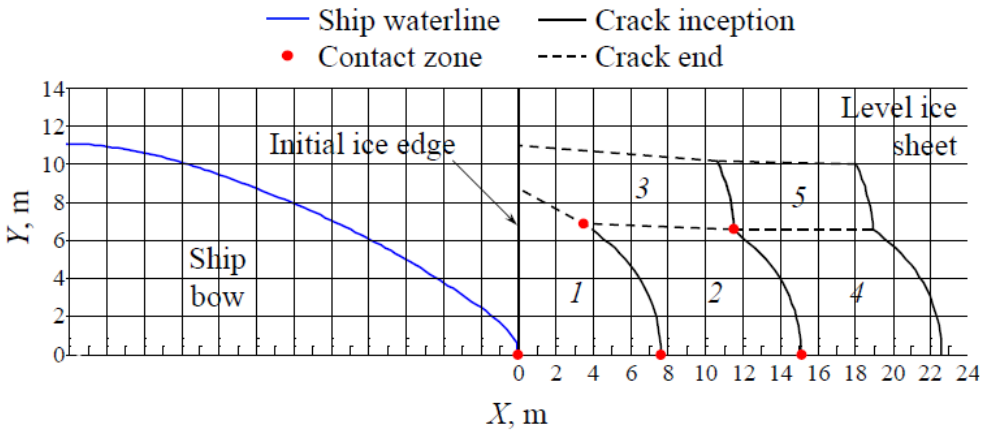

Figure 28. Icebreaking pattern for MT *Uikku* in 0.5m FS level ice using Erceg's discretized beam model (Erceg et al 2015)

2.2.8 Numerical – Valanto's 3D Hydrodynamic Solution (2001)

Valanto (2001)'s icebreaking solution is one of the more complicated solutions using a heavier reliance in numerical calculations to generate the dynamic interaction between the vessel, ice, and the water. A computation grid showing the influence of the three interacting components under the model is shown in Figure 29. His solution is an extensive analysis of the ice, water, and the advancing ship's disturbance to them under steady flow and the appropriate responses when the ice fails by a combination of crushing and bending. The cusp formation has a degree of randomness to its formation and is isolated from the interaction of other cusps. The result is independent cases of interaction of cusp formation based on the loading from the ship and the level ice. A stress field is generated on the ice cover due to the advancing vessel that induces a cantilevered beam like mechanism failure or a membrane stress at steeper frame angles onto the ice cover that fails under the maximum principal stress. The location of the maxima dictates the length and geometry of the broken cusp. The result has a strong dependency on the dynamic and hydrodynamic effects of reality, but the nature of the high complexity excludes the interdependency of the cusps interaction and demands large computation time and power. Figure 30 shows a demonstration of the level ice grid with the induced stresses and deformations due to the influence of the moving vessel in Valanto (2001)'s model.

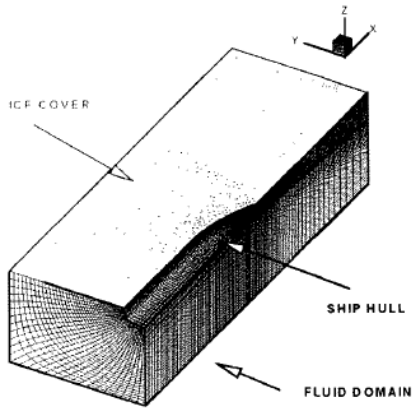

Figure 29. Computational grid domain in Valanto '01 Model (Valanto 2001)

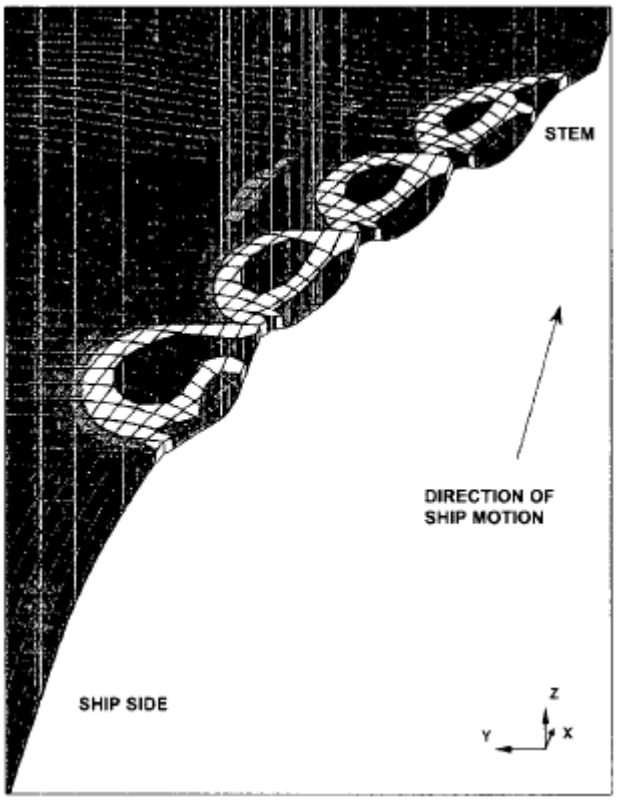

Figure 30. Cusp formation in Valanto ’01 Model (Valanto 2001)

2.2.9 Numerical – Sawamura FEM Solution (2008)

Another approach was completed by Sawamura (2008) who used the FEA tool, ABAQUS, to approximate the breaking pattern. The ABAQUS code allowed the water and ice plate to be modelled as separate entities that could then interact with the structure. The water had its own unique fluid mesh and the code was able to account for fluid-structural interaction. The fluid was modeled as a simple hydrodynamic material and its nature was governed by Navier-Stokes and assuming an incompressible, inviscid fluid. The ice was modelled as a homogeneous elastic material. A contact algorithm was also built between the water and ice. Built with an adaptive mesh, the local interactive nature in crushing and bending was simulated. Additionally, line loads and point loads representing the large pressure loads were used in the simulation as well. Using this model, various wedges ranging from 30 to 150

degrees were simulated. Circles were also used as the geometric failure mechanism, simulating that of the circumferential failure seen in ice. The breaking length of radius of the circle was found for when the load would exceed the bending strength of the ice. Conclusions from the work claim the importance of dynamic and free surface effects of the water and the method does present differences from the analytical methods with some agreements. A diagram representing the general nature of the FEM solution is presented in Figure 31. Due to the calculative intensity of the method, Sawamura compiled the set of solutions from these interactions into a database, allowing for quick access to breaking lengths and stresses based on input parameters. (Sawamura 2012)

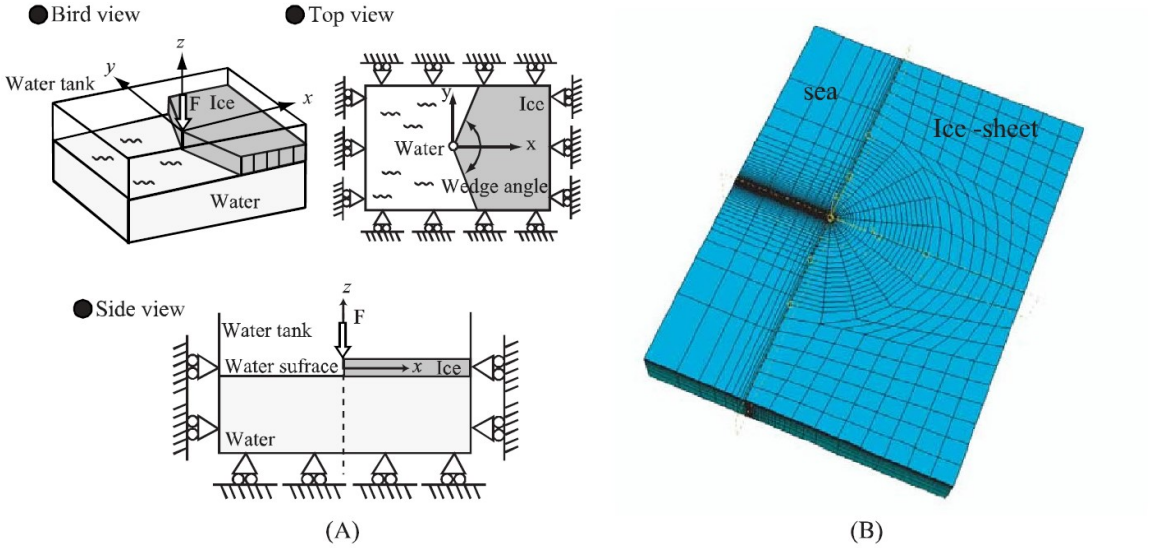

Figure 31. Schematic diagram and FE mesh of the Sawamura FEM model (Sawamura ’12)

2.2.10 Numerical – Summary of Methiod

In summary, various methods have been used to approximate cusps but no standard method has been widely adopted, as the geometry is quite variable and there is a large range of varying complexities from simple analytical formulas to intricate numerical codes. A table containing the major points of each method is summarized in Table 2, regarding the matters of type of solution, scale derivation, structure type origin, solution development method,

speed dependency, geometrical shape approximation, geometric dimensional output, and operative failure regime from Yean et al (1981)'s criterion. Most of these methods have a thickness and strength dependency but speed dependencies are not existent in all the methods.

Table 2. Summary of Cusp Methods of Approximation

CUSP METHOD	TYPE	SCALE	SHIP/ STRUCTURE	SOLUTION METHOD	SPEED DEP.	GEOMETRIC SHAPE APPROX.	DIMENSION OUTPUT	FAILURE REGIME
MCKINDRA & LUTTON (1981)	Statistical	Full	Ship	Log-Normal Distribution Fit to Tug Data	N	N/A	Length	None
IZUMIYAMA et al (1992)	Statistical	Model	Structure	Normal Distribution Fit for Cone Structure	N	Circle	Radius	Strength
KOSTRAS et al (1983)	Analytical	Full	Ship	Dimensionless Linear Fit for a set of 5 ships	Y	Semi-Ellipse	Length, Width	Elastic
TATINCLAUX (1985)	Analytical	Model	Ship	Dimensionless Linear Fit for Simple Wedge	N	Rectangle, Triangle, Trapezoid, Diamond, Arc, Semi-Circle, Ellipse	Width, Area	Strength
WANG (2001)	Analytical	Full	Ship	Linear Fit for a set of 3 ships	Y	Circle	Radius	Elastic
NEVEL (1958)	Theoretical	-	-	Quasi-static	N	Circle	Radius	Elastic
LUBBAD & LØSET (2011)	Theoretical	-	-	Quasi-static	N	Half Circle	Radius	Elastic
ERCEG et al (2015)	Theoretical	-	-	Quasi-static	N	Quarter Circle and less	Radius	Elastic
LI et al (2019)	Theoretical	-	-	Quasi-static	N	Arced Wedge	Wedge Ends and Center Length	Elastic
VALANTO (2001)	Numerical	-	-	Dynamic	Y	Half Circle	Radius	Elastic
SAWAMURA (2008)	Numerical	-	-	Dynamic	Y	Arced Wedge	Radius	Elastic

2.3 Model Testing in Ice

The nature of model testing in ice is a method developed as a cheaper option to test the physical properties of vessels operating in ice-covered waters. Typically, it is performed to assess ice resistance, power requirements, and the flow of ice around the hull during transit. The physical basis of the interaction is usually scaled using non-dimensional numbers in

maintaining the scaling of the most significant physical phenomena. Geometric similarity is maintained by the scaling ratio λ, while kinematic and dynamic similarity is maintained through Froude and Cauchy scaling as opposed to Froude and Reynolds in open water scaling. The Froude Number is a ratio between the gravitational and inertial forces while the Cauchy Number is the ratio between the inertial and elastic forces. These two numbers help in scaling the physical phenomenon associated with the interaction between the ship and the fluid nature of the water as well as the elastic material nature of ice. The equations for these two non-dimensional numbers and are shown in equations 29 and 30. A table of properties and how there are scaled based on these three scaling conditions completed by Timco (1984) and are presented in Table 3.

$$Fn = \frac{V}{\sqrt{g * L_c}} \tag{29}$$

$$Cn = \frac{\rho V^2}{E} \tag{30}$$

Table 3. Summary of scaling laws based on Froude, Cauchy, and geometric similarity (Timco 1984)

Variable	Scaling
ice thickness	$[h]_P = \lambda[h]_M$
ice compressive strength	$[\sigma_c]_P = \lambda[\sigma_c]_M$
ice flexural strength	$[\sigma_f]_P = \lambda[\sigma_f]_M$
ice shear strength	$[\sigma_s]_P = \lambda[\sigma_s]_M$
ice elastic modulus	$[E]_P = \lambda[E]_M$
velocity	$[V]_P = \lambda^{1/2}[V]_M$
time	$[T]_P = \lambda^{1/2}[T]_M$
force	$[F]_P = \lambda^3[F]_M$
mass	$[M]_P = \lambda^3[M]_M$
ice critical stress intensity factor	$[K_{I_c}]_P = \lambda^{3/2}[K_{I_c}]_M$
acceleration	$[a]_P = [a]_M$
the ratio of elastic modulus and flexural strength	$[E/\sigma_f]_P = [E/\sigma_f]_M$
ice frictional coefficient	$[f]_P = [f]_M$
ice density	$[\rho]_P = [\rho]_M$
Poisson ratio	$[\nu]_P = [\nu]_M$

Model testing in ice is typically performed in ice model basins, large tanks usually have a mist spraying system and variable temperature settings to create the ice on top of the tank. The water also contains a dopant to weaken the ice into its required strength and properties as per required for the scaling when frozen. The tanks are also equipped with a carriage to push the model vessel across the ice and various instrumentation to measure resistance and other properties as well as potentially cameras analyze flow of the broken ice or breaking patterns.

In analyzing the resistance for ice, it is typically assumed that the total resistance in ice-covered waters (R_{tot}) is divide into an open water component (R_{OW}) and an ice component (R_{ice}); called the open water resistance and the ice resistance respectively as shown in Equation 31. The open water resistance is from testing the resistance of the model in open water and generating a plot. The total ice resistance could be found by testing the model in level ice and the open water resistance is found by testing the model in open water. The difference between the two is the ice resistance. The ice resistance is also divided into primarily three components crushing, breaking (by bending), and submergence (Lindqvist ’87). Two types of tests are typically performed to decompose the ice resistance, level ice and pre-sawn ice. The level ice is considered to include all the three components where the ice resistance could be found, and the pre-sawn level ice then is considered to contain all the components excluding the breaking component. The ice resistance from the pre-sawn test is considered to contain the rest ice resistance (R_{ir}). The difference between the ice resistance and the rest ice resistance is the breaking component of the ice resistance (R_{br}). This component division of the ice resistance is shown in Equation 32 (Von Bock und Polach ’10).

$$R_{tot} = R_{ice} + R_{OW} \tag{31}$$

$$R_{ice} = R_{br} + R_{ir} \tag{32}$$

3 Method

3.1 Aalto Ice Tank

The location of the test was in the Aalto Ice Tank, a 40 by 40 meter tank with a depth of 2.8m. An area of approximately 35 by 35 meters serves as the usable portion of the tank. The tank had recently undergone a renovation over much of the decade of the 2010s and returned to service in 2019. In cooperation with the completed renovation, tests were also included to compare the performance to tests of the same model before the tank's renovation. All tests performed were to match to the best ability of the previous projects for level ice conditions. All the tests discussed in this section were tests performed in the Aalto Ice Tank before the renovation. A picture of the Aalto Ice Tank is presented in Figure 32.

Figure 32. Aalto Ice Tank

The tank is doped with ethanol to weaken the ice to its desired properties for Froude and Cauchy scaling. The water contains approximately 0.3% ethanol. The ice is created from

multiple layers from a spray that creates a dense frozen mist that would settle on top of the tank water. Sprayed from approximately 1.7m above the tank at -12°C, the process is continued until the desired thickness of the ice is obtained. Due to this process, the ice is fine-grained and grown upward from the water surface unlike sea ice, which is typically grown downward due to the cold air temperature that freezes it. This form of model ice produces a more consistent ice property profile. The desired strength is adjusted to, through a consolidation phase at -15°C degrees Celsius and then at 0°C to -2°C for further strength and property tinkering and for the actual tests (von Bock und Polach ’16).

An important matter to address about the model ice in the Aalto Ice Tank was that the ice was found to experience a dominantly plastic failure mechanism as opposed to an elastic mechanism that is more prevalent in full-scale ice. This raises some questionability of the standard Cauchy scaling that is based on elastic deformation (von Bock und Polach ’16). In addition, many of the fundamental theories and approaches to model-scale ice testing is founded on the assumption that the ice acts elastically. The simplicity of elasticity has allowed the assumption to stand the test of time; however, this now known phenomenon may present some difficulties that stretch throughout the foundations of this and former works in relation to model scale. Nevertheless, the traditional elasticity assumption will still be used for the general analysis due to the nature of former methods and simplicity.

An additional concern was the nature of the ice that was formed during the test. Due to the recently completed renovations of the tank and the sheets used was one of the first, the nature the columns of the ice were atypical. The ice contained an exceptionally hard top layer and a considerable layer of slush underneath the top layer representing a decent amount of variation in mechanical properties across the thickness of the ice. Because of this matter, the ice may behave more unusually compared to other model or full-scale ice.

3.2 MT Uikku Testing

The model to be used in the test is MT *Uikku*, which is a 16000 DWT tanker that was extensively instrumented for measurements for the ARCDEV project (ARCDEV 1988). As part of the ARCDEV project, the ship thus has full-scale ice test data along with hull loading data. Additional work at the Aalto ice tank also includes model scale test results. The vessel was designed to have mixed capabilities such that its bow was to have good operational profiles for forward action in both ice and water, while the aft was designed for heavier ice conditions. Entering operation in the 1970s, the vessel was a very advanced tanker in ice. The model used in the experiment is the Azipod version of the model and is thus a 1:31.56 scale version of the ship. A table demonstrating the general characteristics of the model and full-scale equivalents is presented in Table 4. A general diagram of the MT *Uikku* is also presented in Figure 33.

Table 4. General characteristics of MT *Uikku*

MT *UIKKU* CHARACTERISTICS		**MODEL**	**FULL**
λ		31.56	1
LOA	**(m)**	5.21	164.4
LBP	**(m)**	4.75	150
Displacement	**(ton)**	0.50	15748
B	**(m)**	0.70	22.2
T	**(m)**	0.30	9.5
α	**(deg)**	21	21
φ	**(deg)**	30	30

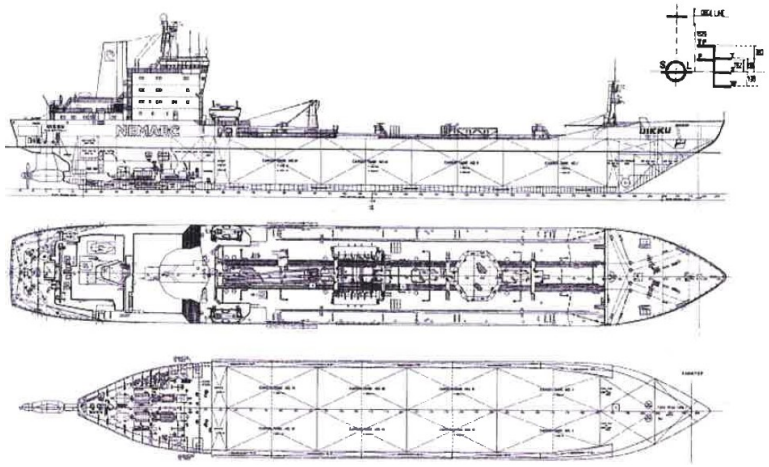

Figure 33. General Arrangements of MT *Uikku* (Garvin 2003)

3.2.1 Past MT *Uikku* Tests

In terms of model scale, two major test series were performed on the MT *Uikku*. The first were the tests by Garvin (2003) who tested a model of MT *Uikku* in level ice and pre-sawn ice and published the results. The second series of tests were performed by von Bock und Polach (2010) who performed tests on the same model of the MT *Uikku* in free and vertically constrained arrangements in level ice, pre-sawn ice, and open water. The results from these previous tests along with the test conditions are presented in Table 5 and Table 6. It should be noted in the tables that it is assumed that Garvin (2003) did not remove the open water resistance in his presentation of his results and in the 2010 tests, the ice resistance and total resistance with open water is include in the table. The extent of tests for this thesis looks primarily at level ice cusp formation, and thus the additional results Garvin (2003) performed for brash ice and the constrained condition Von Bock and Polach (2010) performed are not presented in the tables.

Table 5. MT *Uikku* test results and parameters from Garvin's tests in 2003

MT *UIKKU* - GARVIN ' 03

ICE CONDITION	hm (mm)	Vm (m/s)	σ_f (kPa)	σ_c (kPa)	E (kPa)	Rtot(N)
LEVEL ICE	28	0.162	31.9	66.3	29.4	-24.0
	28	0.270	31.9	66.3	29.4	-26.4
	28.3	0.348	32.7	69.5	26.5	-33.3
	28.3	0.463	32.7	69.5	26.5	-37.9

Table 6. MT *Uikku* test results and parameters from von Bock und Polach tests in 2010

MT *UIKKU* –VON BOCH UND POLACH '10

ICE CONDITION	hm(mm)	Vm (m/s)	σ_f (kPa)	σ_c (kPa)	E (kPa)	Rice(N)	Rtot(N)
LEVEL ICE	20	0.26	19	28	51	32.6	33.6
	20	0.56	18	35	51	47.6	51.5

3.2.2 Experiment Preparations

In preparation of the MT *Uikku* for tests, the model was ballasted to its design draft and two GoPro Black 7s were mounted to the starboard bow region of the model. The mounts were completed with two-aluminum extrusion that allowed for lateral and transverse variability in positioning. The GoPros were controlled remotely to capture a video of the cusps in the bow region at a resolution of 1440 and at 60 FPS. The two cameras were mounted roughly at station 9 and 10 to examine the cusp locations. At such a position, a complete view of the cusp formation zone could be obtained and the overlap between the views assisted in stitching the perspectives. Knowing the height and the relative approximate location of the cameras along with the angle of orientation, a general approximate view of the ice was found. Using the footage taken from the camera, additional modifications were made to get the view of the camera to be correlated to known geometric measurements. Figure 34 shows the region approximately examined by the cameras in the purple region of the bow, and Table 7 shows the location of the camera in reference to the station lines and the cameras' field of vision settings.

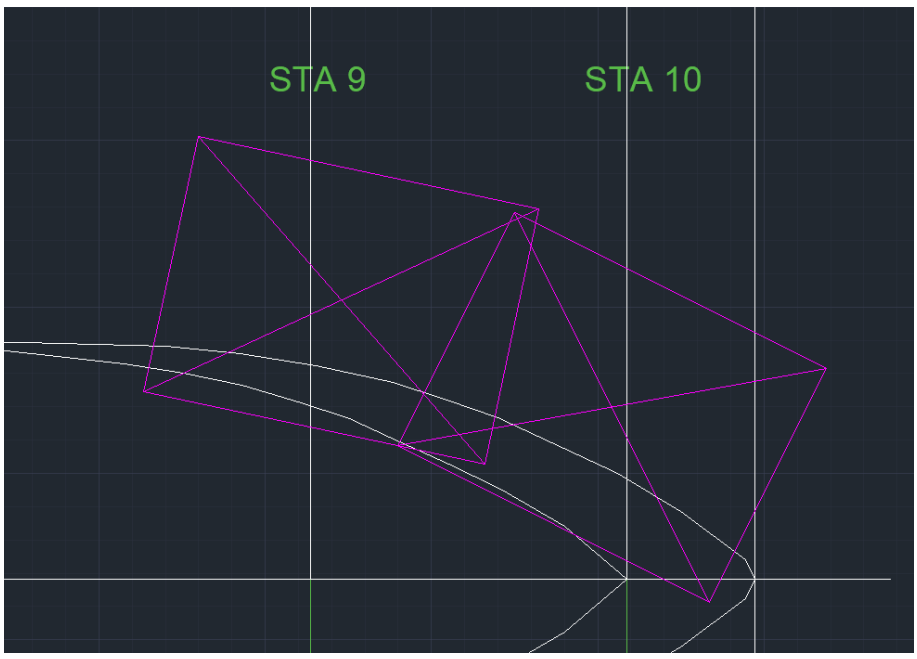

Figure 34. Diagram of the field of vision from the cameras in reference to the model

Table 7. Location and settings of the GoPro cameras

		STATION 9 CAMERA	STATION 10 CAMERA
VERTICAL POSITION	**(cm)** (cm from DWL)	28.5	28.5
HORIZONTAL POSITION	**(cm)** (cm from CL)	41.9	25.8
LONGITUDINAL POSITION	**(cm)** (cm from ST10 aftward)	42.9	2.3
ORIENTATION ANGLE	**(cm)** (deg from CL)	78.8	63.3
ANGLE OF VISION	**(deg)** (deg in Y Direction)	78.1	71.0
ANGLE OF VISION	**(deg)** (deg in X Direction)	86.7	86.7

From the testing, a display of the camera location in reference to its main deck can be seen in Figure 35. As seen in the figure, the cameras were mounted only on one side on top of two layers of aluminum extrusions that can allow for variation of the camera's location. The aluminum extrusions have dimensions of approximately 4.5cm by 4.5cm. The camera is then mounted at the end on top of the extrusion facing down. Due to how it is mounted, the lens would be at approximately 0.5cm below the height of the extrusion giving the lens location of 8.5cm above the main deck.

Figure 35. Depiction of camera locations on the hull in reference with the ice sheet

3.2.3 Model Tank Testing

The tests were performed on May 15th, 2019, where the pre-ballasted model was moved from the outfitting hall into the Aalto Ice Tank. The model, over a crane system, was placed on the tank by the edge of the tank where the model would run across the length of the ice tank. A demonstration of this arrangement could be best seen in Figure 36. Properties of the ice were measured from the main carriage across the tank shortly before the test and the ice property values were averaged and used for the analysis. Thickness, flexural strength, compressive strength, density, and modulus of elasticity were measured before the testing.

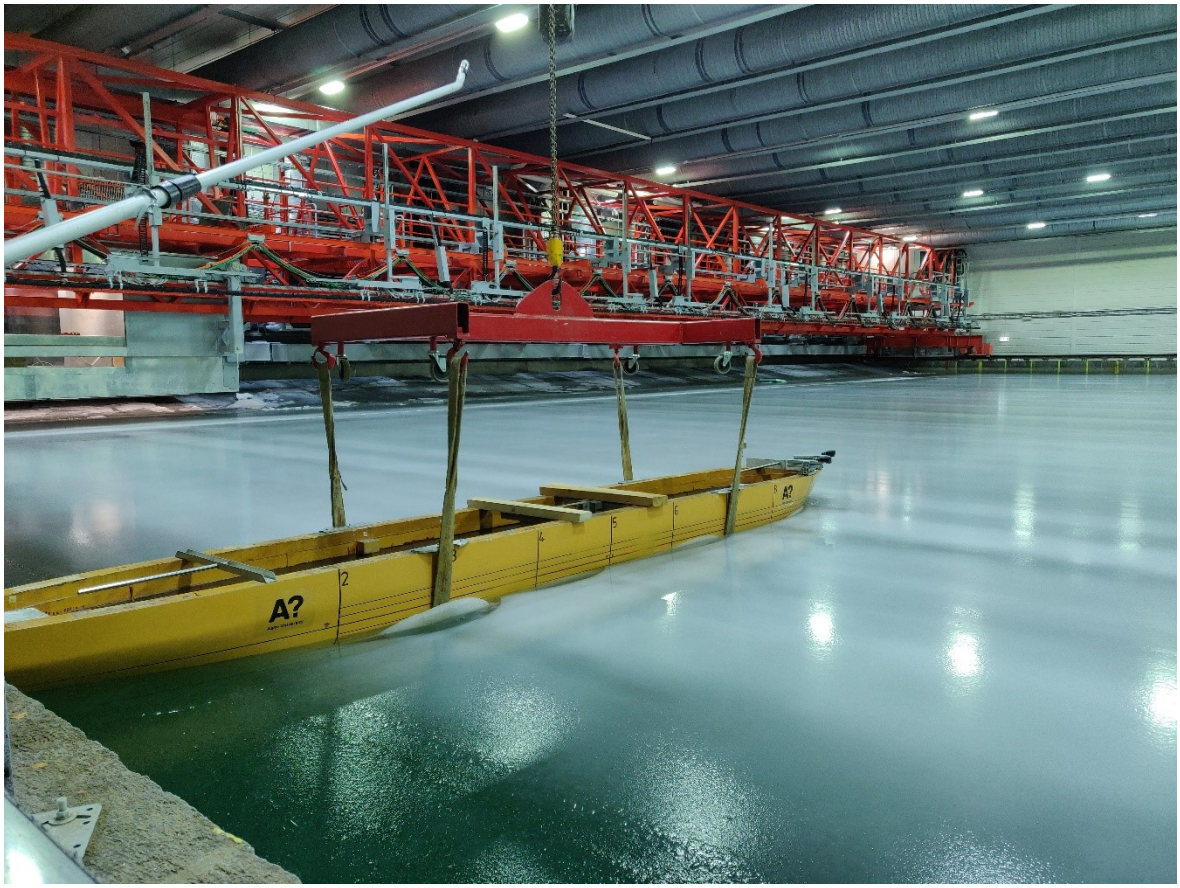

Figure 36. MT *Uikku* in the Ice Tank

The model was then attached to the main red carriage where metal frames were used to attach the carriage to the model. Force blocks and counterweights were used to set the resistance measurement system according to the Aalto University Ice Tank standards. The setup was

completed by the Ice Tank technicians. Figure 37 shows the completed setup of the model attached to the carriage. The carriage moved the model at the set speeds of the experiment, 0.162m/s and 0.270m/s across the 35m of operable test length. These were the only speeds that were tested, and the GoPros recorded the cusp formations through the duration of these tests.

Figure 37. MT *Uikku* attached to the ice tank main carriage

3.3 Digital Processing

3.3.1 Video Processing

The videos from the two cameras were extracted and Adobe Premier Pro CC 2019 was used to process the videos. The first process was to match the timing and locations of the two cameras. This was done easily with arranging the videos into its appropriate positions and orientations so the videos appropriate overlap to see the entire cusp during the process of the video. A picture depicting the overlap could be seen in Figure 38. The overlap was slightly modified to ensure that perspective issues were resolved at the waterline level where the cusp dimensions would be measured.

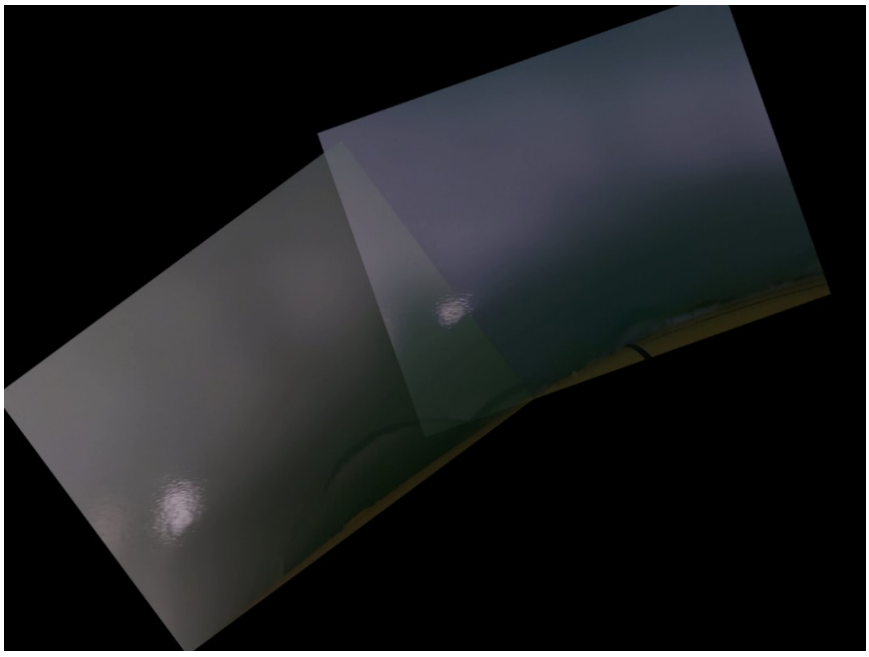

Figure 38. Pre-visual adjustment overlapped video example frame

The next step was to perform some visual adjustments due to the shadow created by the model onto the primary cusp creation zone on the level ice sheet. As a result, the contrast and brightness was modified using Adobe Premier Pro to a level to see the cusps easier. Additional references were also placed such as the hull mask and along with the station and centerline markers. The resulting visual adjustments in an example frame can be seen in Figure 39.

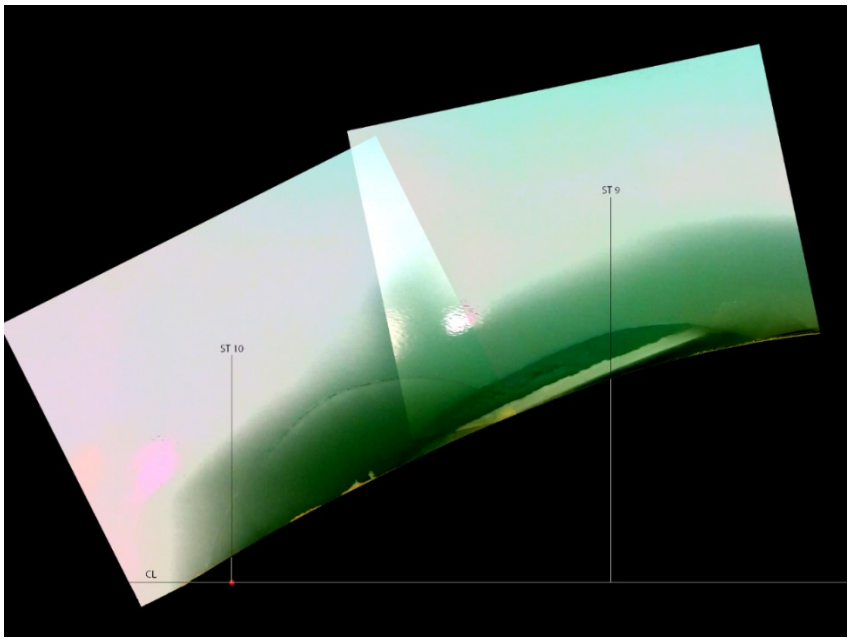

Figure 39. Post-visual and marker additions video example frame

3.3.2 Image Processing

From the videos, each frame was extracted from the 60FPS frame rate resulting in approximately 7500-12000 frames depending on the speed of the vessel. The frames were then manually sorted to find the frames when the cracks have propagated to the cusp formation on the ice sheet. The resulting viable frames for each video was approximately 500-600 frames or cusps valid for the analysis.

A MATLAB code was developed to analyze the cusps based around a six-point interface to take the geometry of the cusp. The six points were centered about capturing six important points to capture the geometry and the contact nature of the cusp. The first point represents the approximate contact at the center of the cusp closest to the hull. The following points represent the extremes of the cusp going in a clockwise direction. The second and last points are used to calculate the length of the cusp and the first and fourth point are used to calculate the width of the cusp. The first, second, and sixth point is used to calculate the approximate contact angle. The six points create a polygon that is used to calculate the area. All these geometric properties are then stored in a large matrix, after appropriate conversions from

pixels to geometric lengths that was calibrated using initial calibrations and reference distances from the vessel. All geometric points were measured from the origin of the intersection of Station 10 and the CL as seen by the red point. Figure 40 demonstrates the before and after image of a cusp drawing.

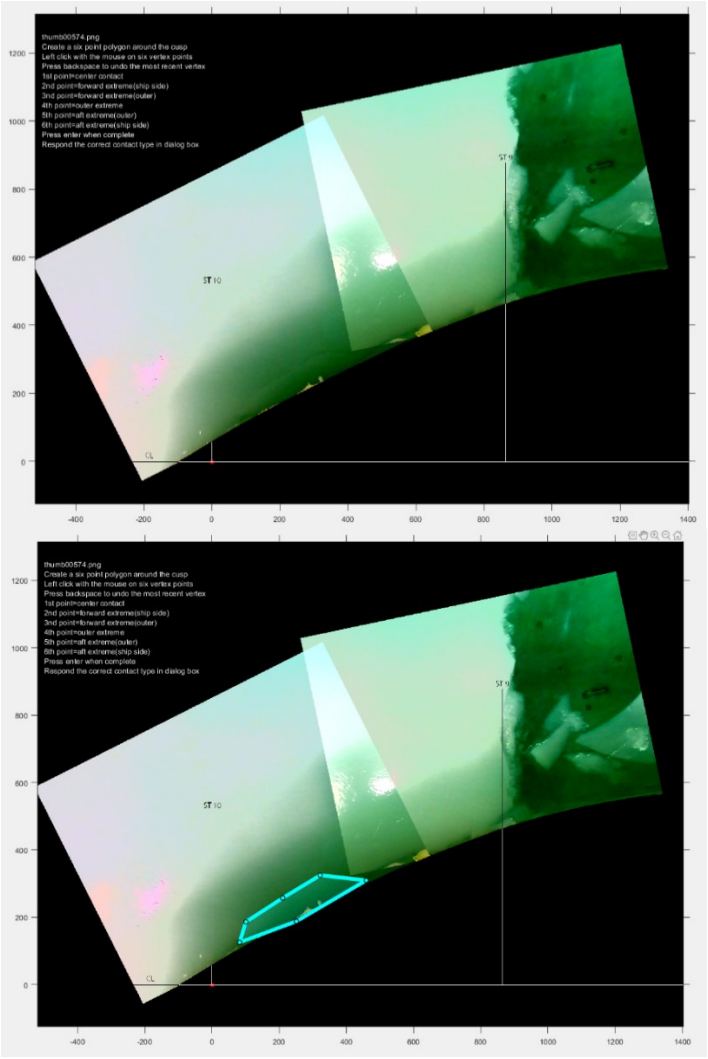

Figure 40. Example of single point contact cusp sketching

After the selection of points, a popup would appear asking if the cusp type was a single point/region contact or a multiple point/region contact. The appropriate selection should be made at this point to appropriately divide the data into the proper classification of the cusp in the following analyses. An example of a multiple contact cusp can be seen on Figure 41. The cusp shown is a multiple contact cusp as it formed from the ice sheet contacting the hull forward and aft-ward of the cusp in Figure 40 and thus has two regions of contact. As seen

by the polygon, a similar sketching mechanism is performed, and the multiple contact button should be selected after the sketching. Despite the multiple contact locations, these locations were not specified, and no previous work has examined this multiple contact cusp formation to provide any comparison.

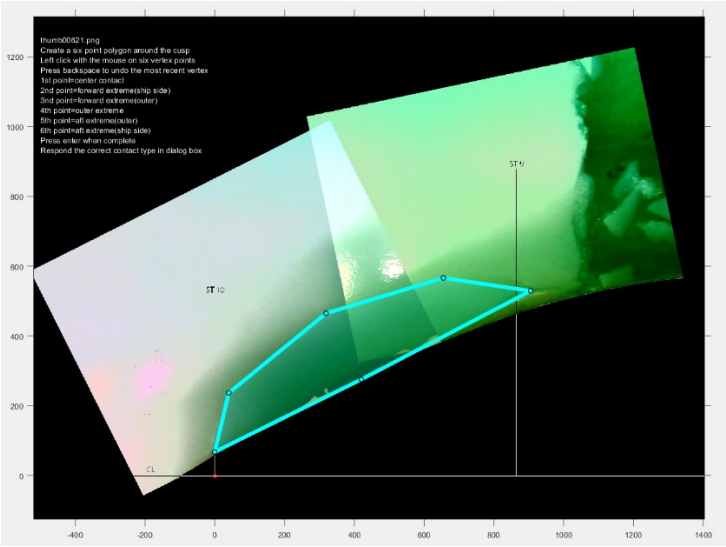

Figure 41. Example of multiple point contact sketching

3.4 Prediction Methods

In workings with the measurements of the icebreaking cusps, comparisons using the various methods from section 2.2 would be performed as an assessment of current methods. Despite the methods being originated from both model and full-scale measurements or analysis, standard geometric scaling was assumed for the sake of testing the hypothesis of cusp scalability. It should be noted that the numerical solution methods would not be used in the predictive comparisons as per the complexity and time-consuming processing and operation of the software, but more importantly due to the proprietary nature of those codes to the original creators. Nevel (1958)'s method of Lubbad and Løset (2011) will be equated for this case as the radius from the two methods are to be theoretically the same and as the angle of the wedges are measured, there is no need for Lubbad and Løset (2011)'s modification in this case.

3.4.1 Statistical Prediction

With the known statistical data from the McKindra and Lutton (1981) ´s Bay Class tests at full scale, the results were scaled down from full scale at the same scaling factor as the MT *Uikku* model. The average values, or the expected value as per the authors, from each test speed were plotted against vessel speed to generate a plot of the expected cusp length as a function of speed as shown in Figure 42. With the known function and the two known speeds, expected cusp sizes were found for the test conditions through simple interpolation from the line function (McKindra and Lutton ’81).

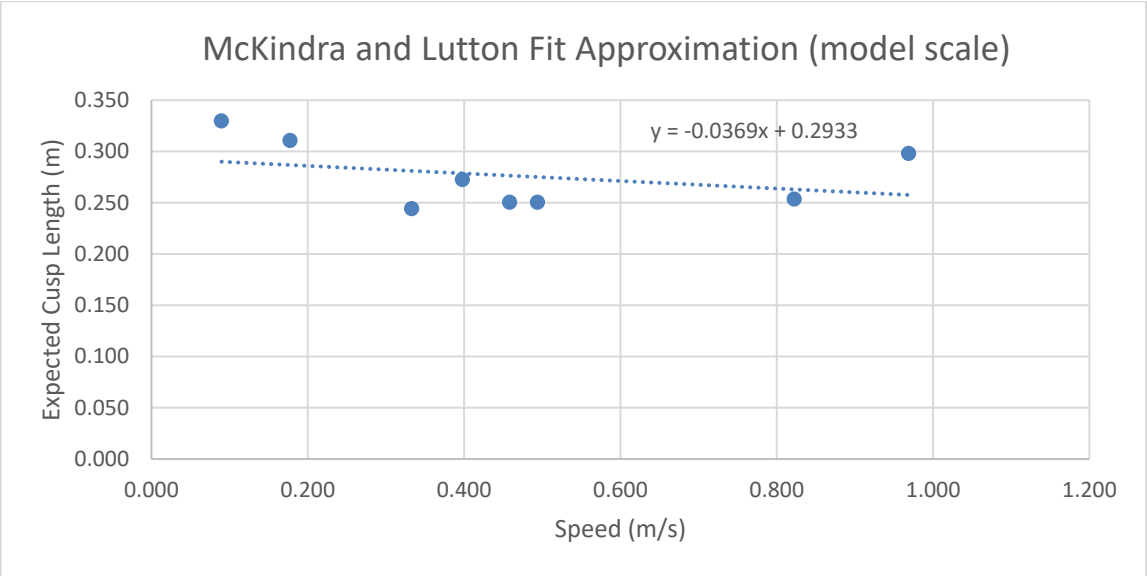

Figure 42. McKindra and Lutton Scaled Cusp Fit

The Izumiyama et al (1992) data only provides one distribution as a function of the ice properties. Thus, Equations 4 and 5 were combined and modified to account for downward bending instead of the original upward bending such that the flexural strength, σ_f, would be used instead of the upward bending strength, σ_u. The value of Z_m from Izumiyama et al (1992) of 0.937 was inserted to the final equation as well such that the resultant expected mean cusp radius is shown in Equation 33.

$$R_m = 0.937 * \left(\frac{\sigma_f h}{\gamma}\right)^{0.5} \tag{33}$$

3.4.2 Analytical Prediction

In the Kostras Semi-Circle cusp approximation, the equation was performed locally for each cusp (Kostras et al 1983). With a wedge approximation of the bow, the directional cosine is the same as the sine of the normal frame angle resulting in the final cusp width equation as shown in Equation 34 based on Equation 9. The Kostras width to depth ratio (Equation 10) was also used, rearranged into the final cusp length equation as shown in Equation 35. The final cusp length equation was also modified as the 10-meter constant was intended for full-scale use and thus the full-scale ice thickness was selected to work with this ratio.

$$W = \sin\beta_c{}' \, l_c(1.7153 + 4.2653\left(\frac{\sin(\alpha)}{\tan(\beta_c{}')}\right)\left(\frac{V}{\sqrt{g l_c}}\right))^{-1} \tag{34}$$

$$L = W\sqrt{\frac{10.0meters}{hm * \lambda}} \tag{35}$$

Through Tatinclaux (1985) model scale shapes analytical method, Equations 11 and 12 were simply rearranged to solve for the length and area for the test conditions. The rearranged equations are shown in Equation 36 and 37. The equations from the urea ice equation was used due to the proper doping in urea ice was more appropriate strength scaling as opposed to synthetic ice that behaves more differently than doped ice. No shape classification was performed on the cusps so only the geometric values of area and length were used in the overall comparison.

$$\mathrm{A} = 0.105 * \left(\frac{h\sigma_f}{\gamma}\right) \tag{36}$$

$$\mathrm{L} = 0.540 * \left(\frac{h\sigma_f}{\gamma}\right)^{\frac{1}{2}} \tag{37}$$

Wang's circle radius approximation was also performed for each cusp based on the local interaction angle and local directional velocity at the contact point and the local directional

velocity. To do this, a MATLAB code takes the known interaction criteria of each cusp formation and calculates the radius as per Equation 38 from combining Equations 13, 14, and 15 and the reverse engineered constant values of C_l and B_e. This equation also modifies the angles to corresponding ship definitions as opposed to the offshore definition used by Wang.

$$R = 0.320\, l_c(1 - 0.144\ \tan\psi \cos\alpha\ V_n) \tag{38}$$

3.4.3 Theoretical Prediction

For the theoretical approximation comparison, the state of the art method of the discretized wedges presented by Li et al (2019) as described in Section 2.2.6.2 is used. A database method was adopted like that of the ABAQUS solution set found in Sawamura (2008) in his integrated model. The Li et al (2019) database used operates on five inputs: the crushing line inclination k, the crushing center location d_c, the wedge angle θ, the crushing depth r_c, and the flare angle ψ.

All these dimensions are measured from the central point of crushing and primarily describing the nature of the interaction between the vessel and the ice sheet. Correspondingly, the database provides five outputs, the first two being the stresses of the maximum stress due to the vertical loading, σ_v, and the horizontal compression stress, σ_h, that combined forms the maximum radial stress, σ_m. The final three outputs are the lengths that represents the geometry of the wedge, based on the max stress line. The three output lengths are the two edge lengths, l_{edge1} and l_{edge2}, as well as the length of the wedge at the center, l_{center}. The database input and output values are summarized in Figure 43. A diagram of all the dimensional parameters in the inputs and outputs are also shown in Figure 44.

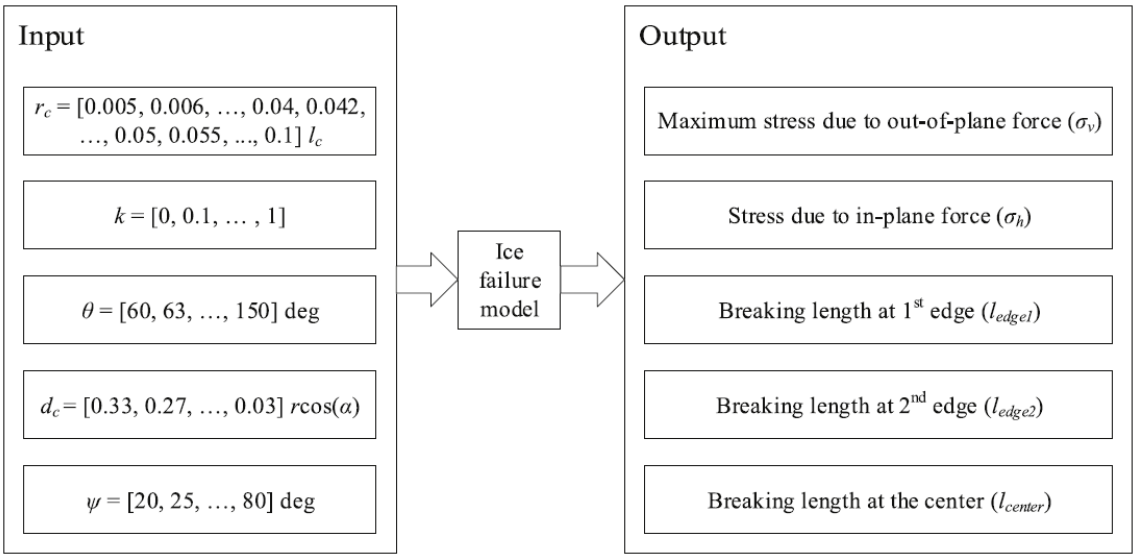

Figure 43. Database inputs and outputs
Source: Li et al '19

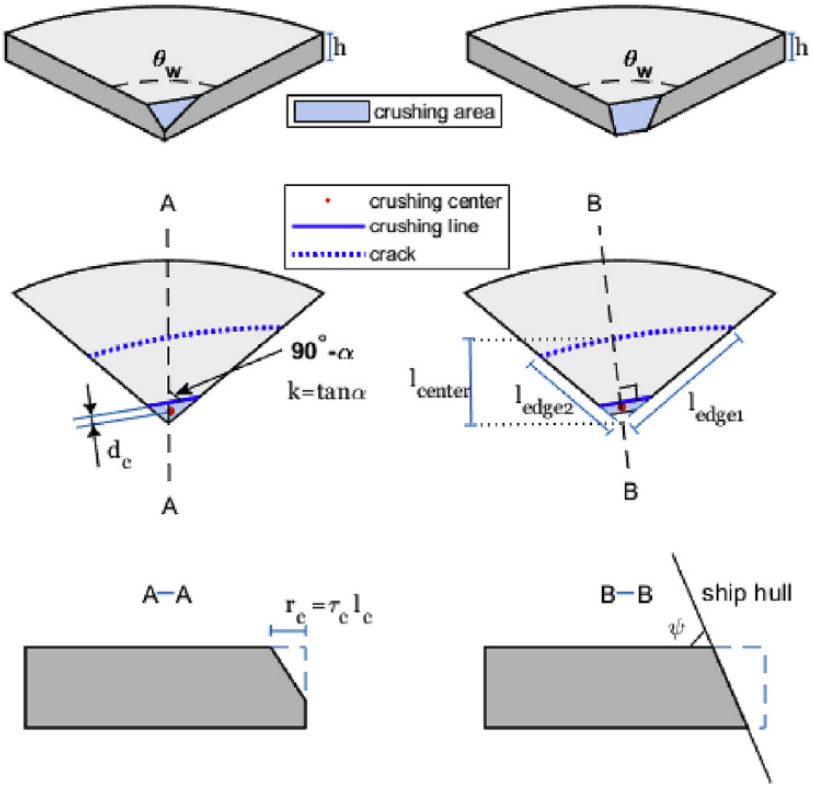

Figure 44. Diagram of ice wedge relevant dimensional parameters
Source: Li et al '19

The last matter of attention concerning the database is the scalability. All the scaling equations use a set of the base reference value that dictate the scaling. The references are the elastic modulus E_{ref}, the reference ice thickness h_{ref}, and the reference crushing strength of

ice $\sigma_{c,ref}$ and they equate to 1GPa, 1m and 1MPa respectively. First, the length values are scaled as per the non-dimensional characteristic length of the wedge. As a result, the scaling of the length can be summarized in Equation 39, where l_{sc} is the scaled length value and l_{db} is the database length value. A version of the database with a non-dimensional length was used, and thus an alternate modification was applied to arrive at the scaled length from the product of the database value and the characteristic length as shown in Equation 40.

$$l_{sc} = l_{db}\left(\frac{E}{E_{ref}}\right)^{0.25}\left(\frac{h}{h_{ref}}\right)^{0.75} \tag{39}$$

$$l_{sc} = l_{db} * l_c \tag{40}$$

The stress scaling additionally includes the scaling from the crushing strength. The vertical stresses is directly related to the crushing strength, while the horizontal stresses is assumed to distributed evenly throughout the area and has additional scaling like the length providing a combined stressed equation as shown in Equation 41.

$$\sigma_m(\theta) = \sigma_{v,db}\left(\frac{E}{E_{ref}}\right)^{0.5}\left(\frac{h}{h_{ref}}\right)^{-0.5}\left(\frac{\sigma_c}{\sigma_{c,ref}}\right) + \sigma_{h,db}\left(\frac{E}{E_{ref}}\right)^{0.25}\left(\frac{h}{h_{ref}}\right)^{-0.25}\left(\frac{\sigma_c}{\sigma_{c,ref}}\right) \tag{41}$$

An assumption was made to simply model the Nevel (1958)'s or Lubbad and Løset (2011) method using Li et al (2019)'s database method. By continuing to assume the zero inclination and symmetrical crushing, and additionally included a consistent crushing area by solving for an equilateral triangle wedge case. Doing so represents the loading scenario from Nevel (1958)'s original method in terms of the resultant radius (and correspondingly would be the same as Lubbad and Løset (2011)'s method). With the given properties, the dependency is just the flare angle of the vessel that varies the crushing radius to solve for a solution that in theory is the same as Nevel (1958)'s.

3.4.4 Dimension Conversion

Various methods provide different outputs such as the radius of the cusp if it was approximated as a circle or a specific length of the cusp. To accommodate this, all prediction methods were converted to the standard length and width values.

Working with radii outputs, the cusp is assumed symmetrical with a contact angle θ and a conversion could be simply approximated as seen by Figure 45 resulting in the conversion equations 42 and 43 using trigonometry. These conversions are used for the conversion from the Izumiyama et al (1992), Wang (2001), and Nevel (1958) radii values to cusp length and width values.

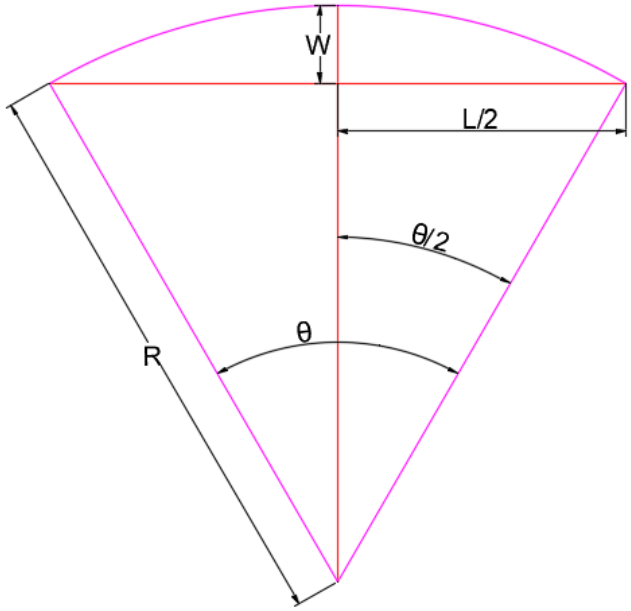

Figure 45. Cusp Radius to Cusp Length/Width Diagram

$$W = R\left(1 - \cos\frac{\theta}{2}\right) \tag{42}$$

$$L = 2R\sin\frac{\theta}{2} \tag{43}$$

The Li et al (2019) database outputs are isolated lengths for a unique output wedge geometry. For simplification purposes, an inclination of the ice cusps of 0 degrees and a triangular crushing zone were assumed such that d_c would always be 33% of r_c. This was the assumption for all the cusp creation cases. The value of r_c was found for when the sum of or σ_m(the

sum of σ_v and σ_h) equaled the flexural strength of the ice. Knowing the symmetrical nature, a similar conversion mechanism as the radius was developed but modified, as the center length would be different from the edge lengths. This is demonstrated in Figure 46 and summarized in Equations 44, 45, and 46.

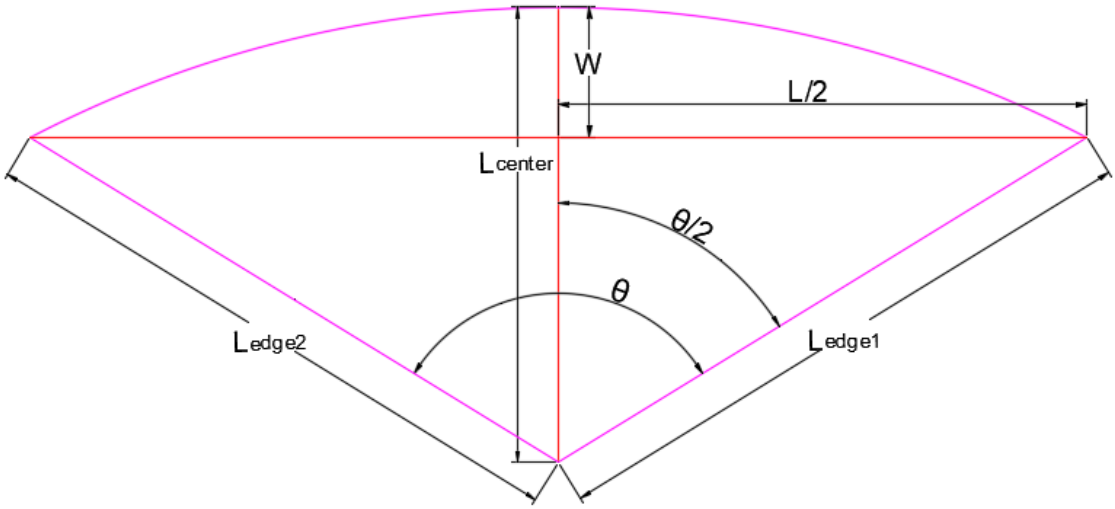

Figure 46. Cusp Radius to Cusp Length/Width Diagram

$$L_{edge} = L_{edge1} = L_{edge2} \tag{44}$$

$$W = L_{center} - L_{edge} \cos\frac{\theta}{2} \tag{45}$$

$$L = 2L_{edge} \sin\frac{\theta}{2} \tag{46}$$

4 Results and Discussions

4.1 Results and Observations

The tests performed were intended to be a recreation of the original test set from the Garvin (2003) experiments. As best as the test conditions were to be to the original, primarily the thickness matched the original test. The various strengths were higher in the new test and the modulus of elasticity was lower than the original. Overall, the ice was harder and more rigid than the original test, but the test was still carried out, but the results were not expected to be exactly as the same as the original. The test ice properties showed alongside the intended original Garvin (2003) test ice properties are shown in Table 8.

Table 8. Test and Original Garvin Ice Property Values

ICE PROPERTY		TEST VALUE	GARVIN VALUE
Thickness	**(m)**	0.028	0.028
Ice Density (Assumed)	**(kg/m^3)**	900	900
Flexural Strength	**(kPa)**	45	31.9
Compressive Strength	**(kPa)**	108	66.3
Modulus of Elasticity	**(MPa)**	14.8	29.4
Specific Weight of Water	**(N/m^3)**	9810	9810
Poisson Ratio of Ice (Assumed)		0.3	0.3
Characteristic Length	**(m)**	0.023	0.028

In regards to the cusp dimensions that were measured from the video and image analysis of the two speeds, Table 9 summarizes the result with the average area, length and area correspondingly for both test speeds and a corresponding direct full-scale value of the scaled geometric values and scaled velocity. The values were scaled directly with the geometric scaling factor and the velocity as per Froude scaling of the velocity.

Table 9. Cusp Geometry Results

		MS		FS	
Cusp Geometry		**V=0.162m/s**	**V=0.270m/s**	**V=1.77knots**	**V=2.95knots**
Area Mean	**(m^2)**	0.0208	0.0171	20.7	17.0
Area Mean Multiple	**(m^2)**	0.0543	0.0384	54.1	38.2
Area Mean Single	**(m^2)**	0.0074	0.0055	7.37	5.48
Length Mean	**(m)**	0.276	0.258	8.69	8.15
Length Mean Multiple	**(m)**	0.536	0.465	16.91	14.67
Length Mean Single	**(m)**	0.171	0.145	5.40	4.58
Width Mean	**(m)**	0.086	0.078	2.71	2.46
Width Mean Multiple	**(m)**	0.145	0.119	4.57	3.76
Width Mean Single	**(m)**	0.062	0.059	1.97	1.87

With the test area, length, and width values from the tests as shown from Table 9, it is evident that the speed reduces the size of the cusp. In every dimension, regardless of contact type, the size of the cusps decreased with speed. This agreement from this widely accepted idea was expected. Tests were not performed with looking at ice thickness variation, thus no test based reconfirmation of that theory could be performed from this paper.

4.2 Single vs Multiple Contact

This work performs one of the first examinations into the variation of contact types in the matter of cusp formations, according to the knowledge of the author. Very evidently from quick examinations of Figure 9 that dimensions are universally larger for the multiple contact point cusps than the single contact cusps. The points of multiple contact are usually along the length and thus easily make the cusps naturally long encompassing all contact points in generating the cusp. Additionally, the width grows as well as the multiple contact decreases the line load and correspondingly the load rate. The nature of this slower bending

result in the large cusps. Additionally, it is also worthwhile to observe the length-width ratio for the different contact types of the cusps and can be seen in Table 10. The length over width ratio is larger in the multiple contact cusps than the single contact cusps. This relation makes sense in agreement with the hypothesis regarding the contact length and line load on the ice sheet. An interesting phenomenon from the data is that the multiple contact ratio seems to increase with speed. This may correlate with the loading rate increasing with the increased speed. The bending rate would also increase and thus reduce the width of the cusp more, relative to the lower speed. This hypothesis could also be supported from the significantly less decline of the cusp width in single contact cusps as see on Table 9.

Table 10. Length/Width Ratio for different contact types

h=0.028m	**MS**	
Length/Width Ratio	**V=0.162m/s**	**V=0.270m/s**
Length/Width	3.21	3.31
Length/Width Multiple	3.70	3.91
Length/Width Single	2.75	2.45

The length/width ratio for single contact decreases, a possible explanation for this is the change of contact type as the speed increases. Conditions that would result in longer single contact cusps (large contact entrance angles that generally take longer to fail than small contact entrance angles that result in high local pressures) may be taken over by the multiple contact cusps. Such a conclusion requires looking at the variation in the total interaction between the two speeds and contact types; this is shown in Table 11 and Table 12. Here it is evident that in terms of the number of cusps, the single cusps are dominant in the interaction type encompassing approximately two-thirds of the interaction counts. The interaction count also clearly decreases for the single contact and increases for the multiple contact, potentially demonstrating a shift of normally single contact cusp failures to multiple contact failures. Another thing worth mentioning is the amount of broken ice area (represented by the sum of

all the cusp areas). The decline in the total area of cusps is expected as all the major dimensions are decreasing. However, it is also evident that most of the ice that was broken are from multiple contact failures despite representing a smaller fraction of the interactions compared to the single contacts. With more of the area broken as multiple contact cusps, potentially demonstrating that overall the multiple contact cusp failures become more prevalent with higher speeds and potentially linking with the condition shift hypothesis. Such observations were not completed with the current observation system to see the contact angles of the contact points in multiple contact cusps.

Table 11. Cusp count and area for v=0.162m/s

V=0.162M/S

Cusp Contact Type	Count	Count %	Area (m^2)	Area %
All Contact	507	100 %	10.55	100 %
Multiple Contact	145	29 %	7.88	75 %
Single Contact	362	71 %	2.68	25 %

Table 12. Cusp count and area for v=0.270m/s

V=0.270M/S

Cusp Contact Type	Count	Count %	Area (m^2)	Area %
All Contact	557	100 %	9.55	100 %
Multiple Contact	197	35 %	7.56	79 %
Single Contact	360	65 %	1.98	21 %

Due to the variation in the cusps, methods of approximation may only approximate a portion of the ice cusp geometries. It becomes thus important to assess the different prediction methods and to compare each type of cusp that is formed to get a stronger idea of which methods would come better.

4.3 Prediction Method Comparison

The various geometric values for each contact type were compared between the actual measured values and the theoretical calculated values are summarized in Tables 10, 11, and 12 for the 0.162m/s speed and in Table 13, 14, and 15 for the 0.270m/s speed with each corresponding table representing the single, multiple, and all contact types. The values listed are the mean values and corresponding relative difference from the experimental results. Many of the methods could be calculated for each interaction (determined from the contact information, such as local modifications based on a calculated radii) while some methods find general averages based on the ice properties and thus would not have any standard deviations. The formulation of these values were completed primarily with MATLAB, and alarger table containing all key calculation parameters in the calculations could be found in Appendix A.

Table 13. Cusp Geometrical Comparison – V=0.162m/s – Single Contact

Single Contacts	**(m)**	**%**	**(m)**	**%**	**(m^2)**	**%**
V=0.162m/s	**Length**	**Rel. Dif**	**Width**	**Rel. Dif**	**Area**	**Rel. Dif**
Actual	0.1712	0%	0.0623	0%	0.0074	0%
McKindra and Lutton	0.2873	68%	-	-	-	-
Izumiyama	0.6298	268%	0.2248	261%	-	-
Kostras	0.2421	41%	0.0720	16%	-	-
Tatinclaux	-	-	0.1935	211%	0.0135	82%
Wang	0.1389	19%	0.0496	20%	-	-
Nevel	0.1351	21%	0.0482	23%	-	-
Li	0.2229	30%	0.0383	39%	-	-
Erceg (Alt. Conditions)	0.2111	23%	0.1167	87%	-	-

Table 14. Cusp Geometrical Comparison – V=0.162m/s – Multiple Contact

Multiple Contacts	**(m)**	**%**	**(m)**	**%**	**(m^2)**	**%**
V=0.162m/s	**Length**	**Rel. Dif**	**Width**	**Rel. Dif**	**Area**	**Rel. Dif**
Actual	0.5359	0%	0.1447	0%	0.0543	0%
McKindra and Lutton	0.2873	46%	-	-	-	-
Izumiyama	0.6480	21%	0.2479	71%	-	-
Kostras	0.2321	57%	0.0690	52%	-	-
Tatinclaux	-	-	0.1935	34%	0.0135	75%
Wang	0.1429	73%	0.0547	62%	-	-
Nevel	0.1389	74%	0.0531	63%	-	-
Li	0.2398	55%	0.0419	71%	-	-
Erceg (Alt. Conditions)	0.2111	61%	0.1167	19%	-	-

Table 15. Cusp Geometrical Comparison – V=0.162m/s – All Contact

All	**(m)**	**%**	**(m)**	**%**	**(m^2)**	**%**
V=0.162m/s	**Length**	**Rel. Dif**	**Width**	**Rel. Dif**	**Area**	**Rel. Dif**
Actual	0.2755	0%	0.0858	0%	0.0208	0%
McKindra and Lutton	0.2873	4%	-	-	-	-
Izumiyama	0.6350	130%	0.2314	170%	-	-
Kostras	0.2392	13%	0.0711	17%	-	-
Tatinclaux	-	-	0.1935	126%	0.0135	35%
Wang	0.1401	49%	0.0510	41%	-	-
Nevel	0.1362	51%	0.0496	42%	-	-
Li	0.2277	17%	0.0393	54%	-	-
Erceg (Alt. Conditions)	0.2111	23%	0.1167	36%	-	-

Table 16. Cusp Geometrical Comparison – V=0.270m/s – Single Contact

Single Contacts	**(m)**	**%**	**(m)**	**%**	**(m^2)**	**%**
V=0.270m/s	**Length**	**Rel. Dif**	**Width**	**Rel. Dif**	**Area**	**Rel. Dif**
Actual	0.1452	0%	0.0593	0%	0.0055	0%
McKindra and Lutton	0.2833	95%	-	-	-	-
Izumiyama	0.6189	326%	0.2148	262%	-	-
Kostras	0.2293	58%	0.0682	15%	-	-
Tatinclaux	-	-	0.1935	226%	0.0135	145%
Wang	0.1354	7%	0.0470	21%	-	-
Nevel	0.1330	8%	0.0461	22%	-	-
Li	0.2157	49%	0.0367	38%	-	-
Erceg (Alt. Conditions)	0.2111	45%	0.1167	97%	-	-

Table 17. Cusp Geometrical Comparison – V=0.270m/s – Multiple Contact

Multiple Contacts	**(m)**	**%**	**(m)**	**%**	**(m^2)**	**%**
V=0.270m/s	**Length**	**Rel. Dif**	**Width**	**Rel. Dif**	**Area**	**Rel. Dif**
Actual	0.4647	0%	0.1119	0%	0.0384	0%
McKindra and Lutton	0.2833	39%	-	-	-	-
Izumiyama	0.6476	39%	0.2473	121%	-	-
Kostras	0.2129	54%	0.0633	43%	-	-
Tatinclaux	-	-	0.1935	73%	0.0135	65%
Wang	0.1416	70%	0.0541	52%	-	-
Nevel	0.1388	70%	0.0461	53%	-	-
Li	0.2394	48%	0.0418	63%	-	-
Erceg (Alt. Conditions)	0.2111	55%	0.1167	4%	-	-

Table 18. Cusp Geometrical Comparison – V=0.270m/s – All Contact

All	(m)	%	(m)	%	(m^2)	%
V=0.270m/s	**Length**	**Rel. Dif**	**Width**	**Rel. Dif**	**Area**	**Rel. Dif**
Actual	0.2582	0%	0.0779	0%	0.0171	0%
McKindra and Lutton	0.2833	10%	-	-	-	-
Izumiyama	0.6291	144%	0.2263	191%	-	-
Kostras	0.2235	13%	0.0664	15%	-	-
Tatinclaux	-	-	0.1935	148%	0.0135	21%
Wang	0.1376	47%	0.0495	36%	-	-
Nevel	0.1350	48%	0.0486	38%	-	-
Li	0.2241	13%	0.0385	54%	-	-
Erceg (Alt. Conditions)	0.2111	18%	0.1167	50%	-	-

Starting from the statistical methods, McKindra and Lutton (1981)'s full-scale statistics works primarily with the length of the cusp and their study made no differentiation with contact type, and is thus best compared with all the contact type data. Overall, the average value provided from McKindra and Lutton (1981) provides a strong similarity to the mean values for both speeds but seems to be ideal at only lower speeds as the deviation increases from the test values with increased speed.

Izumiyama et al (1992)'s model scale normal distribution was an extremely poor fit to the data, even though the data source was also in model scale. There are also additional differences such that the origin of the method was for cone structure with an inclined angle of 60 degrees from the horizontal breaking upward. The nature of cone interact failure typically would imply a single contact failure, but the dimensions are much too large compared to the

single contact ice. The method also operates in the model scale stiffness strength regime. Nevertheless, the dimensions of both the length and the width calculated from his method were much too large and outside the range of all the other methods as well.

Examining Kostras et al (1983) full-scale derived values in comparison to the measured values, there is a reasonable comparability between the two. Similarly, Kostras et al (1983) did not make any single contact or multiple contact differentiation and thus the Kostras et al (1983) values should only be compared with all contact type values. The width values were calculated from the original equation and the length value is derived from a scaled down thickness dependent ratio value. Overall, this state of the equation gave good values compared to the measured although the values slightly under predict the cusp values.

Tatinclaux (1985)'s model-scale shape equations also seem to over predict the geometric values measured from the test. The value is not speed dependent and overpredicts the length of all the cusps for all contact types. Nevertheless, the equation is too rigid and not able to account for the large variations in the average area based on differences in the test conditions. This method also operates in the model scale stiffness strength regime. Really intended to only be compared to all contact types due to no differentiation in the original study, the area is still underpredicted and the length is overpredicted. This gives concerns that the original tests perhaps gave much narrow cusps in comparison to the tests performed.

Wang (2001)'s full-scale approximation method slightly underpredicts the cusp geometries. The values calculated are much closer to single contact cusp values. This would make sense as the equations were theoretically derived from cusps formed from a cone structure (although the data was fitted from ships). Wang (2001)'s equation is one of the only ones that is speed dependent, but the equation appears it may be more accurate at a medium speed of icebreaking than the ones tested. Nevertheless, the value is quite close to the tested.

The Nevel (1958)'s method is rather limited but should only be applied to the single contact at low speeds, particularly strongest in the width that is least affected by the speed and hydrodynamics of the vessel. Strangely it seemed to reach its best accuracy at the higher speed for the length (and finds values very similar to Wang (2001)'s value). The main variation factor applied here is the flare angle and thus little variation is available regarding the type of interaction occurring from the vessel. Nevertheless, in a static case it represents a value of the ice bearing capacity and can serve as a good comparison reference value.

Li et al (2019)'s purely theoretical method does also reasonable job of approximating the single cusp value. The theory is purely for single contact and over predicts the length of the cusp and underpredicts the width of the cusp. With the measured large entrance angles that may have some uncertainty from the measurements, it results in the large length over width ratios that may stretch the length longer and width shorter. Overall, it does a considerable job in approximating without taking empirical values. The theoretical method has no accounts for speed and as speed naturally reduces the size of the cusps. The method by Li et al (2019) also focuses more on an elliptical shape, and with converting the measured values back into the edge and center lengths the circularity of the cusps could be assessed. A ratio of the edge length over the center length is thus assessed as shown in Figure 47 and Figure 48 for the slower speed and faster speed respectively. Based on the figures it can be seen the ice is certainly slightly elliptical, Li et al (2019)'s method is able to capture the general most frequent ratios in the single contact cusps. Values of L_{edge}/L_{center} close to 1 represent circular cusps, and higher values represent a longer cusp as opposed to the lower values representing wider cusps. L_{edge} from the measured is the average value of the two edges measured and L_{center} in this case is the same as the width of the cusp. Thus the figures demonstrate the method is able to capture a reasonable amount of the elliptical nature of he ice.

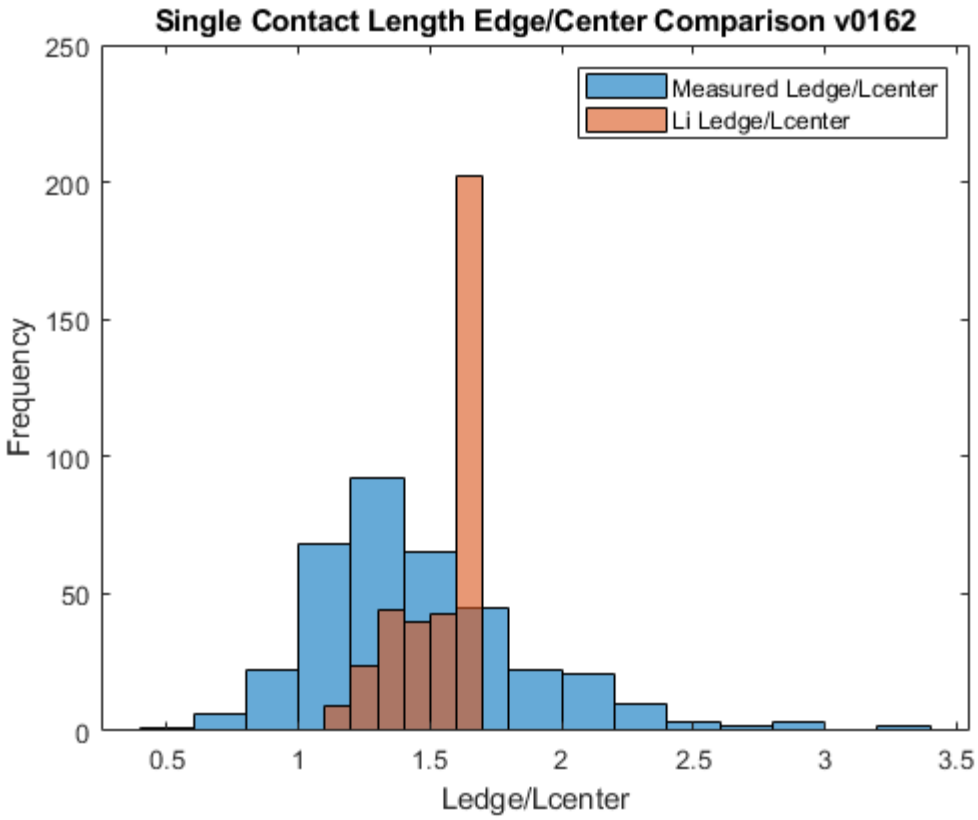

Figure 47. Single Contact Length Edge/Center Comparison for V=0.162m/s

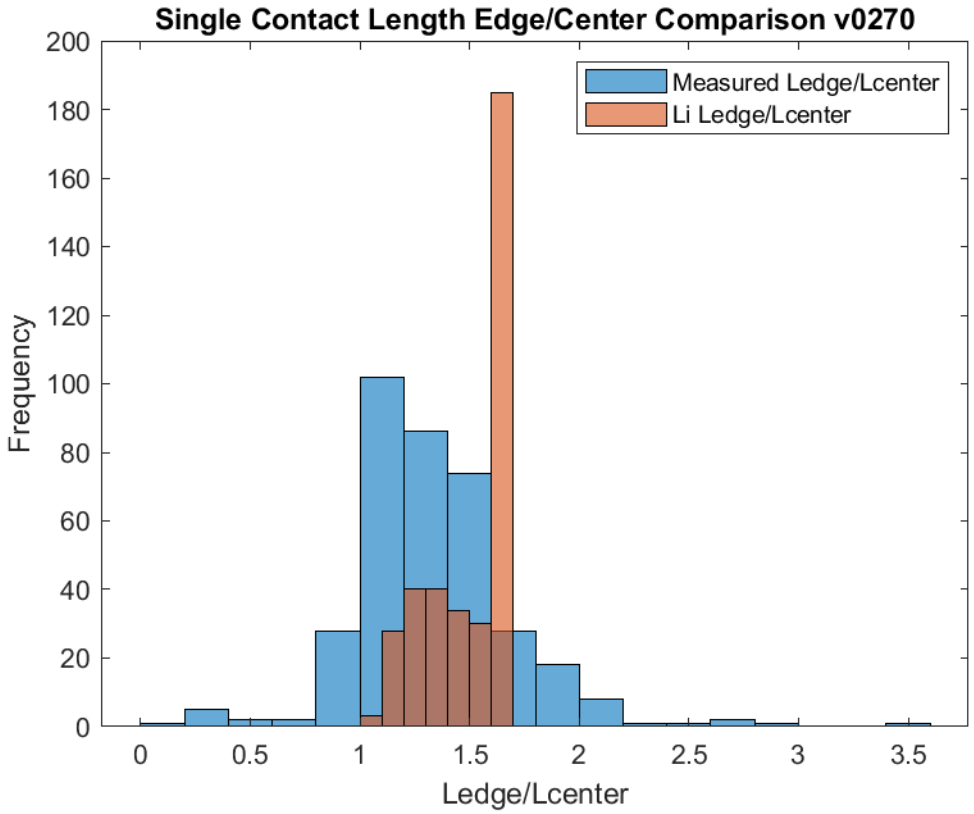

Figure 48. Single Contact Length Edge/Center Comparison for V=0.270m/s

Lastly, the value from Erceg et al (2015)'s plot of the MT *Uikku* simulated full-scale ice-breaking in 0.5m, 500kPa ice provides a reasonable mid-ground value to compare the values to. The contact type is not considered with Erceg's method, but it does a reasonable job in approximating a reasonable value for the cusp length but generally overpredicts the cusp width. The Erceg values are not intended to be comparable as the test conditions are quite different, but it gives another value regarding the current state of cusp calculation methods. Overall, looking at all the comparable methods it appears that the values calculated from full-scale data or on pure theory does a much better job in predicting the cusp values from the test than any of the model-scale derived methods. This is an interesting phenomenon and raises some potential regarding if the Aalto model scale ice does a uniquely good job in developing comparable cusp sizes. All the model scale methods are based on the strength regime and all the methods based on the elastic regime is more accurate. It is typically common with the lower ratios of ice properties that ice would lie in the strength regime as opposed to the elastic regime. This conclusion may support that with the elastic assumption that the ice cusp is very much scalable to full scale. This is interesting as well as the ice in the ice tank was found to be very inelastic as well (von Bock und Polach 2016). However, without any full scale cusp data from the MT *Uikku* there is currently no way to tell how well the comparability is but so far the past works of full scale equations all seem to do more or less a reasonable job in getting a reasonable approximation of the geometric cusp values.

4.4 Scalability

Looking at the scalability of the cusp, the reasonability of the scaled values must be assessed. The properties of the ice are rather unusual compared to typically seen field values of ice properties when scaled. The flexural strength of the ice was rather high when scaled to full scale, and the modulus of elasticity of the ice is very low as well. Returning to Yean et al (1981)'s criterion regarding the elastic and strength regime we can properly understand the ratio between the flexural strength and the elastic modulus. For low modulus over strength ratios, we see that the strength of the ice dominates the nature of cusp formation. Specifically, in this case the ratio E/σ_f is only approximately two times $\sigma_f/\gamma h$ and thus strongly fits in the strength dominancy regime. This regime is typically common in model scale due to various ratios of ice properties making it different from the full scale that operates more in the elastic regime. Accepting this regime and that the strength is abnormally high, the ice is thus expected to be larger as the strength of the ice is exceptionally high. However, the results seem to show the opposite phenomenon as all the elastic based methods scale much better to the ice properties than do the strength based. Regardless of the scale origin, the elastic methods scaled best and thus presents the possibility that scaling is quite possible with cusps under a standard elastic regime.

Another method to assess the scalability is to look at the dimension over thickness ratio and compare it to Keinonen (1983)'s initial investigation of cusp dimension ratios being in the range of 3-6 times the thickness in model scale and 0.5-2 times the thickness in full scale. Table 19 shows the ratio of the measured dimension over the thickness for each contact type. It can be assumed that Keinonen (1983)'s observation dimension would have been the width as it is also the most easily measurable in full-scale observations, despite no clear clarification in the original paper. Nevertheless, the values fit moderately in the upper end of that

range for the single contact width ratios and raises some concerns potentially regarding the type of contact in full scale as opposed to model scale.

Table 19. Dimension/Thickness Ratios

h=0.028m	MS	
Dimension/Thickness Ratio	**V=0.162m/s**	**V=0.270m/s**
Length Mean	9.84	9.22
Length Mean Multiple	19.14	16.60
Length Mean Single	6.11	5.19
Width Mean	3.06	2.78
Width Mean Multiple	5.17	4.25
Width Mean Single	2.23	2.12

4.5 Icebreaking Pattern

After the model tests, the model was reversed to reveal the icebreaking pattern of the models at each speed. The icebreaking patterns were photographed, and sketches were created of the patterns for simplification purposes in eliminating the re-broken ice cusps and creating additional labelling. The sketch of the icebreaking pattern for the two speeds is shown in Figure 49 and Figure 50. The black line represents the primary or circumferential cracks formed, the red lines represent radial cracks, and the green line represents the centerline of the model extended onto the ice. The black hatching was the model in the photograph.

In agreement of the many other previous conclusions, a few observations could be found. First is that many of the cusps in the higher speed are general smaller and feel to have a higher length over width ratio with many being rather narrow. This fits some of the conclusions stated in sections 4.1 and 4.2 (with exceptions to the conditional failure type shift, as the diagrams does not really provide information on failure conditions). Additionally, the 0.162m/s exhibit a breaking pattern more similar to the type A Yamaguchi et al (1997) conventional icebreaking pattern of longer arching cusps in the pattern while the 0.270m/s speed

exhibit a breaking pattern more similar to the type B Yamaguchi et al (1997) spoon icebreaking pattern with cusps being more circular and bar like. Even though the hull is the same, there is potential a change in the type of contact or failure mechanism that changes the overall nature of the icebreaking pattern. Both speeds still fit in the low speed regime and qualify for low speed analysis. Nevertheless, further observations could be done with icebreaking patterns with more testing and comparisons. The original photographs of the icebreaking patterns could be seen in Appendix B.

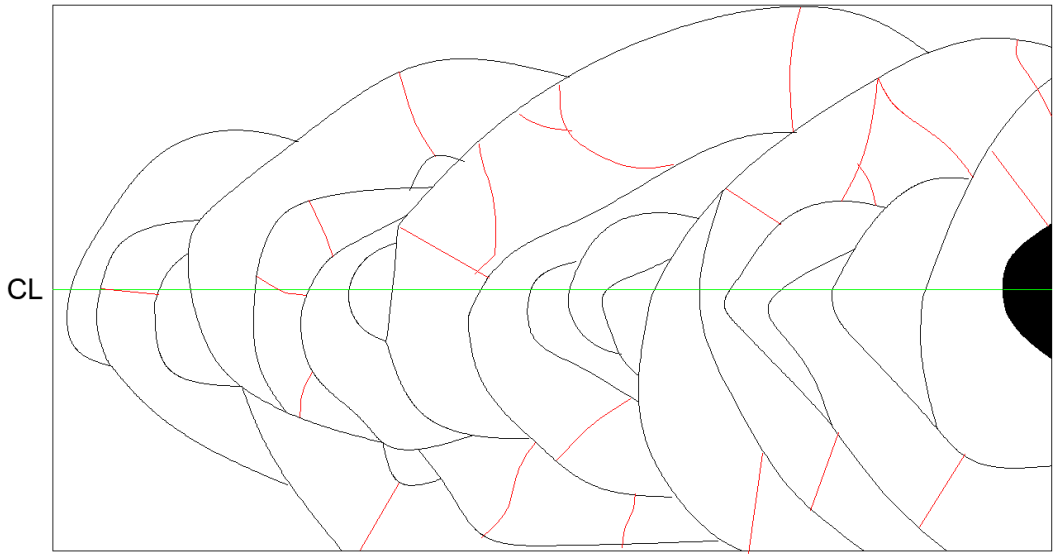

Figure 49. MT *Uikku* model scale icebreaking pattern for 0.162m/s speed

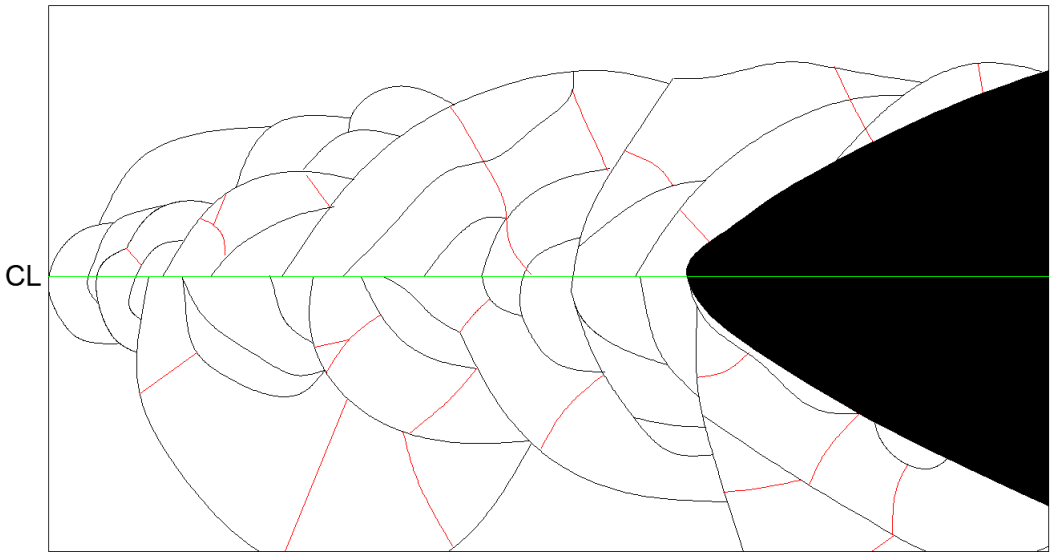

Figure 50. MT *Uikku* model scale icebreaking pattern for 0.270m/s speed

4.6 Distribution Fitting

With so many cusps that were analyzed, a distribution was thought to be best to represent the general large data set for the geometric properties. The distribution selected was the lognormal distribution as per the work from McKindra and Lutton (1981) who performed fittings for cusp geometry as well. A lognormal fit distribution was then automatically fitted using MATLAB's automatic distribution fitting to the measured data. The lognormal distribution proved to be a strong fit for the data as shown by an example figure with a strong fit in Figure 51 where the distribution is shown with a histogram to demonstrate the wellness of the fit. The figure shows the distribution for single contact cusp lengths and the distribution represents the data quite well. Generally, the area, length, and width of the cusps fit quite well within a lognormal distribution.

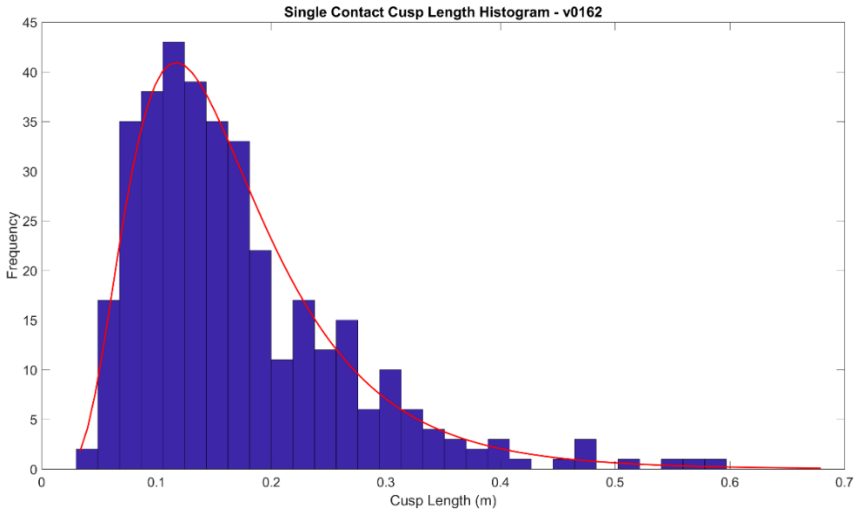

Figure 51. Single contact cusp length histogram and distribution for V=0.162m/s

The distribution works less optimally with multiple contact cusps as the values are less concentrated and can appear more spread out as shown in Figure 52. This fit is one of the poorer fits to the data of all the distributions but still does a reasonable job at representing the data. The multiple contact cusp also contains a smaller sample size compared to the single contact and thus more data would improve the distribution. A table summary of all the generated

distributions parameters (the lognormal parameters) and a goodness of fit values are displayed in Table 20. The values mu and sigma are essential the mean and standard deviation from Table 9 undergone a standard log transformation to the lognormal values for the distribution. The test statistic value as per the chi squared goodness of fit value is included where a lower value designate a stronger fit. All the distributions with histograms are shown in Appendix C.

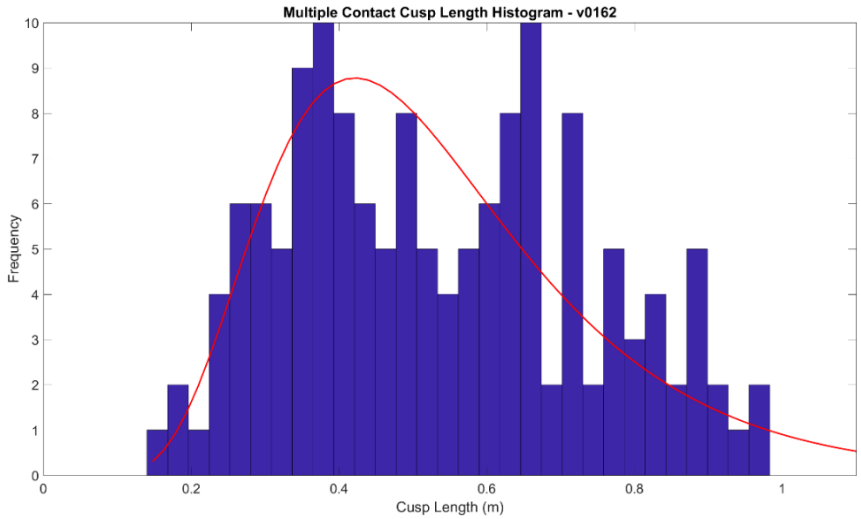

Figure 52. Multiple contact cusp length histogram and distribution for V=0.162m/s

Table 20. Lognormal distribution values for the cusp geometric properties

	V=0.162m/s			V=0.270m/s		
Distribution Values	**mu**	**sigma**	**chi² test statistic**	**mu**	**sigma**	**chi² test statistic**
Length Single Contact	-1.893	0.502	3.1	-2.025	0.435	2.20
Length Multiple Contact	-0.700	0.405	16.6	-0.864	0.450	5.68
Length All Contact	-1.552	0.719	36.3	-1.614	0.708	26.23
Width Single Contact	-2.873	0.433	11.7	-2.886	0.332	12.00
Width Multiple Contact	-2.015	0.414	10.1	-2.252	0.358	3.39
Width All Contact	-2.628	0.578	24.6	-2.662	0.456	19.90
Area Single Contact	-5.348	0.913	7.9	-5.478	0.714	10.89
Area Multiple Contact	-3.161	0.744	6.2	-3.535	0.753	2.83
Area All Contact	-4.722	1.316	18.7	-4.791	1.181	9.49

Additionally, a brief analysis was completed with looking at comparing the distributions of the various prediction methods and the measured. Of course, the distributions would not match incredibly well as the equations take one average properties value and applies it to the all cusps and most have unique slight variations that make them unique. Overall, it presents that the equations can place themselves quite well within the range of the data set and for best seeing the validity of the mean value for comparisons. The prediction to actual measured geometry values histograms are shown in Appendix C.5. The only method distributions compared were Kostras et al (1983), Wang (2001), and Li et al (2019) as those three allowed for values to be calculated for each cusp contact conditions uniquely as well as values that were close enough to the measured to be considered reasonable for comparison. These values are only theoretically valid for single contact cusps and thus the distributions are only comparable with single contact cusps. Thus, the appendix only compares values for single contact cusps.

5 Conclusion

In conclusion, the model tests were slightly difference than the intended tests from the start of the work but work still moved on to analyze the cusps as best as possible. The process was still successful, as a method was developed to analyze cusps with relative simplicity, and then to then compile, process, and analyze the data. A mounting system was built on the model of the MT *Uikku* to allow for further testing and the installation method could be a starting point for future improved installations for cusp analysis. The shadow of the model should be considered in future testing to reduce the amount of light adjustment required in post-processing. A light should be mounted at an angle to illuminate the cusp formation zone but prevent direct reflection of the light directly at the camera from the ice. A better system would also be to use only one camera instead of combining the perspective of two cameras. This method would require more post processing to adjust the perspective of a flat layer, but it is doable. This would allow for a greater field of visions and saves trouble and potential difficulty from a two-camera perspective. A detection method of the cusps could also be developed to avoid the manual labor in analyzing all the frames from the video. An edge detection method could be used to determine automatically the boundaries of the cusps on the ice sheet. This edge detection method becomes difficult with overlapping cameras and the poor lighting situation in the tests performed. This could also help when looking at more complicated contact conditions potentially extracting multiple contact point conditions that would be useful in understanding the dynamic types of interactions that occur over the course of the icebreaking. The addition of also being able to obtain local ice load measurements would be extremely helpful in further developing an understanding of ice cusp formations. The local stresses and time series relation with ice cusp formation can give significant addition detail of the how the ice is loaded on the ship and give a stronger idea of the cyclical nature of the formations.

Beyond the methodology, it was very interesting that out of all the prediction methods, the theoretical and full-scale methods seem to provide the best approximation of the cusp dimensions. This was unexpected as the nature of them may be more far away from model scale testing. The dimension over thickness ratios are still rather high to be comparable to full scale but the predictive methods derived from them seem to show a good fit. This raises some potentials about the viability of proper scaling from model scale to full scale. The main concern is potentially questioning the validity in Yean et al (1981)'s criterion regarding the importance of strength or the elastic modulus, as the characteristic length had a considerable relation to the thickness of the ice than the strength relation in this case. This was also very unexpected as the ice from the Aalto Ice Tank was found to be very inelastic (von Bock und Polahc 2016). Nevertheless, despite this, the ice can be modeled elastically at least in the manner of cusp formation from full scale and the previous approaches from the criterion had created some over-approximations. Additionally, the theory may not be valid for this case due to the cusp like failure as opposed to the beam like failure of Yean et al (1981)'s concerns, and the unusual cases of emersion from the water during the upward bending that may explain the inapplicability of this in ship ice pattern formation. Overall, the testing performed was very limited and much more data will be needed to truly understand the scaling of cusps and icebreaking pattern geometries.

The testing was successful in affirming the speed dependency on cusp geometry, but thickness dependency tests were not carried out so no affirmation of that is performed besides theoretical support from this study. Another success from the testing was the observations and differentiation between the single and multiple contact conditions for the cusp formations. This clearly told that many of the larger cusp experience multiple contact points with the hull and likely then a longer loading. The long bending resulted in a larger cusp that

is different from the single point high-pressure cusps. The multiple contact point cusps dominated the area of the ice that was broken, and the single contact points dominated the interaction count. The nature of this phenomenon needs to be investigated further in full-scale to deem if this matter of contact information is important in large scale or if a different phenomenon takes over in full scale past a certain criterion. Nevertheless, in model scale, these dominant multiple contact cusps could explain why cusps historically in model scale have been recorded to be so much larger than the ones observed in full scale. The multiple point contact cusp formation can be understood in a larger scale sense that they reduce the likelihood of crushing involved with each cusp formation due to the longer load length or as a design intention to maximize that most of the ice fails through bending as opposed to crushing in the single contact cusps.

Lastly, a pleasant conclusion is the fitting of the lognormal distributions to the cusps seem to be a strong a fit to the data. In support of the full-scale distribution fitting from McKindra and Lutton (1981), there is at least a similarity in the distribution nature from model scale to full scale. The distributions are also a strong way to represent the data and the general icebreaking nature of the model in a certain condition and perhaps there is some potential that these distributions could be useful in the future understanding of icebreaking patterns.

Overall, the two tests serve as a limited data set to make major conclusions. The ice was still rather unusual due to the layer, property, elasticity abnormalities. Nevertheless, the testing still gave reasonable results. Further testing in model scale and especially in full scale is needed to gather a stronger knowledge of cusp formations and icebreaking pattern. This study serves as an update on the state of the art on the matter, at least to the knowledge of the author, and further work could be done with now ever coming modern tools to assist in the developing a strong understanding of the nature of icebreaking.

6 Bibliography

Aamot, S. K., 2015. *A Sensitivity Study of Ice Resistance Prediction Methods Using a Developed Bow Shape Modelling Tool,* Trondheim, Norway: NTNU.

ARCDEV, 1988. *Final Public Report of the ARCDEV Project,* s.l.: s.n.

Daley, C., 1992. *Aspects of Ship-Ice Interaction in a Natural Ice Cover, M-120,* Otaniemi, Espoo, Finland: Helsinki University of Technology.

Enkvist, E., 1972. *On the ice resistance encountered by ships operating in the continuous mode of icebreaking.* Helsinki: The Swedish Academy of Engineering Sciences in Finland.

Erceg, S. & Ehlers, S., 2014. *A Numerical Model to Initiate the Icebreaking Pattern in Level Ice.* San Francisco, California, USA, Proceedings of the ASME 2014 33rd International Conference on Ocean, Offshore and Arctic Engineering, OMAE2014.

Ettema, R., Stern, F. & Lazaro, J., 1987. *Dynamics of Continuous-Mode Icebreaking by a Polar-Class Icebreaker Hull ,* Iowa City, Iowa, USA: US Department of Transporation Maritime Administration.

Garvin, M., 2003. *Model Tests of MT Uikku in Level Ice and in Brash Ice, S-3,* Espoo, Finland: Helsinki University of Technology.

Izumiyama, K., Kitagawa, H., Koyama, K. & Uto, S., 1992. *A numerical simulation of ice-cone interaction.* Banff, Alberta, IAHR.

Keinonen, A., 1983. *Major scaling problems with ice model testing of ships.* Hoboken, New Jersey, USA, s.n., pp. 595-612.

Kerr, A. D., 1976. The Bearing Capacity of Floating Ice Plates Subjected to Static or Quasi-Static Loads. *Journal of Glaciology,* 17(76), pp. 229-268.

Kostras, T., Baird, A. & Naegle, J., 1983. Predicting Ship Performance in Level Ice. *SNAME Transactions Vol 91,* pp. 329-349.

Külaots, R., 2012. *Numerical and experimental modelling of ship resistance in compressive ice channels,* Espoo, Finland: Aalto University.

Li, F., Kotilainen, M., Goerlandt, F. & Kujala, P., 2019. An extended ice failure model to improve the fidelity of icebreaking pattern. *Ocean Engineering 176,* pp. 169-183.

Lindqvist, G., 1989. A straightforward method for calculation of ice resistance of ships. *Port and Ocean Engineering Under Arctic Conditions,* pp. 722-735.

Lindstrom, C. A., 1990. *Numerical Estimation of Ice Forces Acting on Inclined Structures and Ships in Level Ice.* Houston, Texas, OTC.

Liu, J., Lau, M. & Williams, F. M., 2006. *Mathematical Modeling of Ice-Hull Interaction for Ship Maneuvering in Ice Simulations.* Banff, Alberta, Canada, s.n.

Lubbad, R. & Sveinung, L., 2011. A numerical model for real-time simulation of ship-ice interaction. *Cold Regions Science and Technology,* Issue 65, pp. 111-127.

Mckindra, C. & Lutton, T., 1981. *Statistical analysis of broken ice dimensions generated during 140' WTGB icebreaking trials,* Washington, D.C., USA: United States Coast Guard.

Myland, D. & Ehlers, S., 2014. *Theoretical Investigation on Ice Resistance Prediction Methods for Ships in Level Ice.* San Francisco, California, USA, ASME.

Nevel, D. E., 1958. *The Narrow Infinite Wedge on an Elastic Foundation,* Wilmette, Illinois, USA: U.S. Army Snow Ice and Permafrost Research Establishment - Corps of Engineers.

Nevel, D. E., 1961. *The Narrow Free Infinite Wedge on an Elastic Foundation,* Hanover, New Hampshire, USA: U.S. Army Cold Regions Research and Engineering Laboratory - Corps of Engineers.

Rodenheber, A., 2002. *Open water resistance and propeller test for MT Uikku,* Espoo: Helsinki University of Technology.

Sanderson, T., 1988. *Ice Mechanics and Risks to Offshore Structures.* London, UK: Graham and Trotman.

Sawamura, J., 2012. *Numerical Investigation of Ice Bending Failure and Ice Submerging Force for Ship Maneuvering in Level Ice.* Dalian, China, 21st IAHR International Symposium on Ice.

Sawamura, J., 2018. *2D numerical modeling of icebreaker advancing in ice-covered water.* Osaka, Japan, International Journal of Naval Architecture and Ocean Engineering.

Sawamura, J., Riska, K. & Moan, T., 2008. *Finite Element Analysis of Fluid-Ice Interaction during Ice Bending.* Vancouver, British Columbia, Canada, 19th IAHR International Symposium on Ice.

Sawamura, J., Riska, K. & Moan, T., 2009. *Numerical Simulation of Breaking Patterns in Level Ice at Ship's Bow.* Osaka, Japan, ISOPE.

Su, B., 2011. *Numerical Predictions of Global and Local Ice Loads on Ships,* Trondheim, Norway: Norwegian University of Science and Technology (NTNU).

Su, B., Riska, K. & Moan, T., 2010. A numerical method for the prediction of ship performance in level ice. *Cold Regions Science and Technology,* Issue 60, pp. 177-188.

Su, B., Skjetne, R. & Berg, T. E., 2014. Numerical assessment of a double-acting offshore vessel's performance. *Cold Regions Science and Technology,* pp. 96-109.

Suominen, M. & Kujala, P., 2012. *Ice Model Tests in Compressive Ice.* Dalian, China, 21st IAHR International Symposium on Ice.

Suominen, M. & Kujala, P., 2013. *A Study of Measured Line Load Lengths and Maximum Ice Loas on Model Ship Hull.* Espoo, Finland, Proceedings of the 22nd International Conference on Port and Ocean Engineering Under Arctic Conditions (POAC).

Suominen, M. & Montewka, J., 2012. *WP 4: Compression in ship scale,* Espoo: Aalto University.

Tatinclaux, J.-C., 1985. *Level ice breaking by a simple wedge,* Hanover, New Hampshire, USA: US Army Corps of Engineers: Cold Regions Research and Engineering Laboratory.

Timco, G. W., 1984. *Ice forces on structures, physical modelling techniques.* Hamburg, Germany , 2nd IAHR State-of-the-Art Report on Ice Forces on Structures. Proceedings 7th International Association for Hydraulic Research Symposium on Ice, pp. 117-150.

Valanto, P., 2001. The Resistance of Ships in Level Ice. *SNAME Transactions Vol 109,* pp. 53-83.

von Bock und Polach, R. U. F., 2011. Heave and pitch motions of a ship in model ice: An experimental study on ship. *Cold Regions Science and Technology 68,* pp. 49-59.

von Bock und Polach, R. U. F., 2011. *Heave and pitch motions of a ship in model ice: An experimental study on ship.* Lahti, Finland, s.n.

von Bock und Polach, R. U. F., 2016. *The mechanical behavior of model-scale ice: experiments, numerical modeling and scalability,* Espoo, Finland: Aalto University.

Wang, S., 2001. *A dynamic model for breaking pattern of level ice by conical structures,* Espoo, Finland: Aalto Unviersity.

Yamaguchi, H., Suzuki, Y., Uemura, O. & Kato, H., 1997. *Influence of bow shapre on icebreaking resistance in low speed range.* Yokohama, Japan, s.n., pp. 51-61.

Yean, J., Tatinclaux, J. & Cook, A., 1981. *Ice forces on two-dimensional sloping structures,* Iowa City, Iowa USA: Iowa Institute of Hydraulic Research.

7 List of Appendices

Appendix A - Cusp Data Table....A-1
Appendix A.1 V=0.162m/s Single Contact Cusp Data....A-2
Appendix A.2 V=0.162m/s Multiple Contact Cusp Data....A-10
Appendix A.3 V=0.270m/s Single Contact Cusp Data....A-14
Appendix A.4 V=0.270m/s Multiple Contact Cusp Data....A-22
Appendix B - Icebreaking Pattern Photographs....B-1
Appendix C - Distributions and Histograms....C-1
Appendix C.1 V=0.162m/s Histograms....C-2
Appendix C.2 V=0.162m/s Distributions....C-6
Appendix C.3 V=0.270m/s Histograms....C-10
Appendix C.4 V=0.270m/s Distributions....C-14
Appendix C.5 Prediction Method Histogram Comparison....C-18

Appendix A - Cusp Data Table

Appendix A.1 V=0.162m/s Single Contact Cusp Data

#	L (m)	W(m)	θ(°)	Contact type	Area(m^2)	ψ(°)	β(°)	α(°)
1	0.249	0.050	150	'Single'	0.0084	50.1	44.5	31.5
2	0.172	0.058	150	'Single'	0.0056	59.1	32.4	19.2
4	0.200	0.076	146	'Single'	0.0084	46.5	50.1	37.6
5	0.465	0.142	150	'Single'	0.0431	49.2	45.8	32.9
6	0.101	0.054	122	'Single'	0.0029	57.7	34.1	20.8
7	0.241	0.056	150	'Single'	0.0085	47.0	49.3	36.7
8	0.230	0.070	150	'Single'	0.0090	64.6	26.0	13.3
9	0.088	0.037	127	'Single'	0.0018	60.9	30.2	17.1
11	0.076	0.039	124	'Single'	0.0013	66.0	24.4	11.9
12	0.069	0.040	129	'Single'	0.0015	48.6	46.8	34.0
13	0.594	0.127	150	'Single'	0.0518	51.5	42.4	29.3
14	0.312	0.078	150	'Single'	0.0146	48.3	47.1	34.4
15	0.087	0.048	150	'Single'	0.0022	46.4	50.4	37.9
16	0.098	0.043	139	'Single'	0.0025	48.0	47.6	34.9
18	0.196	0.065	150	'Single'	0.0065	48.2	47.4	34.7
20	0.142	0.068	144	'Single'	0.0047	51.4	42.5	29.4
22	0.117	0.042	150	'Single'	0.0028	46.5	50.3	37.8
23	0.192	0.047	150	'Single'	0.0059	48.0	47.7	35.0
24	0.110	0.041	145	'Single'	0.0025	46.4	50.3	37.8
25	0.078	0.035	130	'Single'	0.0014	46.6	50.0	37.5
26	0.573	0.161	150	'Single'	0.0583	49.3	45.6	32.7
27	0.191	0.057	150	'Single'	0.0069	46.7	49.9	37.4
28	0.407	0.169	150	'Single'	0.0261	48.2	47.3	34.6
29	0.111	0.047	146	'Single'	0.0028	67.8	22.5	10.3
30	0.159	0.046	150	'Single'	0.0035	47.4	48.6	36.0
31	0.143	0.035	150	'Single'	0.0028	46.5	50.1	37.6
32	0.167	0.031	150	'Single'	0.0028	47.0	49.3	36.7
33	0.070	0.031	128	'Single'	0.0010	62.5	28.4	15.4
34	0.449	0.144	150	'Single'	0.0383	50.0	44.6	31.7
36	0.390	0.093	150	'Single'	0.0257	48.4	47.0	34.2
38	0.141	0.032	150	'Single'	0.0030	47.0	49.4	36.8
40	0.136	0.064	137	'Single'	0.0043	59.6	31.8	18.6
41	0.182	0.064	134	'Single'	0.0068	46.5	50.3	37.8
43	0.512	0.147	150	'Single'	0.0447	49.6	45.1	32.2
44	0.145	0.035	150	'Single'	0.0025	46.6	50.1	37.5
45	0.131	0.105	150	'Single'	0.0191	65.3	25.2	12.6
46	0.318	0.070	150	'Single'	0.0161	49.8	44.9	32.0
47	0.103	0.056	128	'Single'	0.0031	57.9	33.8	20.6
48	0.346	0.127	150	'Single'	0.0259	48.4	47.0	34.2
49	0.273	0.093	150	'Single'	0.0147	59.2	32.2	19.0
50	0.128	0.049	140	'Single'	0.0036	46.6	50.1	37.5
52	0.170	0.052	150	'Single'	0.0050	46.9	49.6	37.0
54	0.220	0.057	150	'Single'	0.0082	54.1	38.8	25.5

56	0.542	0.149	150	'Single'	0.0523	50.1	44.5	31.5
57	0.112	0.041	132	'Single'	0.0023	47.7	48.2	35.6
58	0.113	0.046	139	'Single'	0.0028	64.9	25.6	13.0
59	0.161	0.042	145	'Single'	0.0035	47.6	48.4	35.7
60	0.061	0.037	145	'Single'	0.0014	49.1	46.0	33.1
62	0.053	0.045	94	'Single'	0.0013	46.7	49.9	37.4
64	0.186	0.054	150	'Single'	0.0058	46.9	49.5	36.9
65	0.065	0.038	114	'Single'	0.0014	61.3	29.7	16.7
67	0.160	0.080	149	'Single'	0.0072	62.7	28.1	15.2
68	0.085	0.044	134	'Single'	0.0019	59.3	32.1	18.9
69	0.130	0.032	150	'Single'	0.0022	46.6	50.1	37.5
70	0.168	0.039	150	'Single'	0.0039	62.4	28.5	15.5
72	0.324	0.078	150	'Single'	0.0137	58.1	33.6	20.3
74	0.363	0.145	150	'Single'	0.0287	51.3	42.6	29.5
75	0.129	0.089	150	'Single'	0.0065	59.1	32.3	19.1
76	0.127	0.034	150	'Single'	0.0021	47.8	48.0	35.3
77	0.224	0.064	150	'Single'	0.0075	48.2	47.4	34.6
78	0.085	0.057	135	'Single'	0.0036	64.9	25.6	13.0
79	0.277	0.113	141	'Single'	0.0161	59.8	31.5	18.4
81	0.062	0.038	109	'Single'	0.0012	57.9	33.9	20.6
82	0.129	0.060	125	'Single'	0.0041	46.9	49.6	37.0
83	0.061	0.036	119	'Single'	0.0012	63.4	27.3	14.5
84	0.137	0.051	150	'Single'	0.0039	46.7	49.9	37.4
86	0.119	0.024	150	'Single'	0.0017	46.6	50.0	37.5
87	0.180	0.128	146	'Single'	0.0129	48.1	47.6	34.8
88	0.252	0.114	149	'Single'	0.0104	46.5	50.1	37.6
89	0.082	0.031	140	'Single'	0.0013	46.4	50.4	37.9
90	0.209	0.068	148	'Single'	0.0080	46.9	49.5	36.9
91	0.263	0.092	150	'Single'	0.0136	47.7	48.1	35.4
92	0.111	0.036	150	'Single'	0.0024	56.3	35.9	22.6
95	0.136	0.059	150	'Single'	0.0050	46.4	50.4	37.9
96	0.053	0.030	108	'Single'	0.0008	48.1	47.6	34.8
97	0.087	0.038	147	'Single'	0.0018	63.1	27.7	14.8
98	0.074	0.029	146	'Single'	0.0011	50.1	44.5	31.5
99	0.090	0.043	143	'Single'	0.0022	47.7	48.1	35.4
101	0.179	0.050	150	'Single'	0.0051	47.2	49.0	36.4
102	0.149	0.034	150	'Single'	0.0031	48.7	46.6	33.8
103	0.108	0.033	150	'Single'	0.0021	51.5	42.4	29.3
104	0.269	0.071	150	'Single'	0.0134	47.7	48.2	35.6
105	0.140	0.064	150	'Single'	0.0048	52.7	40.6	27.5
106	0.138	0.031	150	'Single'	0.0026	46.8	49.7	37.1
107	0.061	0.026	150	'Single'	0.0010	58.9	32.6	19.4
108	0.160	0.024	150	'Single'	0.0029	46.4	50.3	37.8
109	0.260	0.039	150	'Single'	0.0073	58.8	32.7	19.5
110	0.301	0.093	150	'Single'	0.0171	51.0	43.1	30.1
111	0.206	0.040	150	'Single'	0.0073	47.8	48.1	35.4
112	0.053	0.016	148	'Single'	0.0005	57.7	34.2	20.9

113	0.106	0.031	150	'Single'	0.0019	58.4	33.3	20.0
114	0.077	0.020	150	'Single'	0.0008	66.2	24.2	11.8
116	0.120	0.033	150	'Single'	0.0024	46.8	49.7	37.1
117	0.078	0.028	150	'Single'	0.0012	48.6	46.8	34.0
119	0.064	0.022	150	'Single'	0.0009	49.1	45.9	33.1
121	0.131	0.067	125	'Single'	0.0044	54.9	37.6	24.4
122	0.111	0.038	143	'Single'	0.0023	46.5	50.2	37.7
124	0.075	0.043	102	'Single'	0.0018	60.2	31.1	17.9
125	0.091	0.038	139	'Single'	0.0016	47.6	48.4	35.7
126	0.142	0.041	150	'Single'	0.0034	63.7	27.0	14.2
128	0.098	0.037	145	'Single'	0.0020	46.4	50.4	37.9
129	0.245	0.045	150	'Single'	0.0065	46.4	50.4	37.9
130	0.191	0.062	150	'Single'	0.0063	46.4	50.4	37.9
132	0.244	0.109	150	'Single'	0.0156	46.4	50.4	37.9
133	0.103	0.058	119	'Single'	0.0033	50.3	44.1	31.2
134	0.206	0.076	150	'Single'	0.0090	47.8	48.0	35.3
136	0.310	0.122	140	'Single'	0.0211	47.1	49.1	36.5
137	0.147	0.044	147	'Single'	0.0039	46.4	50.4	37.9
138	0.188	0.044	150	'Single'	0.0048	48.5	46.9	34.2
140	0.273	0.109	150	'Single'	0.0137	47.3	48.9	36.3
141	0.154	0.056	146	'Single'	0.0045	63.3	27.4	14.5
142	0.221	0.038	150	'Single'	0.0043	47.6	48.4	35.7
144	0.418	0.126	150	'Single'	0.0347	47.4	48.7	36.1
145	0.037	0.022	109	'Single'	0.0004	55.8	36.5	23.2
146	0.066	0.029	130	'Single'	0.0010	58.6	33.0	19.8
149	0.101	0.064	150	'Single'	0.0033	46.4	50.4	37.9
150	0.231	0.067	150	'Single'	0.0083	47.0	49.3	36.7
151	0.158	0.051	150	'Single'	0.0051	66.8	23.5	11.2
152	0.155	0.048	150	'Single'	0.0054	46.4	50.3	37.8
153	0.090	0.041	132	'Single'	0.0017	49.3	45.6	32.7
155	0.290	0.084	150	'Single'	0.0139	65.6	24.8	12.3
157	0.045	0.020	135	'Single'	0.0006	58.6	33.0	19.8
158	0.218	0.056	150	'Single'	0.0075	47.7	48.1	35.4
160	0.108	0.044	145	'Single'	0.0029	46.4	50.4	37.9
161	0.083	0.031	148	'Single'	0.0013	51.7	42.0	28.9
163	0.083	0.029	142	'Single'	0.0013	46.4	50.4	37.9
164	0.192	0.058	150	'Single'	0.0065	46.4	50.3	37.8
165	0.076	0.038	122	'Single'	0.0016	50.2	44.3	31.3
167	0.105	0.046	142	'Single'	0.0023	53.0	40.3	27.1
168	0.112	0.030	147	'Single'	0.0019	46.4	50.4	37.9
169	0.095	0.035	138	'Single'	0.0017	46.5	50.2	37.7
171	0.304	0.086	150	'Single'	0.0150	55.6	36.7	23.5
173	0.190	0.072	145	'Single'	0.0068	52.8	40.6	27.4
176	0.174	0.044	148	'Single'	0.0039	47.0	49.3	36.7
177	0.267	0.067	150	'Single'	0.0098	48.1	47.5	34.7
178	0.093	0.050	135	'Single'	0.0024	53.7	39.2	26.0
180	0.138	0.037	150	'Single'	0.0028	46.4	50.4	37.9

181	0.142	0.047	150	'Single'	0.0039	63.5	27.2	14.4
184	0.277	0.076	150	'Single'	0.0121	46.4	50.4	37.9
185	0.099	0.039	135	'Single'	0.0023	67.1	23.3	11.0
187	0.200	0.087	145	'Single'	0.0092	46.5	50.2	37.7
188	0.115	0.047	128	'Single'	0.0027	50.7	43.6	30.6
189	0.176	0.044	146	'Single'	0.0049	47.8	48.0	35.3
190	0.124	0.055	132	'Single'	0.0039	54.2	38.6	25.4
191	0.096	0.042	123	'Single'	0.0021	59.2	32.2	19.0
193	0.180	0.066	147	'Single'	0.0060	46.6	50.1	37.5
194	0.286	0.069	150	'Single'	0.0155	68.7	21.6	9.6
196	0.235	0.077	146	'Single'	0.0102	47.7	48.2	35.5
197	0.321	0.147	150	'Single'	0.0265	57.9	33.9	20.6
198	0.166	0.092	122	'Single'	0.0076	64.6	26.0	13.3
199	0.149	0.091	108	'Single'	0.0072	47.4	48.6	36.0
201	0.140	0.061	126	'Single'	0.0046	46.4	50.3	37.8
202	0.066	0.034	119	'Single'	0.0012	64.3	26.4	13.6
203	0.303	0.106	150	'Single'	0.0201	70.4	19.8	8.2
204	0.290	0.064	150	'Single'	0.0105	48.6	46.8	34.0
205	0.179	0.068	137	'Single'	0.0062	46.8	49.8	37.2
206	0.121	0.059	131	'Single'	0.0039	53.4	39.6	26.4
208	0.088	0.029	144	'Single'	0.0013	46.5	50.3	37.8
209	0.172	0.086	121	'Single'	0.0090	57.8	33.9	20.7
210	0.188	0.059	150	'Single'	0.0062	47.5	48.4	35.8
211	0.168	0.043	150	'Single'	0.0045	50.5	43.8	30.8
212	0.172	0.049	150	'Single'	0.0043	47.2	49.0	36.4
213	0.124	0.046	148	'Single'	0.0032	54.8	37.8	24.5
214	0.156	0.057	141	'Single'	0.0047	47.1	49.2	36.6
215	0.210	0.091	139	'Single'	0.0097	51.2	42.7	29.7
217	0.144	0.046	150	'Single'	0.0037	47.7	48.2	35.5
221	0.230	0.086	150	'Single'	0.0109	47.2	48.9	36.3
223	0.179	0.065	141	'Single'	0.0062	46.5	50.1	37.6
224	0.073	0.030	116	'Single'	0.0011	46.4	50.4	37.9
226	0.299	0.076	150	'Single'	0.0132	48.3	47.2	34.4
227	0.148	0.080	150	'Single'	0.0067	55.3	37.2	23.9
228	0.083	0.048	128	'Single'	0.0023	59.5	32.0	18.8
230	0.307	0.105	150	'Single'	0.0222	68.7	21.6	9.6
231	0.473	0.154	145	'Single'	0.0412	61.0	30.1	17.0
232	0.466	0.150	147	'Single'	0.0371	47.0	49.3	36.7
233	0.267	0.109	150	'Single'	0.0164	47.8	48.0	35.3
235	0.095	0.044	130	'Single'	0.0022	62.8	28.0	15.1
236	0.200	0.089	127	'Single'	0.0097	61.2	29.9	16.8
237	0.101	0.057	102	'Single'	0.0031	46.5	50.1	37.6
238	0.382	0.188	140	'Single'	0.0418	47.5	48.5	35.9
239	0.204	0.077	150	'Single'	0.0096	64.7	25.9	13.2
240	0.175	0.063	150	'Single'	0.0070	67.4	23.0	10.7
242	0.124	0.064	129	'Single'	0.0042	55.6	36.8	23.5
243	0.251	0.059	150	'Single'	0.0084	55.0	37.5	24.2

245	0.222	0.073	150	'Single'	0.0085	47.8	48.0	35.3
246	0.128	0.052	124	'Single'	0.0036	46.4	50.4	37.9
247	0.313	0.114	148	'Single'	0.0219	50.3	44.1	31.1
248	0.146	0.080	107	'Single'	0.0065	46.9	49.6	37.0
249	0.059	0.043	102	'Single'	0.0013	56.8	35.2	22.0
252	0.242	0.064	150	'Single'	0.0091	47.7	48.1	35.4
254	0.071	0.037	117	'Single'	0.0013	62.3	28.6	15.7
255	0.092	0.057	99	'Single'	0.0027	46.4	50.4	37.9
256	0.405	0.165	150	'Single'	0.0413	48.6	46.8	34.0
258	0.161	0.066	123	'Single'	0.0057	62.0	29.0	16.0
259	0.131	0.047	150	'Single'	0.0034	58.3	33.4	20.2
260	0.237	0.068	150	'Single'	0.0094	48.1	47.5	34.8
262	0.124	0.042	128	'Single'	0.0026	63.6	27.1	14.2
263	0.120	0.048	141	'Single'	0.0032	47.8	48.1	35.4
265	0.159	0.054	146	'Single'	0.0051	47.1	49.2	36.6
266	0.083	0.037	126	'Single'	0.0016	55.4	37.1	23.8
268	0.336	0.168	139	'Single'	0.0310	46.7	49.9	37.4
269	0.136	0.077	110	'Single'	0.0056	47.2	49.1	36.5
270	0.086	0.056	114	'Single'	0.0026	56.0	36.2	23.0
271	0.337	0.127	145	'Single'	0.0247	48.6	46.7	33.9
274	0.327	0.127	142	'Single'	0.0247	47.4	48.7	36.1
275	0.071	0.048	100	'Single'	0.0019	61.5	29.5	16.5
276	0.302	0.068	150	'Single'	0.0096	60.5	30.7	17.6
277	0.179	0.062	150	'Single'	0.0070	54.5	38.2	25.0
278	0.077	0.037	146	'Single'	0.0015	68.7	21.5	9.6
279	0.243	0.085	147	'Single'	0.0114	53.6	39.4	26.1
282	0.147	0.065	133	'Single'	0.0050	48.3	47.3	34.5
283	0.110	0.038	150	'Single'	0.0023	48.8	46.5	33.7
284	0.141	0.072	139	'Single'	0.0050	52.9	40.4	27.3
286	0.077	0.043	133	'Single'	0.0020	53.4	39.7	26.5
287	0.266	0.086	150	'Single'	0.0132	46.7	49.9	37.3
288	0.059	0.036	110	'Single'	0.0011	58.8	32.7	19.5
289	0.180	0.077	149	'Single'	0.0080	62.3	28.5	15.6
290	0.137	0.042	142	'Single'	0.0031	46.8	49.7	37.2
292	0.109	0.096	138	'Single'	0.0093	47.2	49.0	36.4
293	0.086	0.089	129	'Single'	0.0044	46.4	50.4	37.9
294	0.134	0.055	135	'Single'	0.0038	46.5	50.3	37.8
295	0.199	0.091	129	'Single'	0.0099	48.2	47.3	34.6
296	0.179	0.073	150	'Single'	0.0076	51.3	42.7	29.6
297	0.231	0.099	147	'Single'	0.0146	47.2	48.9	36.3
299	0.121	0.059	121	'Single'	0.0038	46.4	50.4	37.9
300	0.268	0.079	150	'Single'	0.0132	48.4	47.0	34.2
302	0.355	0.095	146	'Single'	0.0172	48.2	47.3	34.6
303	0.129	0.064	118	'Single'	0.0043	62.6	28.3	15.3
304	0.122	0.058	126	'Single'	0.0036	46.4	50.4	37.9
305	0.234	0.061	150	'Single'	0.0076	48.0	47.7	35.0
308	0.052	0.029	124	'Single'	0.0008	57.7	34.1	20.8

309	0.105	0.051	124	'Single'	0.0029	48.2	47.4	34.6
312	0.155	0.073	127	'Single'	0.0063	46.5	50.3	37.8
313	0.102	0.053	106	'Single'	0.0026	67.1	23.2	10.9
314	0.155	0.091	116	'Single'	0.0065	55.9	36.4	23.1
315	0.113	0.041	144	'Single'	0.0026	48.1	47.5	34.7
318	0.099	0.058	149	'Single'	0.0038	46.4	50.4	37.9
319	0.147	0.059	149	'Single'	0.0044	47.3	48.9	36.3
321	0.121	0.047	119	'Single'	0.0028	46.6	50.1	37.5
322	0.218	0.069	147	'Single'	0.0066	50.1	44.3	31.4
323	0.199	0.069	150	'Single'	0.0074	48.4	47.0	34.2
324	0.115	0.061	128	'Single'	0.0038	55.5	36.9	23.7
325	0.107	0.035	143	'Single'	0.0021	47.4	48.7	36.1
328	0.197	0.067	144	'Single'	0.0075	47.8	48.1	35.4
329	0.189	0.040	150	'Single'	0.0037	48.7	46.5	33.7
330	0.233	0.055	150	'Single'	0.0076	54.1	38.8	25.6
331	0.129	0.057	147	'Single'	0.0036	47.6	48.4	35.7
333	0.143	0.061	150	'Single'	0.0048	47.9	47.9	35.2
334	0.329	0.113	150	'Single'	0.0180	49.4	45.4	32.5
335	0.139	0.042	150	'Single'	0.0037	46.9	49.4	36.9
336	0.180	0.042	150	'Single'	0.0045	47.0	49.4	36.8
338	0.086	0.059	130	'Single'	0.0033	47.7	48.2	35.5
339	0.199	0.055	150	'Single'	0.0056	47.3	48.8	36.2
342	0.122	0.049	150	'Single'	0.0035	68.4	21.9	9.8
343	0.068	0.041	119	'Single'	0.0014	46.6	50.0	37.4
345	0.125	0.069	132	'Single'	0.0052	46.5	50.2	37.7
346	0.124	0.051	139	'Single'	0.0035	57.4	34.5	21.2
348	0.232	0.104	133	'Single'	0.0125	46.4	50.4	37.9
350	0.099	0.044	132	'Single'	0.0021	58.6	32.9	19.7
351	0.083	0.045	127	'Single'	0.0020	63.5	27.3	14.4
353	0.121	0.058	128	'Single'	0.0033	53.6	39.4	26.1
356	0.124	0.034	150	'Single'	0.0024	48.5	46.8	34.1
357	0.121	0.040	150	'Single'	0.0031	46.8	49.8	37.2
359	0.124	0.044	146	'Single'	0.0026	67.8	22.5	10.4
360	0.078	0.028	125	'Single'	0.0011	46.4	50.4	37.9
361	0.124	0.073	150	'Single'	0.0070	63.8	26.9	14.1
362	0.180	0.051	150	'Single'	0.0055	46.9	49.4	36.9
363	0.166	0.069	150	'Single'	0.0069	47.3	48.8	36.2
364	0.128	0.065	150	'Single'	0.0071	50.5	43.8	30.8
365	0.123	0.057	150	'Single'	0.0042	46.8	49.7	37.2
367	0.072	0.031	136	'Single'	0.0011	58.3	33.4	20.1
368	0.225	0.087	141	'Single'	0.0106	46.9	49.6	37.0
369	0.102	0.049	130	'Single'	0.0026	60.2	31.0	17.9
370	0.077	0.038	119	'Single'	0.0014	46.5	50.1	37.6
371	0.113	0.050	138	'Single'	0.0032	65.0	25.5	12.9
372	0.122	0.050	150	'Single'	0.0036	61.1	30.0	16.9
374	0.162	0.057	150	'Single'	0.0046	61.8	29.2	16.2
375	0.102	0.039	150	'Single'	0.0021	68.4	21.9	9.9

376	0.136	0.060	125	'Single'	0.0043	60.2	31.0	17.9
377	0.086	0.030	148	'Single'	0.0014	48.4	47.0	34.2
378	0.168	0.064	145	'Single'	0.0065	47.1	49.2	36.6
380	0.230	0.050	150	'Single'	0.0071	48.1	47.5	34.8
383	0.103	0.030	150	'Single'	0.0015	58.3	33.3	20.1
384	0.143	0.077	150	'Single'	0.0052	54.4	38.4	25.1
385	0.166	0.062	144	'Single'	0.0055	59.1	32.3	19.1
387	0.146	0.059	141	'Single'	0.0046	46.4	50.4	37.9
389	0.188	0.066	150	'Single'	0.0074	46.8	49.7	37.2
390	0.102	0.050	140	'Single'	0.0028	50.2	44.3	31.3
391	0.126	0.039	141	'Single'	0.0025	61.4	29.6	16.6
392	0.206	0.104	138	'Single'	0.0130	46.9	49.5	37.0
393	0.124	0.056	136	'Single'	0.0034	51.1	42.9	29.9
394	0.149	0.034	150	'Single'	0.0034	54.7	37.9	24.7
395	0.083	0.044	106	'Single'	0.0020	46.4	50.4	37.9
397	0.355	0.148	139	'Single'	0.0286	47.1	49.2	36.6
398	0.104	0.042	142	'Single'	0.0023	47.3	48.8	36.2
399	0.120	0.033	143	'Single'	0.0023	46.9	49.5	36.9
400	0.176	0.055	150	'Single'	0.0052	48.8	46.5	33.7
401	0.156	0.054	146	'Single'	0.0038	58.0	33.8	20.5
402	0.184	0.067	141	'Single'	0.0067	51.5	42.3	29.2
403	0.261	0.075	150	'Single'	0.0118	47.3	48.8	36.2
405	0.248	0.042	150	'Single'	0.0068	47.7	48.2	35.5
407	0.302	0.090	150	'Single'	0.0156	46.9	49.5	37.0
408	0.103	0.060	123	'Single'	0.0032	55.9	36.4	23.2
409	0.170	0.062	141	'Single'	0.0057	54.3	38.4	25.2
410	0.144	0.041	150	'Single'	0.0038	60.6	30.6	17.5
412	0.095	0.036	139	'Single'	0.0018	67.2	23.2	10.9
413	0.238	0.058	150	'Single'	0.0089	47.2	49.1	36.5
414	0.194	0.056	150	'Single'	0.0061	66.3	24.2	11.7
415	0.143	0.049	137	'Single'	0.0037	46.4	50.4	37.9
419	0.385	0.108	150	'Single'	0.0244	54.3	38.5	25.3
421	0.059	0.028	123	'Single'	0.0008	62.4	28.5	15.5
422	0.162	0.062	134	'Single'	0.0054	46.4	50.4	37.9
423	0.157	0.048	150	'Single'	0.0043	46.4	50.4	37.9
424	0.073	0.032	130	'Single'	0.0011	63.6	27.1	14.3
425	0.119	0.063	122	'Single'	0.0038	46.4	50.4	37.9
426	0.157	0.060	150	'Single'	0.0042	56.5	35.5	22.3
428	0.183	0.082	150	'Single'	0.0085	46.4	50.4	37.9
429	0.142	0.056	148	'Single'	0.0053	46.9	49.6	37.0
430	0.274	0.068	150	'Single'	0.0119	49.9	44.7	31.8
431	0.348	0.134	150	'Single'	0.0286	47.7	48.2	35.5
432	0.237	0.092	139	'Single'	0.0107	55.9	36.3	23.1
434	0.088	0.030	150	'Single'	0.0013	46.4	50.4	37.9
435	0.174	0.073	150	'Single'	0.0096	68.6	21.6	9.6
438	0.323	0.073	150	'Single'	0.0137	47.9	47.8	35.1
440	0.193	0.045	150	'Single'	0.0051	46.9	49.4	36.9

441	0.153	0.074	137	'Single'	0.0059	50.3	44.1	31.1
442	0.179	0.032	150	'Single'	0.0035	47.4	48.7	36.1
444	0.262	0.069	150	'Single'	0.0109	64.4	26.3	13.5
445	0.272	0.121	150	'Single'	0.0109	47.6	48.4	35.7
446	0.086	0.034	150	'Single'	0.0018	47.2	48.9	36.3
447	0.079	0.022	150	'Single'	0.0009	46.4	50.4	37.9
450	0.158	0.059	150	'Single'	0.0061	46.9	49.5	37.0
452	0.165	0.065	144	'Single'	0.0061	47.1	49.2	36.6
453	0.091	0.052	128	'Single'	0.0024	60.3	31.0	17.8
457	0.201	0.059	150	'Single'	0.0063	52.2	41.4	28.3
459	0.216	0.088	137	'Single'	0.0104	60.8	30.3	17.2
460	0.231	0.088	150	'Single'	0.0115	46.6	50.1	37.5
461	0.105	0.053	137	'Single'	0.0024	52.3	41.2	28.1
463	0.142	0.057	147	'Single'	0.0055	46.6	50.0	37.5
466	0.077	0.037	115	'Single'	0.0015	46.4	50.4	37.9
467	0.102	0.042	147	'Single'	0.0024	54.2	38.6	25.4
468	0.167	0.057	150	'Single'	0.0054	51.3	42.7	29.6
471	0.063	0.042	124	'Single'	0.0013	56.9	35.1	21.8
472	0.252	0.092	144	'Single'	0.0127	46.5	50.2	37.7
473	0.271	0.094	150	'Single'	0.0163	58.7	32.9	19.7
474	0.104	0.057	112	'Single'	0.0027	46.4	50.4	37.9
476	0.171	0.072	150	'Single'	0.0085	46.4	50.4	37.9
477	0.150	0.056	147	'Single'	0.0044	50.0	44.5	31.6
479	0.164	0.062	140	'Single'	0.0057	46.4	50.4	37.9
481	0.093	0.039	134	'Single'	0.0019	46.4	50.4	37.9
483	0.129	0.056	137	'Single'	0.0040	49.8	44.8	31.9
486	0.156	0.052	148	'Single'	0.0046	46.4	50.4	37.9
490	0.095	0.040	150	'Single'	0.0031	46.9	49.6	37.0
492	0.292	0.124	141	'Single'	0.0159	46.4	50.4	37.9
493	0.168	0.061	144	'Single'	0.0063	48.4	47.1	34.3
495	0.259	0.091	150	'Single'	0.0139	57.9	33.9	20.6
497	0.140	0.055	150	'Single'	0.0044	46.5	50.2	37.7
499	0.146	0.053	150	'Single'	0.0042	46.4	50.3	37.8
500	0.117	0.042	150	'Single'	0.0030	58.1	33.6	20.3
504	0.255	0.086	147	'Single'	0.0123	47.5	48.4	35.8
505	0.121	0.056	140	'Single'	0.0037	46.9	49.4	36.9
506	0.153	0.058	146	'Single'	0.0047	52.8	40.5	27.3

Appendix A.2 V=0.162m/s Multiple Contact Cusp Data

#	L (m)	W(m)	θ(°)	Contact type	Area(m^2)	ψ(°)	β(°)	α(°)
3	0.581	0.125	150	'Multiple'	0.0493	52.6	40.8	27.6
10	0.708	0.128	150	'Multiple'	0.0691	53.3	39.8	26.7
17	0.635	0.184	150	'Multiple'	0.0681	53.9	39.0	25.8
19	0.432	0.044	150	'Multiple'	0.0151	48.7	46.6	33.8
21	0.775	0.184	150	'Multiple'	0.0965	51.8	41.9	28.8
35	0.459	0.191	150	'Multiple'	0.0619	64.7	25.8	13.1
37	0.247	0.084	150	'Multiple'	0.0149	61.9	29.1	16.0
39	0.588	0.170	150	'Multiple'	0.0645	50.5	43.8	30.8
42	0.226	0.074	150	'Multiple'	0.0097	65.1	25.5	12.8
51	0.182	0.123	150	'Multiple'	0.0210	71.3	18.8	7.5
53	0.722	0.088	150	'Multiple'	0.0482	52.7	40.6	27.5
55	0.423	0.143	150	'Multiple'	0.0444	66.2	24.2	11.8
61	0.600	0.188	150	'Multiple'	0.0785	67.0	23.4	11.1
63	0.472	0.137	150	'Multiple'	0.0327	51.8	41.9	28.8
66	0.485	0.161	150	'Multiple'	0.0517	48.8	46.5	33.7
71	0.370	0.100	150	'Multiple'	0.0243	48.3	47.2	34.4
73	0.264	0.152	150	'Multiple'	0.0418	70.4	19.8	8.2
80	0.522	0.146	150	'Multiple'	0.0495	49.6	45.1	32.2
85	0.764	0.173	150	'Multiple'	0.0914	56.4	35.7	22.4
93	0.561	0.203	150	'Multiple'	0.0705	59.1	32.4	19.2
94	0.511	0.149	150	'Multiple'	0.0509	48.7	46.5	33.7
100	0.748	0.150	150	'Multiple'	0.0769	57.1	34.9	21.6
115	0.895	0.094	150	'Multiple'	0.0614	58.8	32.8	19.5
118	0.704	0.228	150	'Multiple'	0.0962	57.9	33.8	20.6
120	0.385	0.099	150	'Multiple'	0.0227	47.2	49.0	36.4
123	0.626	0.088	150	'Multiple'	0.0441	50.0	44.6	31.7
127	0.913	0.096	150	'Multiple'	0.0742	54.8	37.8	24.6
131	0.604	0.163	150	'Multiple'	0.0550	53.2	40.0	26.9
135	0.897	0.233	150	'Multiple'	0.1495	57.8	34.0	20.8
139	0.603	0.166	150	'Multiple'	0.0627	49.9	44.8	31.9
143	0.831	0.128	150	'Multiple'	0.0668	57.1	34.9	21.6
147	0.800	0.089	150	'Multiple'	0.0590	54.2	38.7	25.4
148	0.671	0.115	150	'Multiple'	0.0529	49.3	45.6	32.7
154	0.640	0.086	150	'Multiple'	0.0418	59.8	31.5	18.3
156	0.496	0.145	150	'Multiple'	0.0441	47.6	48.4	35.7
159	0.651	0.163	150	'Multiple'	0.0599	60.1	31.2	18.0
162	0.615	0.167	150	'Multiple'	0.0687	50.7	43.5	30.5
166	0.310	0.090	150	'Multiple'	0.0186	47.3	48.8	36.2
170	0.336	0.105	150	'Multiple'	0.0240	47.2	49.0	36.4
172	0.490	0.099	150	'Multiple'	0.0385	67.0	23.4	11.1
174	0.823	0.203	150	'Multiple'	0.1089	52.0	41.6	28.5
175	0.692	0.140	150	'Multiple'	0.0648	53.8	39.1	25.9
179	0.541	0.106	150	'Multiple'	0.0386	51.5	42.4	29.3

182	0.656	0.192	150	'Multiple'	0.0830	50.3	44.2	31.2
183	0.354	0.052	150	'Multiple'	0.0140	68.0	22.3	10.2
186	0.703	0.200	150	'Multiple'	0.0887	51.8	41.9	28.8
192	0.665	0.252	150	'Multiple'	0.1081	49.7	45.0	32.1
195	0.368	0.123	150	'Multiple'	0.0300	48.5	46.9	34.1
200	0.537	0.128	150	'Multiple'	0.0424	51.4	42.4	29.4
207	0.362	0.088	150	'Multiple'	0.0200	51.6	42.1	29.1
216	0.600	0.191	150	'Multiple'	0.0898	66.4	24.0	11.6
218	0.299	0.063	150	'Multiple'	0.0117	56.0	36.2	23.0
219	0.326	0.079	150	'Multiple'	0.0126	50.6	43.6	30.6
220	0.643	0.186	150	'Multiple'	0.0666	56.7	35.3	22.0
222	0.528	0.185	150	'Multiple'	0.0620	50.1	44.4	31.4
225	0.346	0.086	150	'Multiple'	0.0178	49.2	45.8	33.0
229	0.445	0.160	150	'Multiple'	0.0452	50.1	44.5	31.5
234	0.593	0.179	150	'Multiple'	0.0727	49.5	45.4	32.5
241	0.343	0.119	150	'Multiple'	0.0233	60.6	30.5	17.4
244	0.674	0.199	150	'Multiple'	0.0826	57.2	34.7	21.4
250	0.372	0.076	150	'Multiple'	0.0164	50.1	44.4	31.5
251	0.431	0.153	150	'Multiple'	0.0387	58.2	33.5	20.3
253	0.633	0.216	150	'Multiple'	0.0915	49.1	45.9	33.1
257	0.412	0.169	146	'Multiple'	0.0400	67.5	22.9	10.6
261	0.761	0.180	150	'Multiple'	0.0877	53.0	40.3	27.1
264	0.319	0.110	150	'Multiple'	0.0197	48.5	46.8	34.1
267	0.981	0.203	150	'Multiple'	0.1447	60.0	31.2	18.1
272	0.498	0.232	137	'Multiple'	0.0634	57.5	34.4	21.1
273	0.452	0.234	150	'Multiple'	0.0630	50.4	43.9	30.9
280	0.497	0.142	150	'Multiple'	0.0431	50.1	44.3	31.4
281	0.485	0.117	150	'Multiple'	0.0372	65.0	25.6	12.9
285	0.794	0.148	150	'Multiple'	0.0790	53.5	39.5	26.3
291	0.832	0.246	150	'Multiple'	0.1429	56.8	35.2	21.9
298	0.665	0.131	150	'Multiple'	0.0581	52.8	40.5	27.4
301	0.379	0.159	150	'Multiple'	0.0339	54.1	38.7	25.5
306	0.718	0.191	150	'Multiple'	0.0906	58.7	32.8	19.6
307	0.407	0.154	150	'Multiple'	0.0401	48.6	46.7	33.9
310	0.350	0.133	150	'Multiple'	0.0279	48.8	46.5	33.7
311	0.346	0.130	150	'Multiple'	0.0251	58.4	33.2	20.0
316	0.651	0.185	150	'Multiple'	0.0778	53.1	40.2	27.0
317	0.517	0.178	150	'Multiple'	0.0569	46.4	50.4	37.9
320	0.874	0.169	150	'Multiple'	0.1100	56.8	35.3	22.0
326	0.646	0.070	150	'Multiple'	0.0354	56.3	35.8	22.6
327	0.586	0.136	150	'Multiple'	0.0471	53.1	40.2	27.0
332	0.760	0.137	150	'Multiple'	0.0773	59.8	31.6	18.4
337	0.268	0.119	150	'Multiple'	0.0186	48.8	46.4	33.6
340	0.660	0.190	150	'Multiple'	0.0751	53.0	40.2	27.0
341	0.157	0.044	150	'Multiple'	0.0042	62.8	28.1	15.1
344	0.376	0.167	145	'Multiple'	0.0387	47.7	48.2	35.5
347	0.958	0.205	150	'Multiple'	0.1328	57.5	34.3	21.1

349	0.444	0.149	150	'Multiple'	0.0349	50.1	44.5	31.5
352	0.307	0.063	150	'Multiple'	0.0117	48.2	47.4	34.7
354	0.465	0.101	150	'Multiple'	0.0277	54.0	38.9	25.7
355	0.349	0.221	150	'Multiple'	0.0562	70.6	19.6	8.1
358	0.640	0.196	150	'Multiple'	0.0831	49.7	45.0	32.1
366	0.481	0.170	150	'Multiple'	0.0463	50.8	43.4	30.4
373	0.569	0.160	150	'Multiple'	0.0547	50.3	44.1	31.2
379	0.769	0.193	150	'Multiple'	0.1035	60.4	30.8	17.6
381	0.276	0.094	150	'Multiple'	0.0172	50.3	44.2	31.2
382	0.311	0.074	150	'Multiple'	0.0133	48.8	46.4	33.6
386	0.409	0.092	150	'Multiple'	0.0228	51.6	42.2	29.1
388	0.729	0.091	150	'Multiple'	0.0480	55.9	36.4	23.1
396	0.925	0.221	150	'Multiple'	0.1673	59.3	32.2	19.0
404	0.728	0.153	150	'Multiple'	0.0802	57.5	34.3	21.0
406	0.377	0.071	150	'Multiple'	0.0163	49.4	45.4	32.5
411	0.662	0.144	150	'Multiple'	0.0510	53.1	40.2	27.0
416	0.476	0.068	150	'Multiple'	0.0246	49.9	44.7	31.8
417	0.364	0.082	150	'Multiple'	0.0149	58.4	33.2	20.0
418	0.395	0.075	150	'Multiple'	0.0186	49.6	45.1	32.2
420	0.303	0.100	150	'Multiple'	0.0175	48.4	47.0	34.2
427	0.872	0.335	150	'Multiple'	0.2301	60.7	30.5	17.4
433	0.415	0.107	150	'Multiple'	0.0278	55.1	37.4	24.2
436	0.301	0.074	150	'Multiple'	0.0119	47.9	47.9	35.2
437	0.210	0.060	150	'Multiple'	0.0077	56.5	35.6	22.4
439	0.370	0.097	150	'Multiple'	0.0216	54.9	37.7	24.4
443	0.494	0.099	150	'Multiple'	0.0295	50.5	43.9	30.9
448	0.401	0.139	150	'Multiple'	0.0300	63.6	27.1	14.3
449	0.947	0.200	150	'Multiple'	0.1282	53.7	39.2	26.0
451	0.407	0.121	150	'Multiple'	0.0293	50.2	44.3	31.3
454	0.295	0.103	150	'Multiple'	0.0181	49.1	45.9	33.1
455	0.581	0.149	150	'Multiple'	0.0502	58.3	33.3	20.1
456	0.262	0.055	150	'Multiple'	0.0093	47.3	48.8	36.2
458	0.541	0.172	150	'Multiple'	0.0621	49.1	45.9	33.1
462	0.840	0.125	150	'Multiple'	0.0824	54.7	37.9	24.7
464	0.352	0.090	150	'Multiple'	0.0185	48.8	46.4	33.6
465	0.637	0.383	150	'Multiple'	0.0936	56.4	35.8	22.5
469	0.445	0.159	150	'Multiple'	0.0449	47.6	48.3	35.7
470	0.511	0.095	150	'Multiple'	0.0377	68.5	21.7	9.7
475	0.880	0.233	150	'Multiple'	0.1387	53.4	39.7	26.5
478	0.373	0.113	150	'Multiple'	0.0241	49.0	46.2	33.3
480	0.624	0.112	150	'Multiple'	0.0458	52.0	41.6	28.5
482	0.228	0.083	150	'Multiple'	0.0111	46.4	50.4	37.9
484	0.388	0.106	150	'Multiple'	0.0269	48.2	47.3	34.6
485	0.795	0.230	150	'Multiple'	0.1090	56.4	35.7	22.5
487	0.271	0.206	128	'Multiple'	0.0331	51.5	42.4	29.3
488	0.241	0.106	150	'Multiple'	0.0202	48.6	46.8	34.0
489	0.300	0.301	142	'Multiple'	0.0156	46.4	50.4	37.9

491	0.751	0.262	150	'Multiple'	0.1342	49.1	45.9	33.1
494	0.402	0.095	150	'Multiple'	0.0256	49.3	45.6	32.8
496	0.719	0.116	150	'Multiple'	0.0418	53.8	39.2	26.0
498	0.265	0.072	150	'Multiple'	0.0107	48.6	46.8	34.0
501	0.865	0.225	150	'Multiple'	0.1299	61.5	29.5	16.5
502	0.193	0.160	150	'Multiple'	0.0286	46.9	49.5	36.9
503	0.867	0.173	150	'Multiple'	0.0831	57.8	34.0	20.8
507	0.662	0.196	150	'Multiple'	0.0837	49.4	45.5	32.6

Appendix A.3 V=0.270m/s Single Contact Cusp Data

#	L (m)	W(m)	θ(°)	Contact type	Area(m^2)	ψ(°)	β(°)	α(°)	#
2	0.304	0.103	150	'Single'	0.017	46.7	49.9	37.3	43.3
3	0.105	0.045	136	'Single'	0.003	46.4	50.4	37.9	43.6
4	0.165	0.050	150	'Single'	0.004	46.9	49.6	37.0	43.1
7	0.306	0.132	142	'Single'	0.023	50.4	44.0	31.0	39.6
8	0.067	0.049	104	'Single'	0.002	46.4	50.4	37.9	43.6
10	0.193	0.082	150	'Single'	0.010	46.4	50.4	37.9	43.6
13	0.062	0.043	91	'Single'	0.001	56.2	36.0	22.7	33.8
14	0.172	0.057	148	'Single'	0.006	58.3	33.3	20.1	31.7
15	0.168	0.067	145	'Single'	0.006	47.4	48.7	36.1	42.6
18	0.085	0.042	146	'Single'	0.002	63.8	26.9	14.1	26.2
19	0.084	0.050	100	'Single'	0.002	46.4	50.4	37.9	43.6
20	0.093	0.062	91	'Single'	0.003	48.1	47.6	34.9	41.9
21	0.176	0.066	150	'Single'	0.007	46.9	49.4	36.9	43.1
23	0.080	0.049	104	'Single'	0.002	46.4	50.4	37.9	43.6
24	0.178	0.063	135	'Single'	0.006	46.8	49.8	37.2	43.2
26	0.120	0.080	101	'Single'	0.005	51.1	43.0	29.9	38.9
27	0.114	0.053	133	'Single'	0.004	46.6	50.1	37.6	43.4
28	0.162	0.057	148	'Single'	0.004	48.8	46.4	33.6	41.2
29	0.224	0.042	150	'Single'	0.005	56.2	36.0	22.7	33.8
30	0.126	0.066	124	'Single'	0.005	61.5	29.5	16.5	28.5
31	0.086	0.038	129	'Single'	0.002	65.4	25.1	12.5	24.6
33	0.077	0.035	150	'Single'	0.002	46.4	50.4	37.9	43.6
34	0.177	0.054	150	'Single'	0.006	48.6	46.8	34.0	41.4
35	0.160	0.054	150	'Single'	0.005	47.8	48.0	35.3	42.2
36	0.239	0.035	150	'Single'	0.007	56.2	36.0	22.7	33.8
39	0.282	0.089	150	'Single'	0.015	47.6	48.3	35.7	42.4
40	0.196	0.062	150	'Single'	0.007	47.8	48.0	35.3	42.2
42	0.167	0.064	150	'Single'	0.007	65.6	24.8	12.3	24.4
43	0.163	0.061	150	'Single'	0.006	46.4	50.4	37.9	43.6
45	0.114	0.046	126	'Single'	0.003	57.8	34.0	20.7	32.2
46	0.305	0.080	150	'Single'	0.014	47.5	48.5	35.9	42.5
47	0.086	0.045	123	'Single'	0.002	59.3	32.1	18.9	30.7
48	0.172	0.052	150	'Single'	0.005	49.1	45.9	33.1	40.9
49	0.148	0.059	150	'Single'	0.005	47.8	48.1	35.4	42.2
50	0.232	0.063	150	'Single'	0.010	67.6	22.7	10.5	22.4
53	0.355	0.101	150	'Single'	0.022	50.5	43.8	30.8	39.5
54	0.111	0.043	128	'Single'	0.002	47.0	49.4	36.8	43.0
55	0.252	0.052	150	'Single'	0.009	47.8	48.1	35.4	42.2
56	0.138	0.038	150	'Single'	0.003	47.2	49.0	36.4	42.8
59	0.253	0.082	150	'Single'	0.012	47.0	49.4	36.8	43.0
61	0.326	0.116	150	'Single'	0.019	57.7	34.1	20.8	32.3
64	0.125	0.057	128	'Single'	0.004	46.4	50.4	37.9	43.6
65	0.400	0.115	150	'Single'	0.027	51.5	42.4	29.3	38.5
66	0.333	0.105	150	'Single'	0.023	49.3	45.7	32.8	40.7

67	0.064	0.025	128	'Single'	0.001	60.1	31.2	18.0	29.9
68	0.157	0.058	142	'Single'	0.005	57.3	34.6	21.3	32.7
69	0.145	0.076	122	'Single'	0.006	46.9	49.6	37.0	43.1
70	0.343	0.115	150	'Single'	0.024	50.1	44.4	31.4	39.9
71	0.118	0.040	150	'Single'	0.003	65.0	25.5	12.9	25.0
73	0.169	0.041	150	'Single'	0.005	47.6	48.3	35.6	42.4
74	0.431	0.108	150	'Single'	0.020	58.9	32.6	19.4	31.1
75	0.162	0.057	148	'Single'	0.005	46.4	50.3	37.8	43.6
77	0.060	0.034	138	'Single'	0.001	59.0	32.5	19.3	31.0
78	0.104	0.048	137	'Single'	0.003	46.4	50.4	37.9	43.6
81	0.096	0.041	150	'Single'	0.003	46.5	50.3	37.8	43.5
84	0.140	0.060	118	'Single'	0.005	54.2	38.6	25.4	35.8
85	0.308	0.105	150	'Single'	0.020	52.7	40.7	27.5	37.3
89	0.098	0.064	107	'Single'	0.003	58.0	33.7	20.4	32.0
90	0.118	0.056	135	'Single'	0.003	59.3	32.1	18.9	30.7
94	0.179	0.052	150	'Single'	0.005	47.1	49.2	36.6	42.9
95	0.051	0.040	83	'Single'	0.001	49.4	45.4	32.5	40.6
96	0.215	0.086	133	'Single'	0.010	51.7	42.0	29.0	38.3
97	0.172	0.075	135	'Single'	0.007	48.0	47.6	34.9	42.0
98	0.100	0.046	131	'Single'	0.003	46.5	50.2	37.7	43.5
99	0.165	0.058	148	'Single'	0.005	55.9	36.4	23.1	34.1
101	0.284	0.114	145	'Single'	0.018	48.7	46.6	33.8	41.3
102	0.156	0.066	137	'Single'	0.006	47.2	48.9	36.3	42.8
104	0.058	0.034	109	'Single'	0.001	58.9	32.6	19.4	31.1
105	0.133	0.056	130	'Single'	0.004	47.1	49.2	36.6	42.9
107	0.155	0.055	150	'Single'	0.004	49.0	46.1	33.3	41.0
108	0.151	0.047	150	'Single'	0.004	47.4	48.7	36.0	42.6
109	0.203	0.093	150	'Single'	0.008	65.4	25.1	12.5	24.6
111	0.184	0.072	150	'Single'	0.008	46.6	50.0	37.5	43.4
113	0.101	0.072	103	'Single'	0.004	55.9	36.3	23.1	34.1
114	0.148	0.065	130	'Single'	0.005	46.8	49.7	37.2	43.2
116	0.113	0.044	117	'Single'	0.003	46.8	49.7	37.1	43.2
117	0.305	0.107	150	'Single'	0.019	47.7	48.2	35.6	42.3
119	0.253	0.117	150	'Single'	0.018	48.3	47.2	34.5	41.7
120	0.145	0.073	127	'Single'	0.006	53.3	39.8	26.6	36.7
121	0.094	0.040	125	'Single'	0.002	46.4	50.4	37.9	43.6
122	0.190	0.072	150	'Single'	0.008	48.3	47.2	34.4	41.7
124	0.453	0.169	150	'Single'	0.053	49.1	45.9	33.1	40.9
125	0.169	0.043	150	'Single'	0.004	46.7	49.9	37.3	43.3
128	0.092	0.035	141	'Single'	0.002	47.2	48.9	36.3	42.8
129	0.138	0.070	139	'Single'	0.005	48.2	47.4	34.7	41.8
130	0.203	0.055	150	'Single'	0.006	47.3	48.8	36.2	42.7
131	0.073	0.035	148	'Single'	0.001	53.7	39.2	26.0	36.3
132	0.173	0.051	150	'Single'	0.005	52.4	41.0	27.9	37.6
133	0.101	0.052	143	'Single'	0.003	57.4	34.5	21.3	32.6
136	0.181	0.087	150	'Single'	0.009	50.8	43.4	30.4	39.2
137	0.066	0.099	150	'Single'	0.004	47.7	48.2	35.5	42.3

138	0.099	0.047	146	'Single'	0.002	46.4	50.4	37.9	43.6
139	0.199	0.073	144	'Single'	0.007	57.2	34.7	21.4	32.8
140	0.139	0.054	150	'Single'	0.005	48.1	47.6	34.8	41.9
141	0.190	0.052	150	'Single'	0.007	55.5	36.8	23.6	34.5
143	0.163	0.055	150	'Single'	0.005	46.9	49.6	37.0	43.1
144	0.066	0.045	118	'Single'	0.002	61.9	29.0	16.0	28.1
146	0.152	0.059	149	'Single'	0.005	63.5	27.2	14.3	26.5
147	0.231	0.077	150	'Single'	0.010	46.5	50.3	37.8	43.5
148	0.156	0.070	145	'Single'	0.007	46.4	50.4	37.9	43.6
150	0.090	0.041	146	'Single'	0.002	47.7	48.2	35.5	42.3
152	0.122	0.036	150	'Single'	0.003	47.4	48.7	36.1	42.6
153	0.184	0.062	150	'Single'	0.006	51.1	43.0	29.9	38.9
154	0.135	0.047	150	'Single'	0.004	47.3	48.8	36.2	42.7
155	0.143	0.051	147	'Single'	0.004	49.9	44.7	31.8	40.1
156	0.097	0.065	105	'Single'	0.003	54.7	37.9	24.7	35.3
158	0.082	0.049	125	'Single'	0.002	46.4	50.4	37.9	43.6
162	0.089	0.029	135	'Single'	0.001	46.4	50.4	37.9	43.6
163	0.144	0.044	141	'Single'	0.004	47.1	49.2	36.6	42.9
164	0.132	0.051	147	'Single'	0.004	55.1	37.4	24.1	34.9
165	0.153	0.051	150	'Single'	0.005	49.9	44.7	31.8	40.1
166	0.113	0.044	150	'Single'	0.003	46.5	50.3	37.8	43.5
167	0.123	0.047	132	'Single'	0.003	50.5	43.8	30.8	39.5
168	0.140	0.039	150	'Single'	0.003	48.8	46.4	33.6	41.2
170	0.082	0.025	150	'Single'	0.001	47.3	48.9	36.2	42.7
171	0.160	0.059	150	'Single'	0.005	47.9	47.8	35.1	42.1
172	0.151	0.052	150	'Single'	0.004	48.4	47.0	34.2	41.6
173	0.256	0.069	150	'Single'	0.010	47.0	49.3	36.7	43.0
175	0.118	0.053	150	'Single'	0.003	46.6	50.1	37.5	43.4
178	0.098	0.036	124	'Single'	0.002	46.4	50.4	37.9	43.6
181	0.129	0.059	150	'Single'	0.004	49.3	45.6	32.7	40.7
183	0.122	0.050	132	'Single'	0.003	46.4	50.4	37.9	43.6
184	0.181	0.051	150	'Single'	0.005	48.3	47.2	34.4	41.7
186	0.231	0.059	150	'Single'	0.009	59.6	31.7	18.5	30.4
187	0.123	0.048	150	'Single'	0.003	47.0	49.4	36.8	43.0
189	0.128	0.045	148	'Single'	0.003	47.0	49.4	36.8	43.0
190	0.170	0.052	150	'Single'	0.006	58.3	33.4	20.1	31.7
193	0.238	0.095	150	'Single'	0.013	46.8	49.8	37.2	43.2
194	0.140	0.066	129	'Single'	0.005	46.4	50.4	37.9	43.6
196	0.138	0.073	121	'Single'	0.005	46.6	50.0	37.4	43.4
197	0.085	0.044	143	'Single'	0.002	57.1	34.9	21.6	32.9
199	0.134	0.046	150	'Single'	0.003	54.6	38.1	24.9	35.4
201	0.103	0.039	141	'Single'	0.002	47.9	47.9	35.2	42.1
202	0.093	0.039	135	'Single'	0.002	58.5	33.1	19.8	31.5
204	0.082	0.053	94	'Single'	0.002	46.4	50.4	37.9	43.6
205	0.078	0.042	108	'Single'	0.002	62.6	28.2	15.3	27.4
206	0.089	0.053	121	'Single'	0.003	61.8	29.2	16.1	28.2
208	0.135	0.057	127	'Single'	0.004	46.4	50.4	37.9	43.6

209	0.088	0.045	126	'Single'	0.002	51.0	43.1	30.0	39.0
211	0.108	0.048	148	'Single'	0.003	66.0	24.5	12.0	24.0
212	0.113	0.047	150	'Single'	0.003	47.0	49.4	36.8	43.0
215	0.282	0.083	150	'Single'	0.012	58.5	33.1	19.8	31.5
216	0.205	0.099	150	'Single'	0.010	47.5	48.5	35.9	42.5
218	0.087	0.036	129	'Single'	0.002	46.7	49.9	37.4	43.3
219	0.085	0.048	120	'Single'	0.002	48.6	46.7	33.9	41.4
220	0.195	0.069	148	'Single'	0.008	48.1	47.6	34.8	41.9
221	0.095	0.045	135	'Single'	0.002	51.2	42.8	29.7	38.8
223	0.149	0.064	150	'Single'	0.006	68.4	21.9	9.9	21.6
224	0.183	0.062	150	'Single'	0.006	47.0	49.4	36.8	43.0
226	0.365	0.128	150	'Single'	0.031	48.4	47.0	34.2	41.6
227	0.162	0.051	150	'Single'	0.005	60.8	30.3	17.2	29.2
228	0.083	0.048	128	'Single'	0.002	59.5	32.0	18.8	30.5
229	0.222	0.081	150	'Single'	0.011	46.4	50.4	37.9	43.6
231	0.144	0.050	149	'Single'	0.004	47.6	48.3	35.6	42.4
232	0.186	0.084	135	'Single'	0.008	56.9	35.1	21.8	33.1
234	0.152	0.063	135	'Single'	0.005	56.3	35.8	22.6	33.7
235	0.097	0.145	150	'Single'	0.006	46.5	50.1	37.6	43.5
236	0.101	0.050	122	'Single'	0.003	57.2	34.7	21.4	32.8
237	0.084	0.042	106	'Single'	0.002	47.3	48.8	36.2	42.7
239	0.197	0.060	150	'Single'	0.007	47.2	49.1	36.5	42.8
241	0.202	0.055	150	'Single'	0.007	64.1	26.6	13.8	25.9
242	0.128	0.055	145	'Single'	0.004	46.4	50.3	37.8	43.6
243	0.108	0.036	150	'Single'	0.002	67.0	23.4	11.1	23.0
244	0.120	0.042	140	'Single'	0.003	46.5	50.2	37.7	43.5
246	0.091	0.047	131	'Single'	0.002	47.0	49.4	36.8	43.0
247	0.127	0.048	141	'Single'	0.003	53.8	39.1	25.9	36.2
249	0.103	0.040	143	'Single'	0.002	46.4	50.4	37.9	43.6
250	0.141	0.036	150	'Single'	0.003	58.8	32.8	19.5	31.2
252	0.088	0.042	125	'Single'	0.002	46.7	49.9	37.3	43.3
255	0.231	0.089	138	'Single'	0.012	54.9	37.6	24.4	35.1
256	0.167	0.082	126	'Single'	0.008	46.8	49.7	37.2	43.2
259	0.070	0.055	101	'Single'	0.002	46.7	49.9	37.3	43.3
261	0.102	0.052	119	'Single'	0.003	46.5	50.1	37.6	43.5
262	0.213	0.071	145	'Single'	0.008	47.9	47.9	35.2	42.1
263	0.088	0.050	104	'Single'	0.002	46.4	50.4	37.9	43.6
264	0.139	0.063	124	'Single'	0.005	46.4	50.4	37.9	43.6
268	0.109	0.046	126	'Single'	0.003	46.6	50.1	37.5	43.4
271	0.139	0.044	150	'Single'	0.003	47.4	48.7	36.1	42.6
272	0.086	0.034	150	'Single'	0.002	49.2	45.9	33.0	40.8
275	0.111	0.045	139	'Single'	0.003	47.3	48.8	36.2	42.7
277	0.164	0.040	150	'Single'	0.004	47.9	47.9	35.2	42.1
279	0.144	0.051	143	'Single'	0.004	46.8	49.8	37.2	43.2
280	0.301	0.088	150	'Single'	0.016	52.4	41.0	27.9	37.6
281	0.110	0.041	148	'Single'	0.002	49.0	46.1	33.2	41.0
282	0.156	0.060	143	'Single'	0.005	49.6	45.2	32.3	40.4

283	0.073	0.039	106	'Single'	0.001	46.6	50.0	37.5	43.4
284	0.148	0.040	150	'Single'	0.003	47.3	48.8	36.2	42.7
286	0.174	0.055	146	'Single'	0.006	47.3	48.9	36.2	42.7
287	0.127	0.057	141	'Single'	0.004	46.4	50.4	37.9	43.6
289	0.073	0.041	106	'Single'	0.001	46.8	49.7	37.1	43.2
291	0.072	0.048	118	'Single'	0.002	51.4	42.5	29.4	38.6
292	0.048	0.033	109	'Single'	0.001	46.6	50.1	37.5	43.4
294	0.170	0.053	150	'Single'	0.005	58.1	33.6	20.3	31.9
295	0.261	0.090	150	'Single'	0.013	47.7	48.2	35.5	42.3
296	0.170	0.047	150	'Single'	0.005	58.6	32.9	19.7	31.4
297	0.128	0.030	150	'Single'	0.003	54.6	38.1	24.8	35.4
299	0.051	0.270	150	'Single'	0.009	47.0	49.3	36.7	43.0
300	0.119	0.057	124	'Single'	0.004	46.8	49.7	37.2	43.2
301	0.134	0.043	139	'Single'	0.003	46.8	49.7	37.2	43.2
302	0.162	0.068	147	'Single'	0.006	49.7	45.1	32.2	40.3
303	0.143	0.047	148	'Single'	0.004	47.7	48.2	35.5	42.3
306	0.112	0.051	150	'Single'	0.005	46.4	50.4	37.9	43.6
307	0.208	0.067	150	'Single'	0.010	47.5	48.6	35.9	42.5
309	0.068	0.041	110	'Single'	0.001	54.5	38.2	25.0	35.5
310	0.104	0.060	108	'Single'	0.003	46.5	50.3	37.8	43.5
311	0.082	0.032	140	'Single'	0.002	46.7	49.9	37.4	43.3
313	0.074	0.043	114	'Single'	0.002	47.2	49.0	36.4	42.8
316	0.169	0.058	140	'Single'	0.006	47.5	48.5	35.9	42.5
318	0.069	0.037	115	'Single'	0.001	67.3	23.0	10.8	22.7
319	0.252	0.065	150	'Single'	0.009	47.6	48.3	35.6	42.4
321	0.068	0.035	108	'Single'	0.001	46.4	50.4	37.9	43.6
323	0.061	0.030	135	'Single'	0.001	55.2	37.3	24.0	34.8
324	0.233	0.079	150	'Single'	0.011	47.7	48.2	35.6	42.3
325	0.090	0.041	150	'Single'	0.003	55.9	36.3	23.1	34.1
326	0.104	0.059	115	'Single'	0.003	46.4	50.4	37.9	43.6
330	0.139	0.061	150	'Single'	0.006	46.4	50.3	37.8	43.6
331	0.111	0.034	150	'Single'	0.002	61.8	29.1	16.1	28.2
333	0.134	0.060	150	'Single'	0.006	46.9	49.5	36.9	43.1
335	0.162	0.036	150	'Single'	0.004	46.4	50.4	37.9	43.6
337	0.092	0.069	150	'Single'	0.006	46.4	50.4	37.9	43.6
338	0.149	0.058	150	'Single'	0.005	58.9	32.6	19.3	31.1
340	0.174	0.074	140	'Single'	0.007	46.4	50.3	37.8	43.6
341	0.159	0.065	140	'Single'	0.005	47.3	48.8	36.2	42.7
342	0.099	0.049	137	'Single'	0.003	46.4	50.4	37.9	43.6
343	0.048	0.030	103	'Single'	0.001	47.4	48.7	36.0	42.6
345	0.051	0.039	97	'Single'	0.001	46.4	50.4	37.9	43.6
348	0.116	0.039	150	'Single'	0.003	46.4	50.4	37.9	43.6
349	0.185	0.051	150	'Single'	0.006	47.0	49.4	36.8	43.0
350	0.279	0.122	150	'Single'	0.020	50.1	44.4	31.5	39.9
351	0.194	0.102	150	'Single'	0.017	47.4	48.7	36.1	42.6
352	0.104	0.057	113	'Single'	0.003	46.4	50.4	37.9	43.6
353	0.094	0.051	107	'Single'	0.002	46.7	49.9	37.3	43.3

354	0.085	0.055	108	'Single'	0.003	47.9	47.8	35.1	42.1
356	0.078	0.052	101	'Single'	0.002	46.4	50.4	37.9	43.6
357	0.156	0.062	150	'Single'	0.005	47.3	48.9	36.3	42.7
358	0.082	0.042	120	'Single'	0.002	49.2	45.7	32.9	40.8
359	0.171	0.067	150	'Single'	0.007	47.3	48.9	36.3	42.7
361	0.204	0.061	150	'Single'	0.008	47.1	49.2	36.6	42.9
362	0.097	0.047	137	'Single'	0.002	46.4	50.4	37.9	43.6
364	0.097	0.051	131	'Single'	0.003	47.3	48.8	36.2	42.7
365	0.216	0.071	150	'Single'	0.009	61.0	30.1	17.0	29.0
366	0.190	0.067	139	'Single'	0.007	47.6	48.4	35.7	42.4
368	0.041	0.056	150	'Single'	0.002	47.2	49.0	36.4	42.8
369	0.213	0.066	150	'Single'	0.008	47.3	48.8	36.2	42.7
370	0.120	0.058	150	'Single'	0.003	51.2	42.8	29.8	38.8
371	0.065	0.042	104	'Single'	0.001	50.6	43.6	30.6	39.4
372	0.121	0.045	131	'Single'	0.003	46.8	49.7	37.2	43.2
375	0.102	0.037	126	'Single'	0.002	46.4	50.3	37.8	43.6
376	0.070	0.035	114	'Single'	0.001	60.5	30.7	17.6	29.5
377	0.090	0.051	112	'Single'	0.002	47.9	47.8	35.1	42.1
378	0.078	0.068	84	'Single'	0.003	46.8	49.7	37.1	43.2
380	0.135	0.061	131	'Single'	0.005	46.5	50.3	37.8	43.5
381	0.113	0.061	135	'Single'	0.004	59.3	32.1	18.9	30.7
383	0.090	0.035	138	'Single'	0.002	46.4	50.4	37.9	43.6
384	0.071	0.041	112	'Single'	0.001	47.9	47.8	35.1	42.1
385	0.215	0.071	150	'Single'	0.009	47.3	48.8	36.2	42.7
386	0.133	0.048	150	'Single'	0.004	47.1	49.2	36.6	42.9
389	0.160	0.052	150	'Single'	0.004	58.6	32.9	19.7	31.4
390	0.209	0.048	150	'Single'	0.006	47.8	48.0	35.3	42.2
391	0.082	0.044	119	'Single'	0.002	46.4	50.4	37.9	43.6
392	0.193	0.062	150	'Single'	0.007	46.4	50.4	37.9	43.6
394	0.136	0.052	150	'Single'	0.005	58.3	33.4	20.1	31.7
396	0.138	0.049	150	'Single'	0.004	46.7	49.8	37.3	43.3
397	0.067	0.040	114	'Single'	0.002	48.8	46.3	33.5	41.2
401	0.200	0.049	150	'Single'	0.007	47.4	48.7	36.1	42.6
402	0.273	0.049	150	'Single'	0.010	48.4	47.1	34.3	41.6
404	0.110	0.059	134	'Single'	0.004	46.6	50.0	37.5	43.4
405	0.062	0.046	150	'Single'	0.003	48.9	46.2	33.4	41.1
406	0.133	0.048	150	'Single'	0.004	46.9	49.4	36.9	43.1
408	0.112	0.098	150	'Single'	0.006	46.4	50.4	37.9	43.6
409	0.142	0.050	150	'Single'	0.004	46.7	49.9	37.4	43.3
411	0.212	0.074	150	'Single'	0.009	46.5	50.2	37.7	43.5
412	0.224	0.082	149	'Single'	0.011	49.6	45.2	32.3	40.4
414	0.152	0.055	150	'Single'	0.005	69.5	20.8	8.9	20.5
415	0.240	0.094	150	'Single'	0.012	48.3	47.2	34.4	41.7
416	0.077	0.044	103	'Single'	0.002	46.4	50.4	37.9	43.6
419	0.132	0.048	149	'Single'	0.003	47.6	48.4	35.7	42.4
421	0.155	0.054	150	'Single'	0.005	60.6	30.6	17.5	29.4
422	0.201	0.065	150	'Single'	0.007	47.7	48.2	35.6	42.3

423	0.084	0.038	132	'Single'	0.002	59.8	31.5	18.4	30.2
425	0.106	0.198	150	'Single'	0.007	46.6	50.0	37.4	43.4
427	0.052	0.036	109	'Single'	0.001	46.4	50.4	37.9	43.6
428	0.112	0.039	138	'Single'	0.003	47.3	48.8	36.2	42.7
429	0.122	0.049	150	'Single'	0.003	52.6	40.8	27.6	37.4
430	0.164	0.056	150	'Single'	0.005	48.5	46.9	34.1	41.5
431	0.113	0.054	125	'Single'	0.003	46.5	50.3	37.8	43.5
435	0.143	0.080	150	'Single'	0.007	52.3	41.2	28.1	37.7
436	0.110	0.055	150	'Single'	0.004	46.4	50.4	37.9	43.6
439	0.096	0.050	117	'Single'	0.003	46.4	50.4	37.9	43.6
440	0.081	0.038	128	'Single'	0.002	56.8	35.3	22.0	33.2
443	0.204	0.074	150	'Single'	0.012	46.8	49.7	37.2	43.2
445	0.141	0.060	141	'Single'	0.004	46.5	50.2	37.7	43.5
448	0.109	0.060	120	'Single'	0.004	50.8	43.3	30.3	39.2
449	0.151	0.042	150	'Single'	0.003	47.1	49.2	36.6	42.9
451	0.174	0.088	135	'Single'	0.008	47.2	49.0	36.4	42.8
452	0.155	0.067	135	'Single'	0.006	46.4	50.3	37.8	43.6
453	0.071	0.029	134	'Single'	0.001	64.9	25.7	13.0	25.1
455	0.087	0.053	115	'Single'	0.002	46.5	50.2	37.7	43.5
456	0.060	0.039	110	'Single'	0.001	48.8	46.4	33.6	41.2
461	0.100	0.054	116	'Single'	0.003	46.7	49.9	37.3	43.3
462	0.084	0.052	101	'Single'	0.002	46.4	50.3	37.8	43.6
463	0.070	0.041	112	'Single'	0.002	48.9	46.3	33.5	41.1
466	0.216	0.077	144	'Single'	0.011	46.4	50.4	37.9	43.6
467	0.125	0.064	127	'Single'	0.005	46.4	50.4	37.9	43.6
469	0.125	0.054	134	'Single'	0.004	47.1	49.2	36.6	42.9
470	0.042	0.104	150	'Single'	0.003	48.6	46.7	33.9	41.4
471	0.205	0.068	150	'Single'	0.008	48.2	47.4	34.7	41.8
473	0.189	0.052	150	'Single'	0.005	46.8	49.7	37.1	43.2
475	0.107	0.098	150	'Single'	0.007	46.4	50.4	37.9	43.6
476	0.121	0.061	121	'Single'	0.004	55.6	36.7	23.5	34.4
477	0.140	0.065	130	'Single'	0.005	46.7	49.9	37.4	43.3
478	0.099	0.036	150	'Single'	0.002	60.2	31.1	17.9	29.8
481	0.216	0.082	147	'Single'	0.011	47.6	48.3	35.6	42.4
484	0.140	0.079	120	'Single'	0.006	47.8	48.0	35.3	42.2
487	0.101	0.059	102	'Single'	0.003	46.5	50.2	37.7	43.5
489	0.143	0.064	150	'Single'	0.006	47.3	48.9	36.3	42.7
491	0.160	0.052	149	'Single'	0.005	47.0	49.3	36.7	43.0
492	0.158	0.049	142	'Single'	0.004	57.2	34.8	21.5	32.8
493	0.107	0.044	131	'Single'	0.003	47.5	48.6	35.9	42.5
495	0.104	0.038	150	'Single'	0.002	56.2	36.0	22.7	33.8
498	0.099	0.045	135	'Single'	0.002	56.1	36.1	22.9	33.9
499	0.147	0.067	129	'Single'	0.005	46.4	50.4	37.9	43.6
500	0.165	0.064	148	'Single'	0.006	56.3	35.9	22.6	33.7
502	0.148	0.056	150	'Single'	0.005	62.5	28.4	15.4	27.5
503	0.143	0.041	150	'Single'	0.004	67.7	22.6	10.4	22.3
505	0.169	0.070	150	'Single'	0.007	46.4	50.4	37.9	43.6

506	0.164	0.072	150	'Single'	0.009	49.9	44.7	31.8	40.1
509	0.136	0.054	143	'Single'	0.004	46.9	49.6	37.0	43.1
510	0.076	0.051	101	'Single'	0.002	46.4	50.4	37.9	43.6
511	0.123	0.062	121	'Single'	0.004	47.4	48.7	36.1	42.6
512	0.168	0.073	149	'Single'	0.007	50.4	44.0	31.0	39.6
513	0.196	0.072	150	'Single'	0.008	48.3	47.1	34.4	41.7
514	0.237	0.062	150	'Single'	0.008	48.5	46.9	34.2	41.5
515	0.128	0.049	150	'Single'	0.005	56.5	35.6	22.3	33.5
516	0.123	0.054	150	'Single'	0.004	52.8	40.5	27.3	37.2
517	0.204	0.078	150	'Single'	0.010	47.6	48.3	35.7	42.4
520	0.104	0.059	117	'Single'	0.003	46.4	50.4	37.9	43.6
521	0.102	0.064	117	'Single'	0.003	47.9	47.8	35.1	42.1
522	0.136	0.059	118	'Single'	0.004	46.7	49.9	37.3	43.3
524	0.136	0.065	107	'Single'	0.005	46.4	50.4	37.9	43.6
525	0.062	0.036	118	'Single'	0.001	46.9	49.6	37.0	43.1
526	0.102	0.054	115	'Single'	0.003	48.7	46.6	33.8	41.3
527	0.145	0.040	147	'Single'	0.003	46.9	49.5	36.9	43.1
529	0.254	0.046	150	'Single'	0.008	49.2	45.7	32.9	40.8
531	0.196	0.057	150	'Single'	0.007	46.4	50.4	37.9	43.6
532	0.135	0.055	144	'Single'	0.004	49.8	44.8	31.9	40.2
534	0.371	0.150	150	'Single'	0.034	46.5	50.2	37.7	43.5
535	0.141	0.055	150	'Single'	0.004	55.9	36.3	23.1	34.1
537	0.150	0.057	149	'Single'	0.004	61.1	30.0	16.9	28.9
538	0.217	0.086	148	'Single'	0.011	66.5	23.9	11.5	23.5
541	0.130	0.070	117	'Single'	0.005	46.5	50.3	37.8	43.5
544	0.126	0.061	140	'Single'	0.004	47.5	48.6	35.9	42.5
546	0.159	0.064	113	'Single'	0.004	46.4	50.4	37.9	43.6
547	0.052	0.049	65	'Single'	0.001	46.5	50.3	37.8	43.5
548	0.157	0.068	131	'Single'	0.006	48.4	47.1	34.3	41.6
550	0.171	0.087	132	'Single'	0.008	54.4	38.4	25.1	35.6
551	0.056	0.037	95	'Single'	0.001	46.5	50.2	37.7	43.5
554	0.114	0.037	150	'Single'	0.002	47.5	48.5	35.9	42.5
555	0.106	0.042	146	'Single'	0.002	52.4	41.1	28.0	37.6
556	0.122	0.043	144	'Single'	0.003	46.9	49.6	37.0	43.1

Appendix A.4 V=0.270m/s Multiple Contact Cusp Data

#	L (m)	W(m)	θ(°)	Contact type	Area(m^2)	ψ(°)	β(°)	α(°)	#
1	0.650	0.125	150	'Multiple'	0.047	54.8	37.8	24.5	35.2
5	0.589	0.146	150	'Multiple'	0.051	58.1	33.5	20.3	31.9
6	0.207	0.054	150	'Multiple'	0.007	46.8	49.7	37.1	43.2
9	0.453	0.140	150	'Multiple'	0.040	48.4	47.0	34.2	41.6
11	0.384	0.108	150	'Multiple'	0.027	50.1	44.5	31.5	39.9
12	0.477	0.129	150	'Multiple'	0.038	63.5	27.2	14.3	26.5
16	0.436	0.113	150	'Multiple'	0.031	54.6	38.1	24.9	35.4
17	0.452	0.168	144	'Multiple'	0.042	47.4	48.7	36.1	42.6
22	0.913	0.170	150	'Multiple'	0.108	56.8	35.2	22.0	33.2
25	0.278	0.098	150	'Multiple'	0.016	47.3	48.8	36.2	42.7
32	0.723	0.143	150	'Multiple'	0.068	53.6	39.4	26.1	36.4
37	0.359	0.077	150	'Multiple'	0.016	50.7	43.5	30.5	39.3
38	0.699	0.094	150	'Multiple'	0.050	54.6	38.1	24.9	35.4
41	0.658	0.114	150	'Multiple'	0.046	53.0	40.2	27.0	37.0
44	0.420	0.109	150	'Multiple'	0.031	49.5	45.3	32.5	40.5
51	0.506	0.128	150	'Multiple'	0.041	51.6	42.2	29.1	38.4
52	0.388	0.109	150	'Multiple'	0.028	48.7	46.6	33.8	41.3
57	0.314	0.075	150	'Multiple'	0.014	59.7	31.6	18.4	30.3
58	0.516	0.095	150	'Multiple'	0.031	52.3	41.2	28.0	37.7
60	0.649	0.111	150	'Multiple'	0.044	52.1	41.5	28.4	37.9
62	0.917	0.201	150	'Multiple'	0.114	58.1	33.6	20.3	31.9
63	0.418	0.105	150	'Multiple'	0.026	48.7	46.5	33.7	41.3
72	0.540	0.080	150	'Multiple'	0.032	65.6	24.9	12.3	24.4
76	0.317	0.098	150	'Multiple'	0.016	50.1	44.4	31.5	39.9
79	0.376	0.053	150	'Multiple'	0.016	58.0	33.7	20.5	32.0
80	0.468	0.096	150	'Multiple'	0.031	50.9	43.2	30.2	39.1
82	0.304	0.087	150	'Multiple'	0.016	49.3	45.6	32.7	40.7
83	0.672	0.198	150	'Multiple'	0.083	68.4	21.9	9.9	21.6
86	0.285	0.070	150	'Multiple'	0.011	48.5	46.8	34.1	41.5
87	0.579	0.119	150	'Multiple'	0.047	54.1	38.8	25.6	35.9
88	0.400	0.126	150	'Multiple'	0.029	51.2	42.8	29.7	38.8
91	0.392	0.103	150	'Multiple'	0.026	64.9	25.6	13.0	25.1
92	0.330	0.094	150	'Multiple'	0.019	57.4	34.5	21.2	32.6
93	0.713	0.124	150	'Multiple'	0.050	53.3	39.8	26.7	36.7
100	0.884	0.189	150	'Multiple'	0.130	58.6	32.9	19.7	31.4
103	0.455	0.125	150	'Multiple'	0.032	50.8	43.4	30.4	39.2
106	0.170	0.053	144	'Multiple'	0.005	58.8	32.7	19.5	31.2
110	0.620	0.158	150	'Multiple'	0.059	53.2	39.9	26.8	36.8
112	0.430	0.099	150	'Multiple'	0.029	48.9	46.2	33.4	41.1
115	0.707	0.138	150	'Multiple'	0.069	54.1	38.7	25.5	35.9
118	0.324	0.107	150	'Multiple'	0.025	55.0	37.6	24.3	35.0
123	0.931	0.142	150	'Multiple'	0.098	59.4	32.0	18.8	30.6
126	0.353	0.114	150	'Multiple'	0.024	48.2	47.3	34.6	41.8
127	0.745	0.170	150	'Multiple'	0.080	55.2	37.3	24.0	34.8

134	0.221	0.046	150	'Multiple'	0.007	48.5	46.9	34.2	41.5
135	0.437	0.100	150	'Multiple'	0.027	56.5	35.6	22.3	33.5
142	0.927	0.124	150	'Multiple'	0.079	54.5	38.2	25.0	35.5
145	0.627	0.154	150	'Multiple'	0.066	49.3	45.7	32.8	40.7
149	0.328	0.049	150	'Multiple'	0.011	52.2	41.3	28.2	37.8
151	0.674	0.201	150	'Multiple'	0.098	65.1	25.5	12.8	24.9
157	0.684	0.161	150	'Multiple'	0.100	50.3	44.2	31.2	39.7
159	0.306	0.087	150	'Multiple'	0.017	48.3	47.2	34.4	41.7
160	0.253	0.074	150	'Multiple'	0.012	65.5	25.0	12.4	24.5
161	0.743	0.138	150	'Multiple'	0.072	54.2	38.6	25.4	35.8
169	0.771	0.130	150	'Multiple'	0.069	54.9	37.7	24.4	35.1
174	0.714	0.093	150	'Multiple'	0.044	55.7	36.6	23.3	34.3
176	0.406	0.080	150	'Multiple'	0.021	51.8	41.9	28.8	38.2
177	0.472	0.092	150	'Multiple'	0.026	51.2	42.8	29.7	38.8
179	0.633	0.077	150	'Multiple'	0.034	53.9	39.0	25.8	36.1
180	0.820	0.086	150	'Multiple'	0.056	59.4	32.0	18.8	30.6
182	0.447	0.101	150	'Multiple'	0.033	50.4	43.9	30.9	39.6
185	0.309	0.070	150	'Multiple'	0.013	51.2	42.8	29.8	38.8
188	0.318	0.101	150	'Multiple'	0.019	49.7	44.9	32.0	40.3
191	0.638	0.129	150	'Multiple'	0.053	53.4	39.7	26.5	36.6
192	0.379	0.134	150	'Multiple'	0.036	70.3	19.9	8.3	19.7
195	0.354	0.078	150	'Multiple'	0.019	50.7	43.6	30.6	39.3
198	0.361	0.053	150	'Multiple'	0.013	49.2	45.8	33.0	40.8
200	0.425	0.103	150	'Multiple'	0.030	65.9	24.5	12.0	24.1
203	0.540	0.140	150	'Multiple'	0.044	51.2	42.8	29.7	38.8
207	0.199	0.066	150	'Multiple'	0.008	47.4	48.7	36.0	42.6
210	0.245	0.078	150	'Multiple'	0.011	48.7	46.5	33.7	41.3
213	0.420	0.045	150	'Multiple'	0.015	68.5	21.8	9.7	21.5
214	0.397	0.049	150	'Multiple'	0.014	50.4	43.9	31.0	39.6
217	0.481	0.113	150	'Multiple'	0.033	52.8	40.5	27.4	37.2
222	0.645	0.156	150	'Multiple'	0.074	51.8	41.9	28.8	38.2
225	0.311	0.104	150	'Multiple'	0.019	50.7	43.5	30.5	39.3
230	0.278	0.096	150	'Multiple'	0.017	59.0	32.5	19.3	31.0
233	0.363	0.099	150	'Multiple'	0.021	49.5	45.4	32.5	40.5
238	0.379	0.110	150	'Multiple'	0.025	66.5	23.9	11.5	23.5
240	0.761	0.168	150	'Multiple'	0.082	52.4	41.0	27.9	37.6
245	0.247	0.091	150	'Multiple'	0.013	50.0	44.6	31.6	40.0
248	0.267	0.149	150	'Multiple'	0.029	71.8	18.4	7.2	18.2
251	0.558	0.135	150	'Multiple'	0.047	53.3	39.8	26.6	36.7
253	0.164	0.076	150	'Multiple'	0.012	66.0	24.5	12.0	24.0
254	0.331	0.080	150	'Multiple'	0.017	48.3	47.1	34.4	41.7
257	0.275	0.072	150	'Multiple'	0.014	47.8	48.0	35.3	42.2
258	0.855	0.112	150	'Multiple'	0.072	56.3	35.9	22.6	33.7
260	0.143	0.232	150	'Multiple'	0.023	47.3	48.8	36.2	42.7
265	0.448	0.120	150	'Multiple'	0.033	52.7	40.6	27.5	37.3
266	0.279	0.077	150	'Multiple'	0.013	62.2	28.7	15.7	27.8
267	0.208	0.063	150	'Multiple'	0.009	48.1	47.5	34.7	41.9

269	0.307	0.075	150	'Multiple'	0.014	48.9	46.2	33.4	41.1
270	0.293	0.125	150	'Multiple'	0.022	65.2	25.3	12.7	24.8
273	0.315	0.056	150	'Multiple'	0.012	55.5	36.9	23.7	34.5
274	0.968	0.149	150	'Multiple'	0.103	59.8	31.6	18.4	30.2
276	0.227	0.083	150	'Multiple'	0.012	47.7	48.2	35.6	42.3
278	0.661	0.108	150	'Multiple'	0.050	54.2	38.6	25.4	35.8
285	0.494	0.128	150	'Multiple'	0.040	52.2	41.3	28.2	37.8
288	0.895	0.119	150	'Multiple'	0.089	60.4	30.8	17.6	29.6
290	0.242	0.127	112	'Multiple'	0.017	48.2	47.4	34.7	41.8
293	0.413	0.101	150	'Multiple'	0.024	50.9	43.3	30.3	39.1
298	0.726	0.135	150	'Multiple'	0.062	52.5	40.9	27.7	37.5
304	0.469	0.078	150	'Multiple'	0.026	63.5	27.3	14.4	26.5
305	0.949	0.196	150	'Multiple'	0.143	61.2	29.8	16.8	28.8
308	0.345	0.098	150	'Multiple'	0.021	48.1	47.5	34.8	41.9
312	0.302	0.109	150	'Multiple'	0.019	57.4	34.5	21.2	32.6
314	0.266	0.102	150	'Multiple'	0.015	48.7	46.5	33.7	41.3
315	0.283	0.167	137	'Multiple'	0.025	53.6	39.4	26.2	36.4
317	0.699	0.111	150	'Multiple'	0.059	51.9	41.7	28.6	38.1
320	0.555	0.079	150	'Multiple'	0.038	51.7	42.0	28.9	38.3
322	0.374	0.110	150	'Multiple'	0.028	68.7	21.5	9.6	21.3
327	0.326	0.101	150	'Multiple'	0.018	62.3	28.6	15.7	27.7
328	0.382	0.108	150	'Multiple'	0.029	52.0	41.6	28.5	38.0
329	0.184	0.064	150	'Multiple'	0.009	47.7	48.2	35.6	42.3
332	0.201	0.093	150	'Multiple'	0.013	50.2	44.3	31.3	39.8
334	0.551	0.097	150	'Multiple'	0.038	62.6	28.2	15.3	27.4
336	0.467	0.099	150	'Multiple'	0.031	50.7	43.5	30.5	39.3
339	0.588	0.120	150	'Multiple'	0.044	51.7	42.0	29.0	38.3
344	0.372	0.126	150	'Multiple'	0.027	49.8	44.9	31.9	40.2
346	0.377	0.095	150	'Multiple'	0.024	57.8	34.0	20.8	32.2
347	0.416	0.167	150	'Multiple'	0.056	50.1	44.5	31.5	39.9
355	0.936	0.139	150	'Multiple'	0.103	58.9	32.6	19.3	31.1
360	0.781	0.191	150	'Multiple'	0.096	53.8	39.2	26.0	36.2
363	0.454	0.162	150	'Multiple'	0.046	49.2	45.9	33.0	40.8
367	0.611	0.105	150	'Multiple'	0.043	53.7	39.3	26.1	36.3
373	0.453	0.124	150	'Multiple'	0.035	66.2	24.2	11.8	23.8
374	0.500	0.174	150	'Multiple'	0.054	51.2	42.8	29.8	38.8
379	0.341	0.089	150	'Multiple'	0.019	48.3	47.2	34.4	41.7
382	0.792	0.111	150	'Multiple'	0.059	55.6	36.8	23.5	34.4
387	0.374	0.086	150	'Multiple'	0.022	63.3	27.5	14.6	26.7
388	0.465	0.099	150	'Multiple'	0.029	50.2	44.3	31.3	39.8
393	0.324	0.091	150	'Multiple'	0.018	51.1	42.9	29.8	38.9
395	0.152	0.059	150	'Multiple'	0.004	64.6	26.0	13.3	25.4
398	0.358	0.093	150	'Multiple'	0.021	64.2	26.4	13.6	25.8
399	0.328	0.096	150	'Multiple'	0.021	55.7	36.7	23.4	34.3
400	0.527	0.138	150	'Multiple'	0.045	50.4	43.9	30.9	39.6
403	0.895	0.185	150	'Multiple'	0.126	64.3	26.4	13.6	25.7
407	0.511	0.135	150	'Multiple'	0.049	50.8	43.4	30.4	39.2

410	0.332	0.069	150	'Multiple'	0.016	48.6	46.7	33.9	41.4
413	0.503	0.146	150	'Multiple'	0.045	58.4	33.3	20.0	31.6
417	0.145	0.068	150	'Multiple'	0.010	52.6	40.8	27.7	37.4
418	0.190	0.058	150	'Multiple'	0.006	46.9	49.5	37.0	43.1
420	0.488	0.130	150	'Multiple'	0.036	50.9	43.2	30.2	39.1
424	0.524	0.131	150	'Multiple'	0.039	49.9	44.6	31.7	40.1
426	0.375	0.058	150	'Multiple'	0.019	68.1	22.2	10.1	21.9
432	0.656	0.163	150	'Multiple'	0.083	62.4	28.5	15.5	27.6
433	0.246	0.092	150	'Multiple'	0.022	47.2	48.9	36.3	42.8
434	0.207	0.082	150	'Multiple'	0.012	46.7	49.9	37.3	43.3
437	0.321	0.104	150	'Multiple'	0.032	56.3	35.9	22.6	33.7
438	0.382	0.124	150	'Multiple'	0.032	48.6	46.8	34.0	41.4
441	0.236	0.071	150	'Multiple'	0.010	47.3	48.8	36.2	42.7
442	0.733	0.155	150	'Multiple'	0.067	53.5	39.6	26.4	36.5
444	0.458	0.122	150	'Multiple'	0.038	49.1	45.9	33.1	40.9
446	0.525	0.188	150	'Multiple'	0.075	67.6	22.7	10.5	22.4
447	0.273	0.093	150	'Multiple'	0.016	47.0	49.3	36.7	43.0
450	0.557	0.160	150	'Multiple'	0.053	53.5	39.5	26.3	36.5
454	0.185	0.082	138	'Multiple'	0.008	50.6	43.6	30.6	39.4
457	0.320	0.078	150	'Multiple'	0.016	47.9	47.9	35.2	42.1
458	0.223	0.064	150	'Multiple'	0.011	54.8	37.8	24.6	35.2
459	0.609	0.106	150	'Multiple'	0.055	64.5	26.1	13.4	25.5
460	0.654	0.159	150	'Multiple'	0.070	51.2	42.8	29.7	38.8
464	0.293	0.118	150	'Multiple'	0.021	47.7	48.2	35.6	42.3
465	0.312	0.119	145	'Multiple'	0.021	52.6	40.8	27.6	37.4
468	0.673	0.208	150	'Multiple'	0.096	52.2	41.3	28.2	37.8
472	0.520	0.122	150	'Multiple'	0.042	54.5	38.2	25.0	35.5
474	0.287	0.121	150	'Multiple'	0.022	50.1	44.4	31.5	39.9
479	0.327	0.078	150	'Multiple'	0.016	50.2	44.3	31.3	39.8
480	0.315	0.049	150	'Multiple'	0.013	58.8	32.7	19.5	31.2
482	0.607	0.091	150	'Multiple'	0.043	57.8	33.9	20.7	32.2
483	0.233	0.077	150	'Multiple'	0.010	48.1	47.6	34.9	41.9
485	0.423	0.089	150	'Multiple'	0.023	54.4	38.4	25.1	35.6
486	0.238	0.088	144	'Multiple'	0.011	48.0	47.7	35.0	42.0
488	0.817	0.114	150	'Multiple'	0.075	63.0	27.8	14.9	27.0
490	0.317	0.104	150	'Multiple'	0.021	48.4	47.1	34.3	41.6
494	0.440	0.082	150	'Multiple'	0.025	51.4	42.5	29.5	38.6
496	0.338	0.080	150	'Multiple'	0.016	60.2	31.1	17.9	29.8
497	0.421	0.075	150	'Multiple'	0.019	49.9	44.7	31.8	40.1
501	0.347	0.117	150	'Multiple'	0.021	49.1	45.9	33.1	40.9
504	0.612	0.075	150	'Multiple'	0.034	55.0	37.5	24.2	35.0
507	0.181	0.049	150	'Multiple'	0.006	56.2	36.0	22.7	33.8
508	0.995	0.189	150	'Multiple'	0.146	58.0	33.7	20.4	32.0
518	0.847	0.200	150	'Multiple'	0.115	57.6	34.2	21.0	32.4
519	0.254	0.148	131	'Multiple'	0.020	47.5	48.4	35.8	42.5
523	0.750	0.234	150	'Multiple'	0.109	52.9	40.4	27.2	37.1
528	0.306	0.051	150	'Multiple'	0.010	49.2	45.8	32.9	40.8

530	0.714	0.162	150	'Multiple'	0.082	51.8	42.0	28.9	38.2
533	0.632	0.161	150	'Multiple'	0.066	52.4	41.1	27.9	37.6
536	0.514	0.116	150	'Multiple'	0.036	52.0	41.6	28.5	38.0
539	0.441	0.079	150	'Multiple'	0.024	55.8	36.5	23.2	34.2
540	0.211	0.050	150	'Multiple'	0.007	48.1	47.6	34.8	41.9
542	0.877	0.147	150	'Multiple'	0.096	55.2	37.3	24.1	34.8
543	0.308	0.084	150	'Multiple'	0.019	47.7	48.2	35.5	42.3
545	0.721	0.216	150	'Multiple'	0.102	50.4	43.9	30.9	39.6
549	0.350	0.141	150	'Multiple'	0.026	49.3	45.7	32.8	40.7
552	0.192	0.071	144	'Multiple'	0.008	47.6	48.3	35.7	42.4
553	0.404	0.071	150	'Multiple'	0.024	58.8	32.7	19.5	31.2
557	0.294	0.117	150	'Multiple'	0.025	52.3	41.2	28.1	37.7

Appendix B - Icebreaking Pattern Photographs

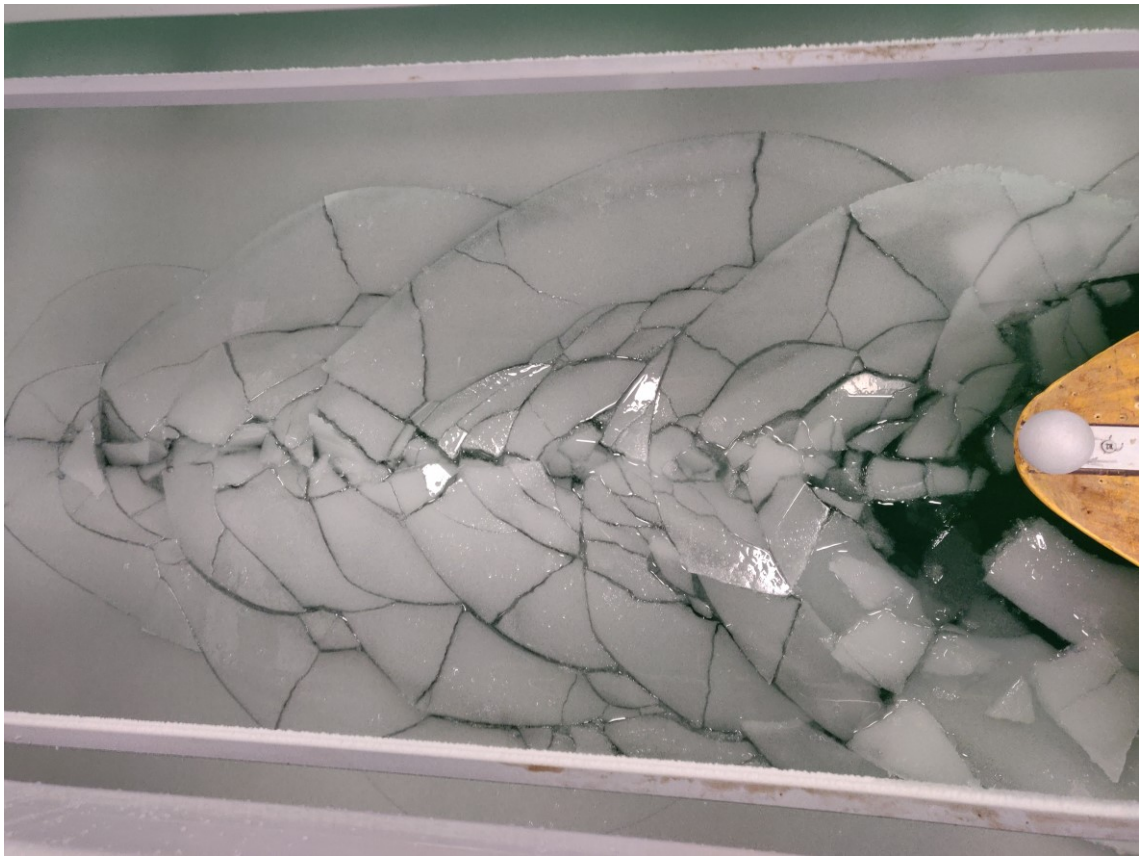

Photograph of V=0.162m/s icebreaking pattern

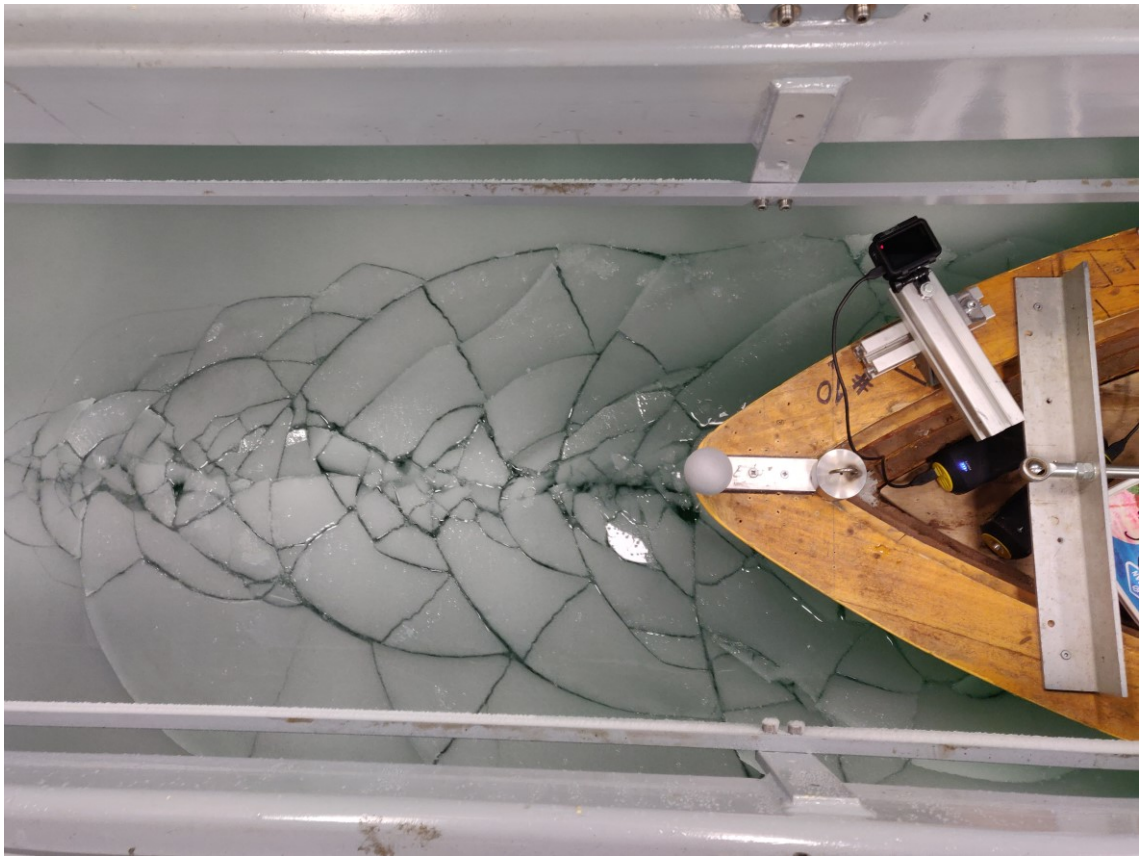

Photograph of V=0.270m/s icebreaking pattern

Appendix C - Distributions and Histograms

Appendix C.1 V=0.162m/s Histograms

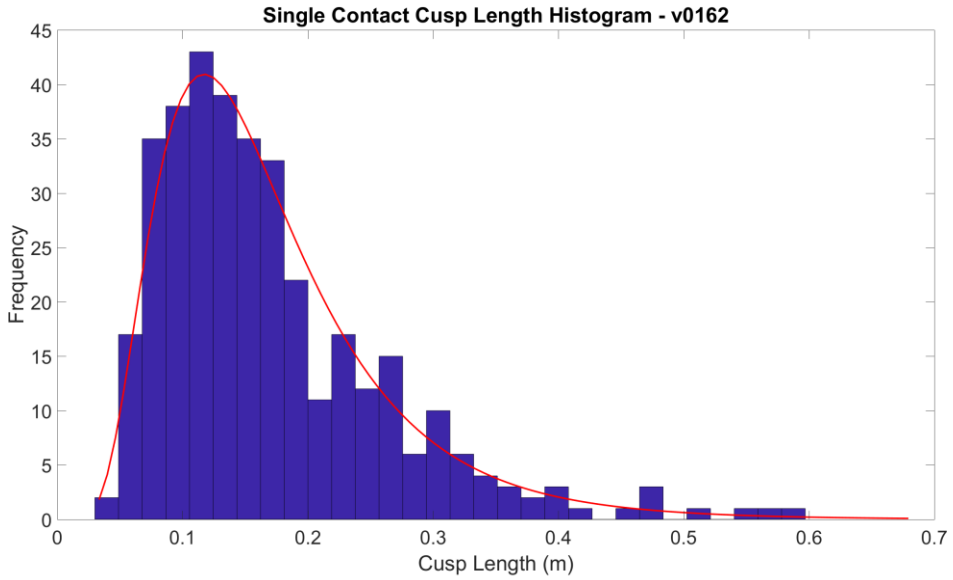
Single Contact Cusp Length Histogram - v0162
Frequency
Cusp Length (m)
0
5
10
15
20
25
30
35
40
45
0
0.1
0.2
0.3
0.4
0.5
0.6
0.7

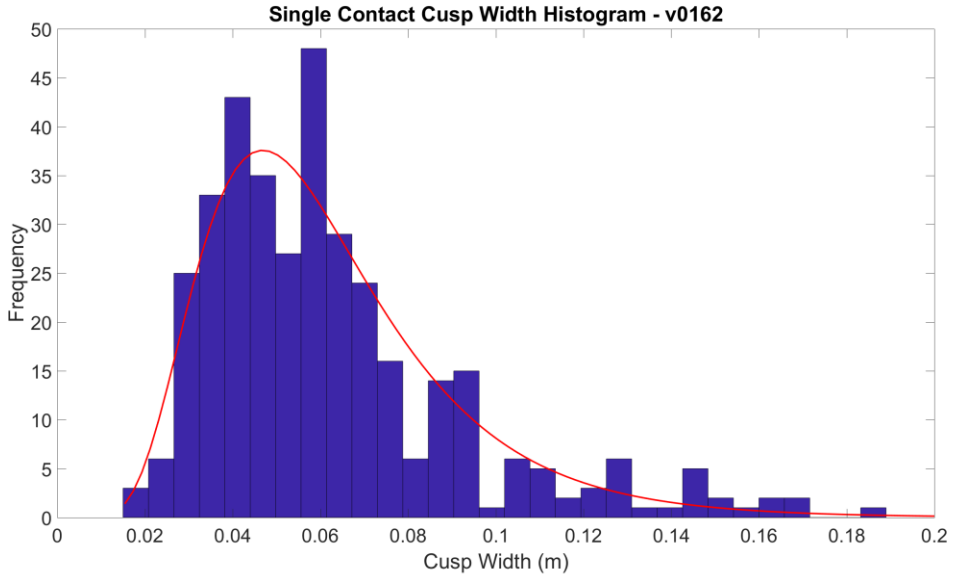
Single Contact Cusp Width Histogram - v0162
Frequency
Cusp Width (m)
0
5
10
15
20
25
30
35
40
45
50
0
0.02
0.04
0.06
0.08
0.1
0.12
0.14
0.16
0.18
0.2

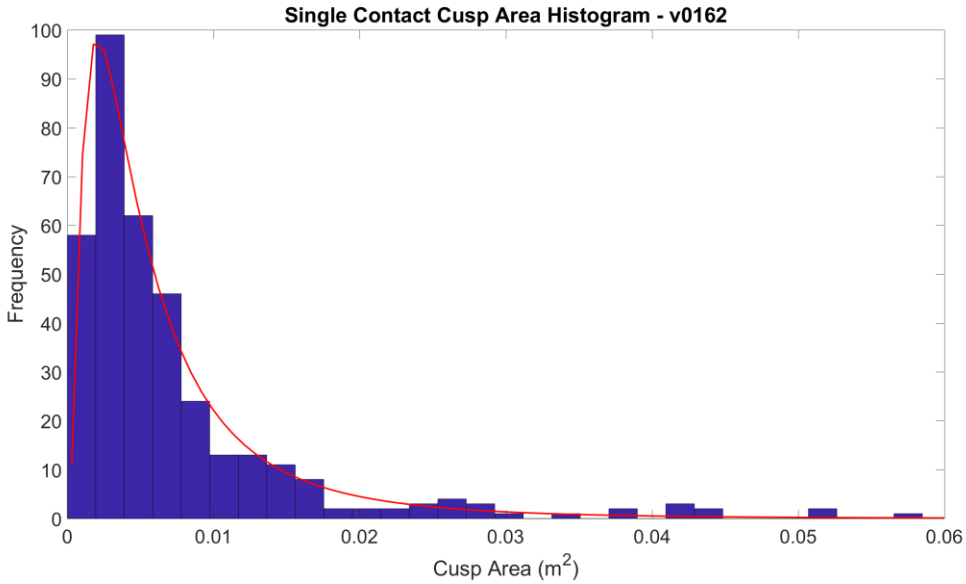
Single Contact Cusp Area Histogram - v0162
Frequency
Cusp Area (m2)
0
10
20
30
40
50
60
70
80
90
100
0
0.01
0.02
0.03
0.04
0.05
0.06

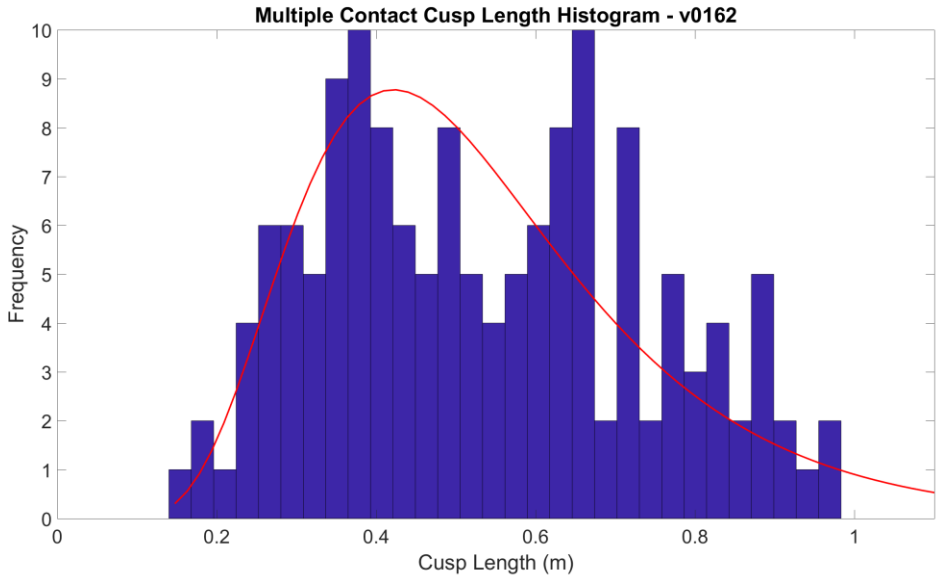
Multiple Contact Cusp Length Histogram - v0162
Frequency
Cusp Length (m)
0
1
2
3
4
5
6
7
8
9
10
0
0.2
0.4
0.6
0.8
1

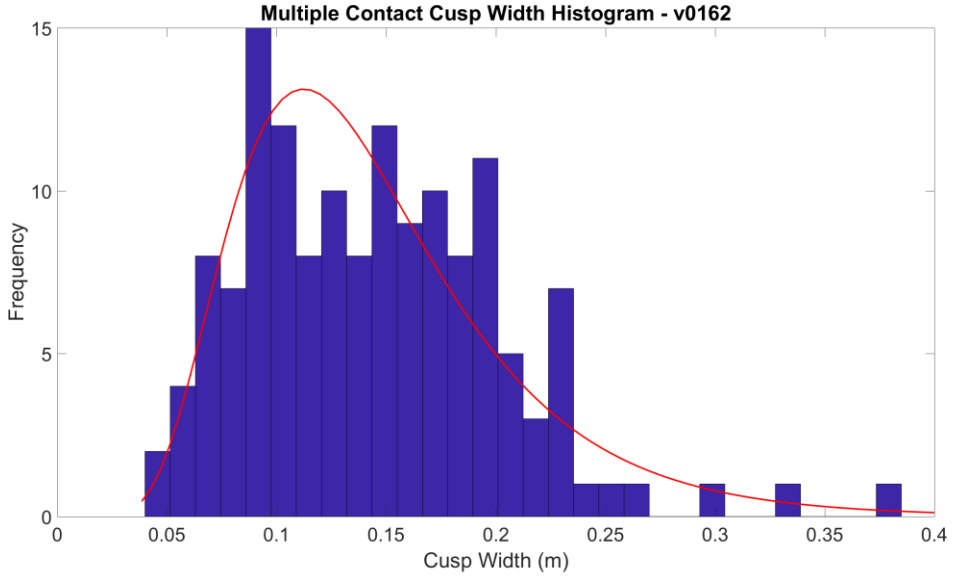
Multiple Contact Cusp Width Histogram - v0162
Frequency
Cusp Width (m)
0
5
10
15
0
0.05
0.1
0.15
0.2
0.25
0.3
0.35
0.4

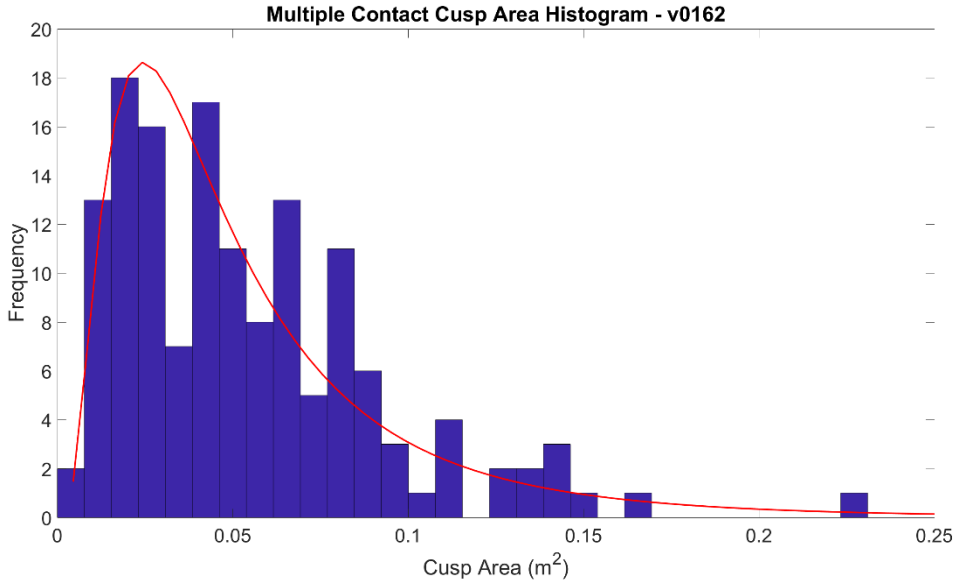
Multiple Contact Cusp Area Histogram - v0162
Frequency
Cusp Area (m2)
0
2
4
6
8
10
12
14
16
18
20
0
0.05
0.1
0.15
0.2
0.25

,

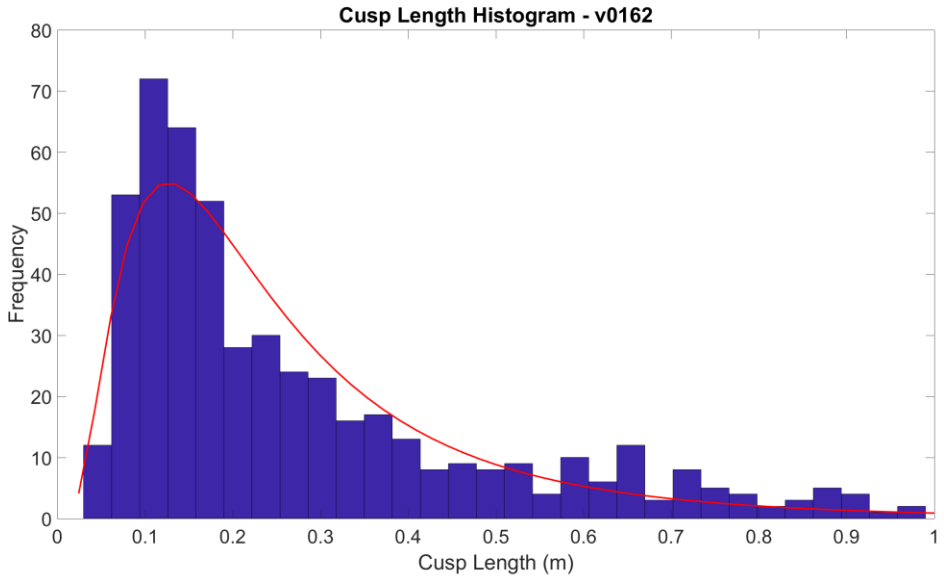
Cusp Length Histogram - v0162
Frequency
Cusp Length (m)
0
10
20
30
40
50
60
70
80
0
0.1
0.2
0.3
0.4
0.5
0.6
0.7
0.8
0.9
1

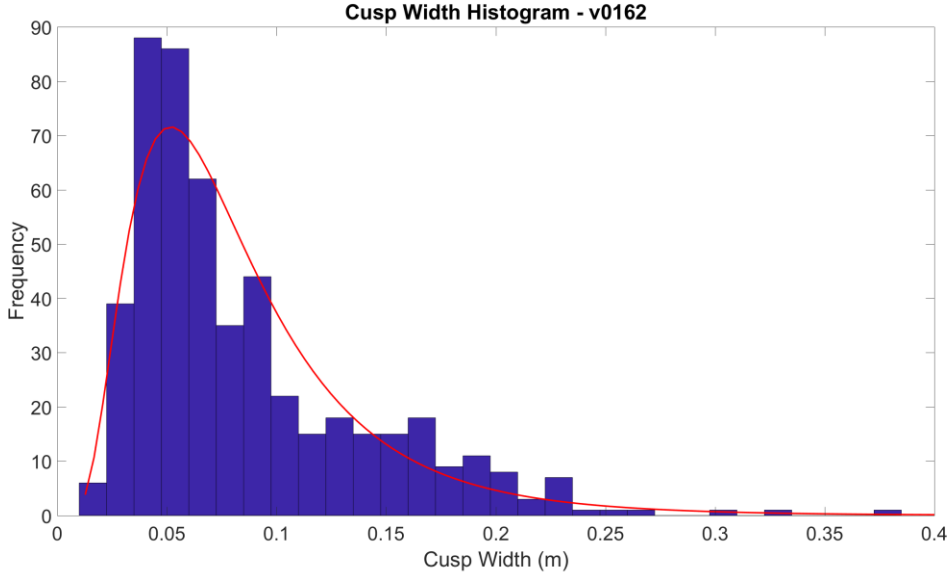
Cusp Width Histogram - v0162
Frequency
Cusp Width (m)
0
10
20
30
40
50
60
70
80
90
0
0.05
0.1
0.15
0.2
0.25
0.3
0.35
0.4

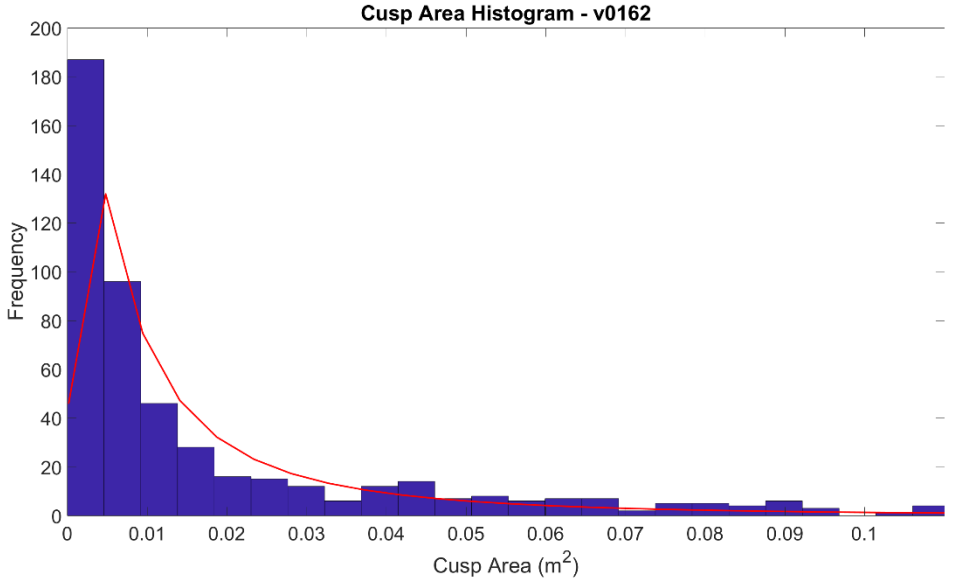
Cusp Area Histogram - v0162
Frequency
Cusp Area (m2)
0
20
40
60
80
100
120
140
160
180
200
0
0.01
0.02
0.03
0.04
0.05
0.06
0.07
0.08
0.09
0.1

Appendix C.2 V=0.162m/s Distributions

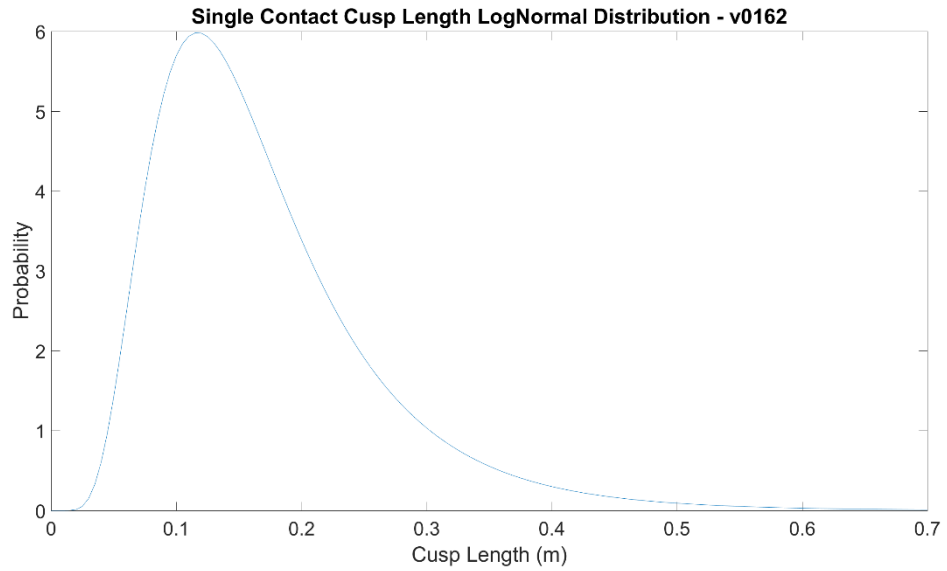
Single Contact Cusp Length LogNormal Distribution - v0162
Probability
Cusp Length (m)
0
1
2
3
4
5
6
0
0.1
0.2
0.3
0.4
0.5
0.6
0.7

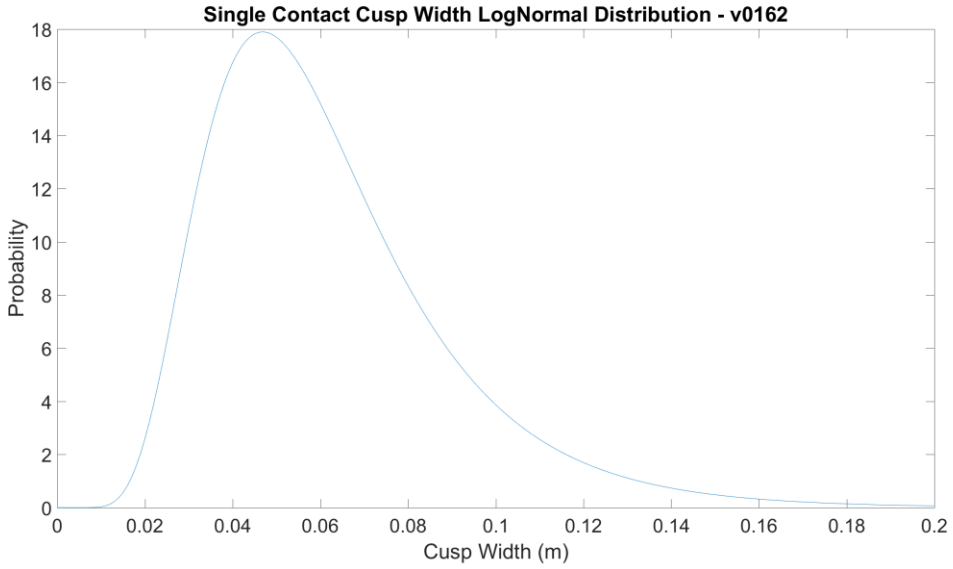
Single Contact Cusp Width LogNormal Distribution - v0162
Probability
Cusp Width (m)
0
2
4
6
8
10
12
14
16
18
0
0.02
0.04
0.06
0.08
0.1
0.12
0.14
0.16
0.18
0.2

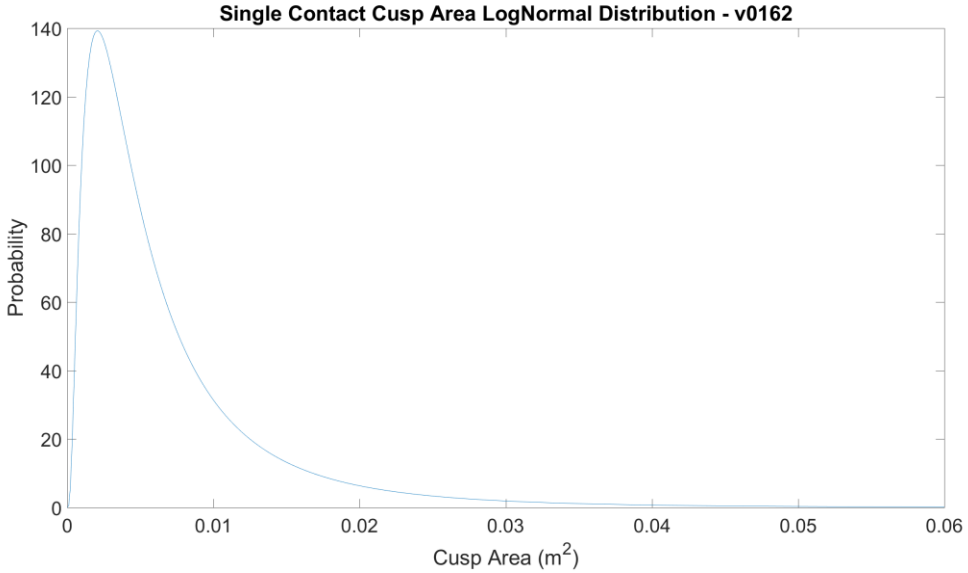
Single Contact Cusp Area LogNormal Distribution - v0162
Probability
Cusp Area (m2)
0
20
40
60
80
100
120
140
0
0.01
0.02
0.03
0.04
0.05
0.06

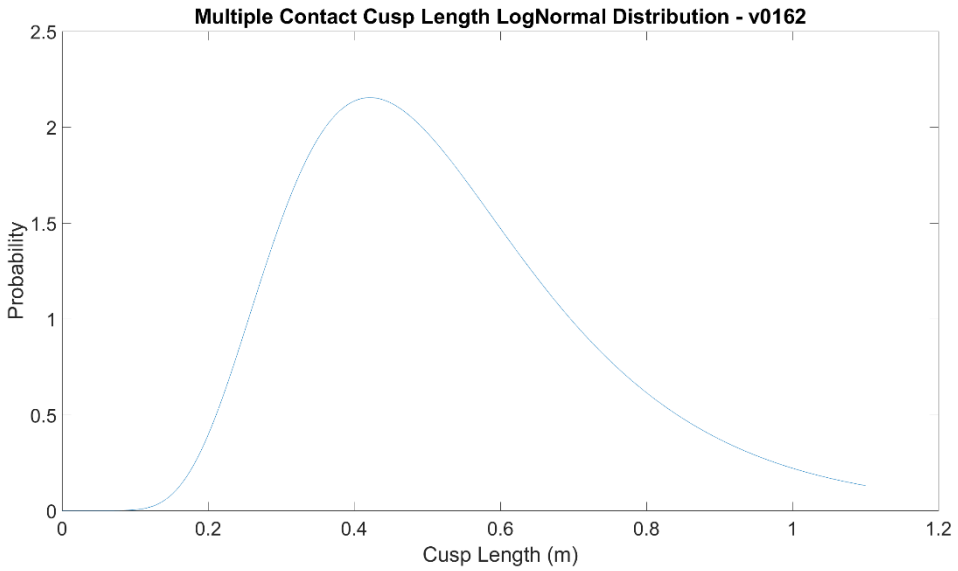
Multiple Contact Cusp Length LogNormal Distribution - v0162
Probability
Cusp Length (m)
0
0.5
1
1.5
2
2.5
0.2
0.4
0.6
0.8
1
1.2

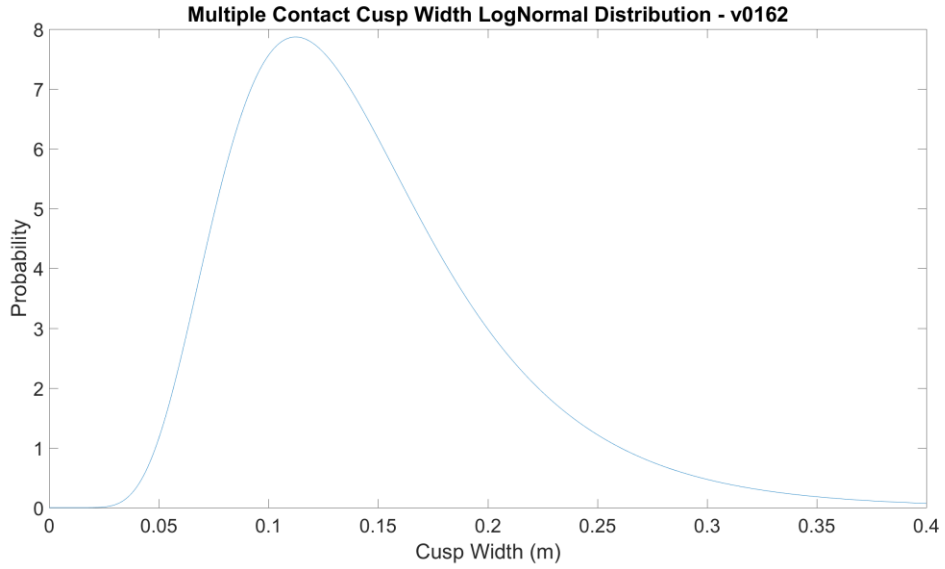
Multiple Contact Cusp Width LogNormal Distribution - v0162
Probability
Cusp Width (m)
0
1
2
3
4
5
6
7
8
0.05
0.1
0.15
0.2
0.25
0.3
0.35
0.4

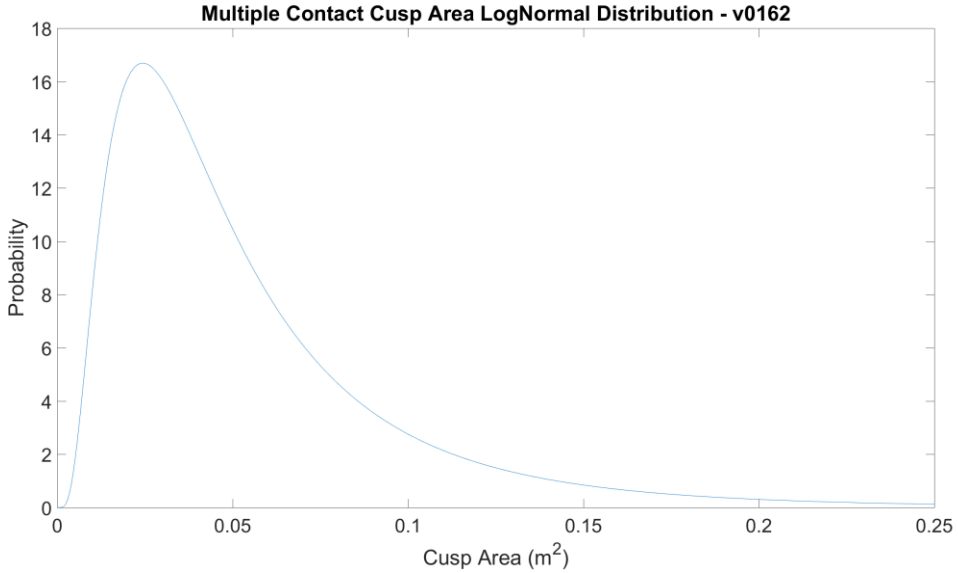
Multiple Contact Cusp Area LogNormal Distribution - v0162
Probability
Cusp Area (m2)
0
2
4
6
8
10
12
14
16
18
0.05
0.1
0.15
0.2
0.25

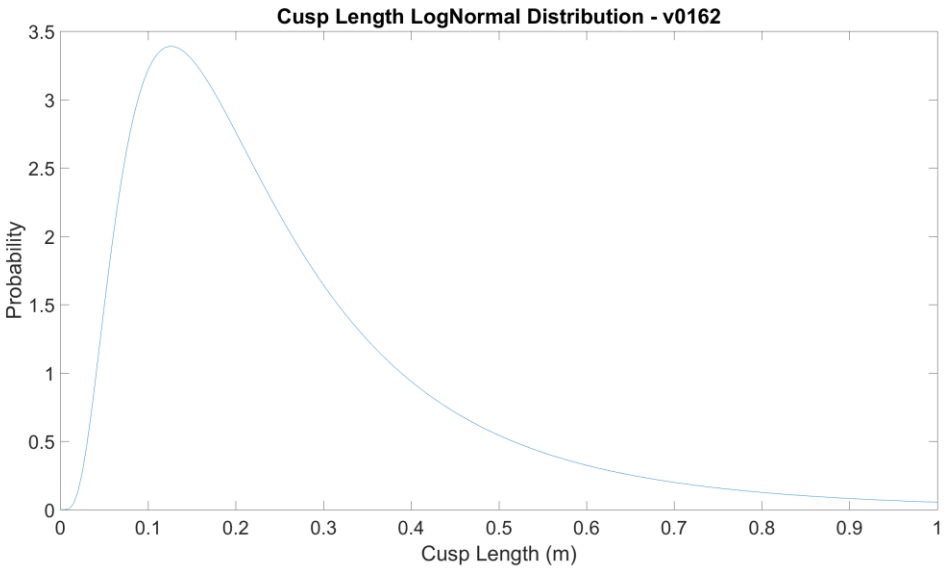
Cusp Length LogNormal Distribution - v0162
Probability
Cusp Length (m)
0
0.5
1
1.5
2
2.5
3
3.5
0.1
0.2
0.3
0.4
0.5
0.6
0.7
0.8
0.9

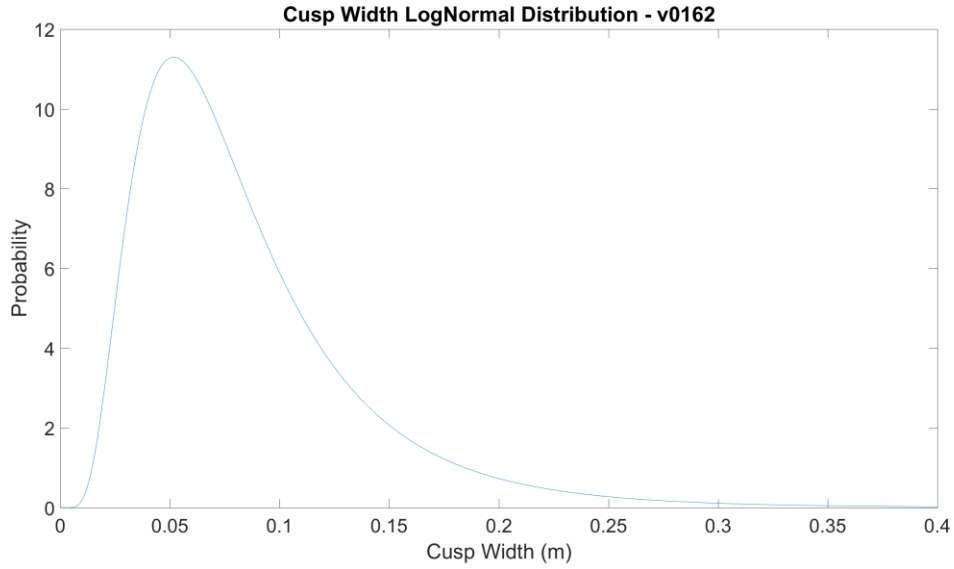
Cusp Width LogNormal Distribution - v0162
Probability
Cusp Width (m)
0
2
4
6
8
10
12
0.05
0.1
0.15
0.2
0.25
0.3
0.35
0.4

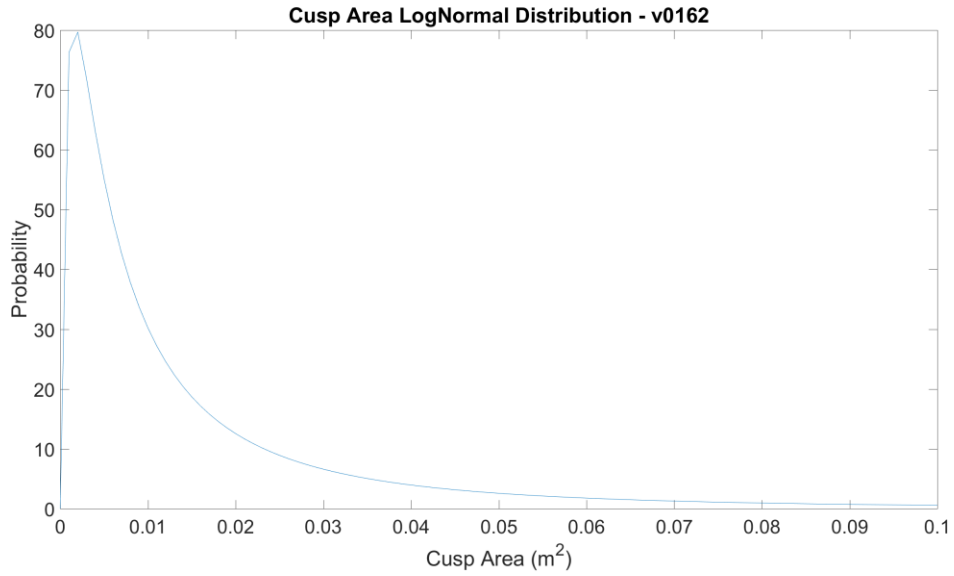
Cusp Area LogNormal Distribution - v0162
Probability
Cusp Area (m2)
0
10
20
30
40
50
60
70
80
0.01
0.02
0.03
0.04
0.05
0.06
0.07
0.08
0.09
0.1

Appendix C.3 V=0.270m/s Histograms

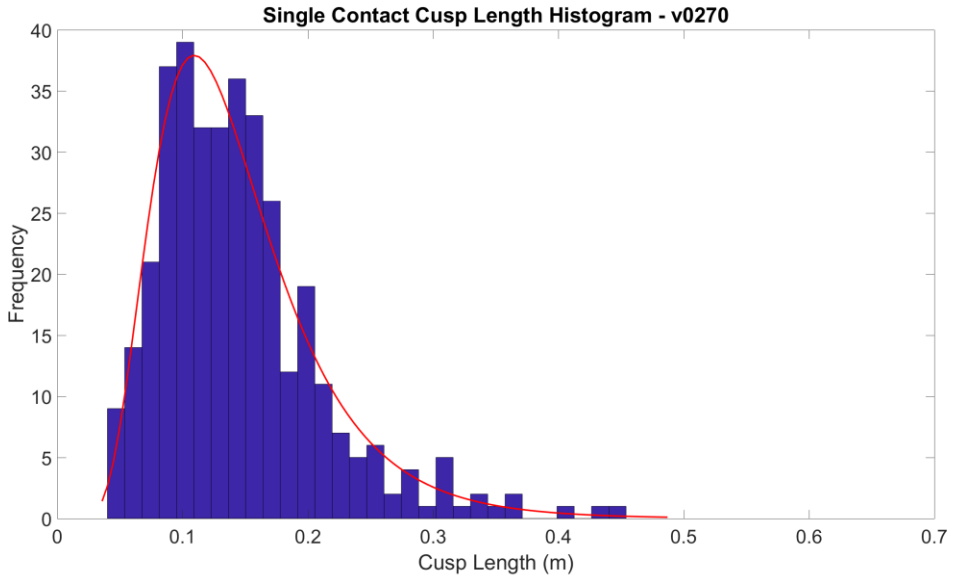
Single Contact Cusp Length Histogram - v0270
Frequency
Cusp Length (m)
0
5
10
15
20
25
30
35
40
0
0.1
0.2
0.3
0.4
0.5
0.6
0.7

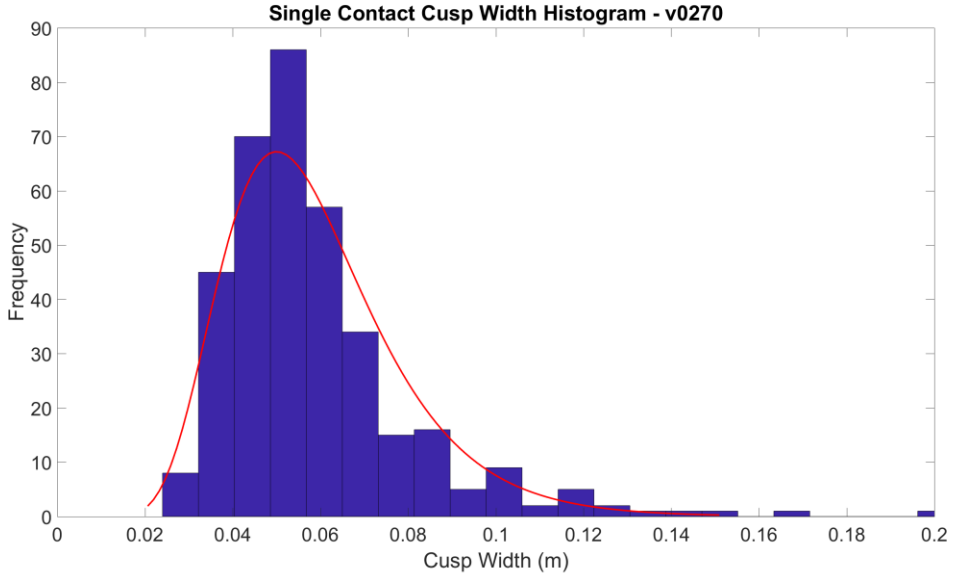
Single Contact Cusp Width Histogram - v0270
Frequency
Cusp Width (m)
0
10
20
30
40
50
60
70
80
90
0
0.02
0.04
0.06
0.08
0.1
0.12
0.14
0.16
0.18
0.2

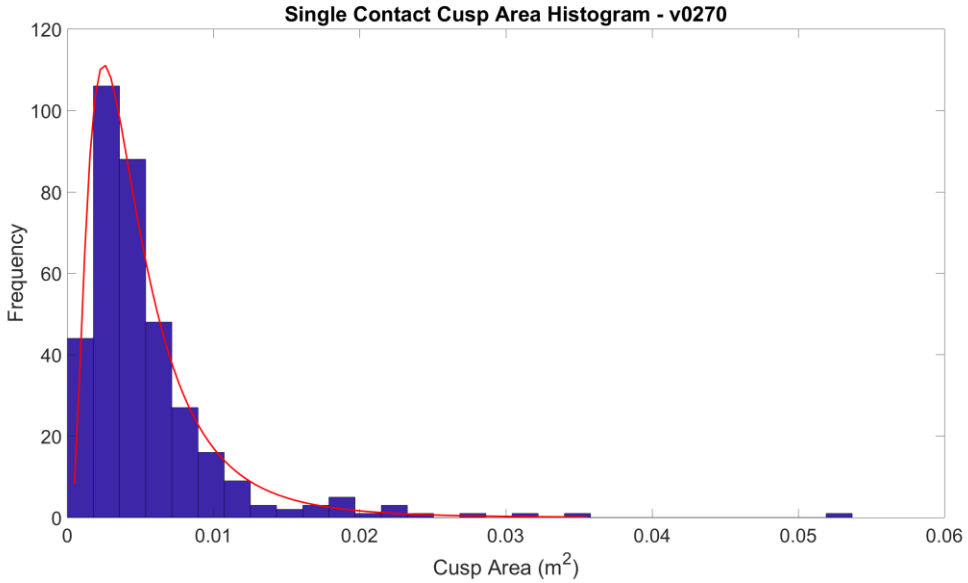
Single Contact Cusp Area Histogram - v0270
Frequency
Cusp Area (m2)
0
20
40
60
80
100
120
0
0.01
0.02
0.03
0.04
0.05
0.06

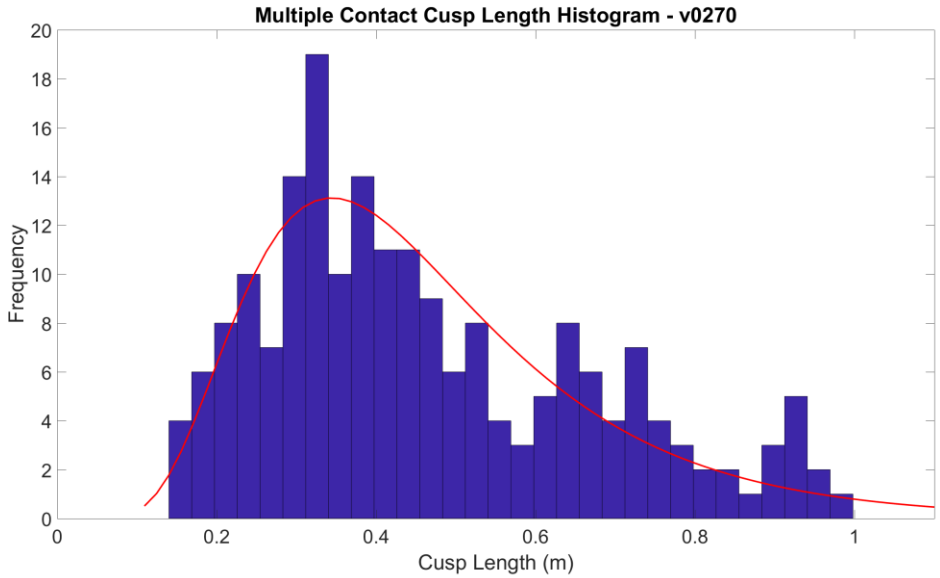
Multiple Contact Cusp Length Histogram - v0270
Frequency
Cusp Length (m)
0
2
4
6
8
10
12
14
16
18
20
0.2
0.4
0.6
0.8
1

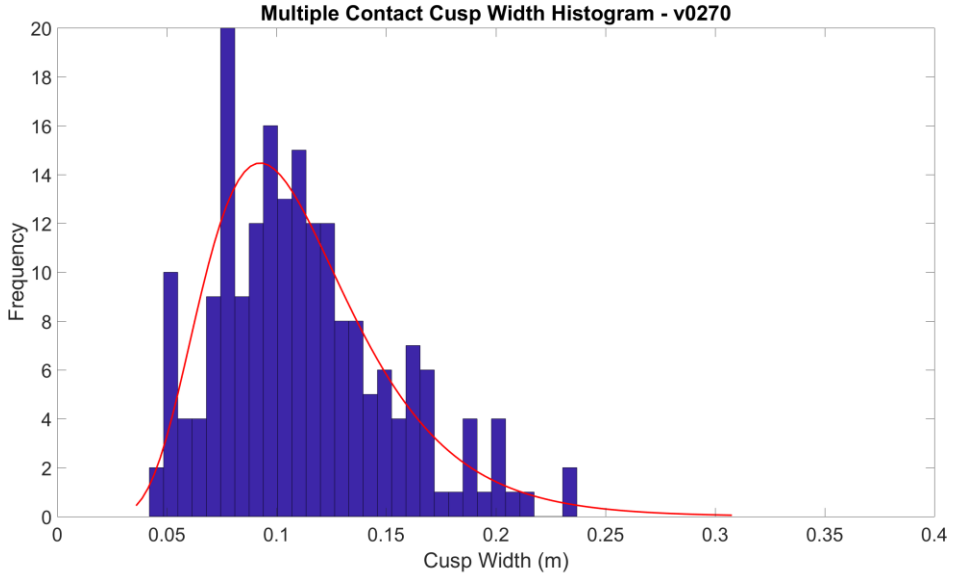
Multiple Contact Cusp Width Histogram - v0270
Frequency
Cusp Width (m)
0
2
4
6
8
10
12
14
16
18
20
0.05
0.1
0.15
0.2
0.25
0.3
0.35
0.4

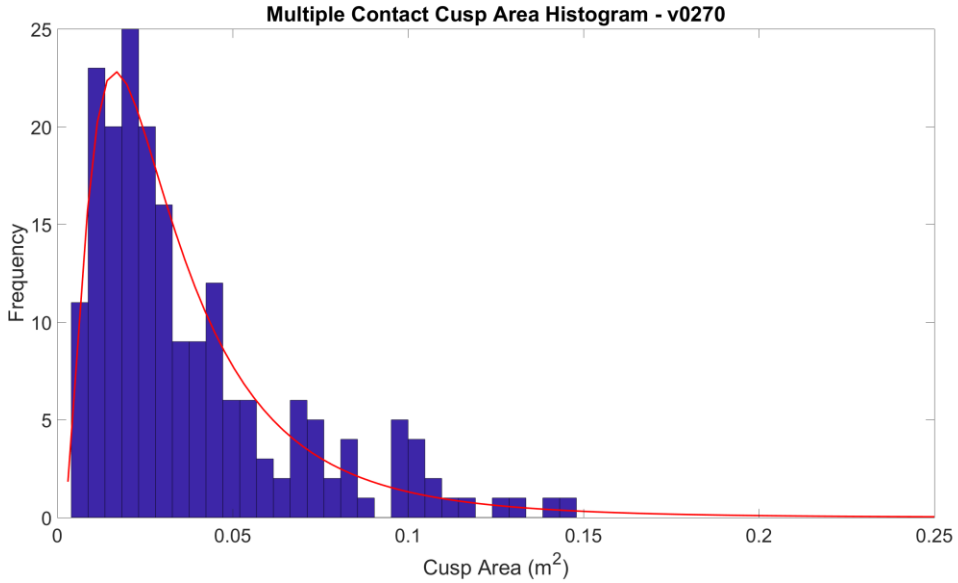
Multiple Contact Cusp Area Histogram - v0270
Frequency
Cusp Area (m2)
0
5
10
15
20
25
0.05
0.1
0.15
0.2
0.25

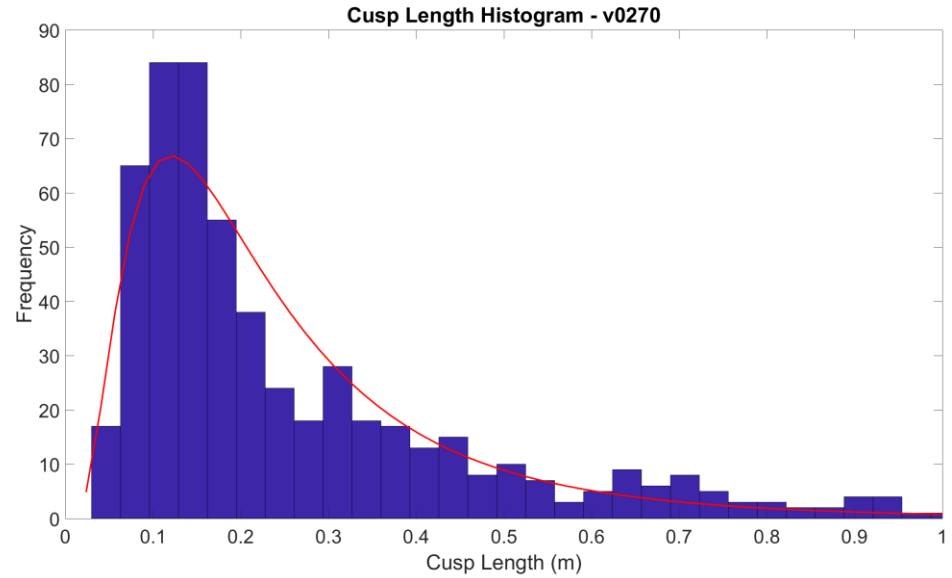
Cusp Length Histogram - v0270
Frequency
Cusp Length (m)
0
10
20
30
40
50
60
70
80
90
0
0.1
0.2
0.3
0.4
0.5
0.6
0.7
0.8
0.9
1

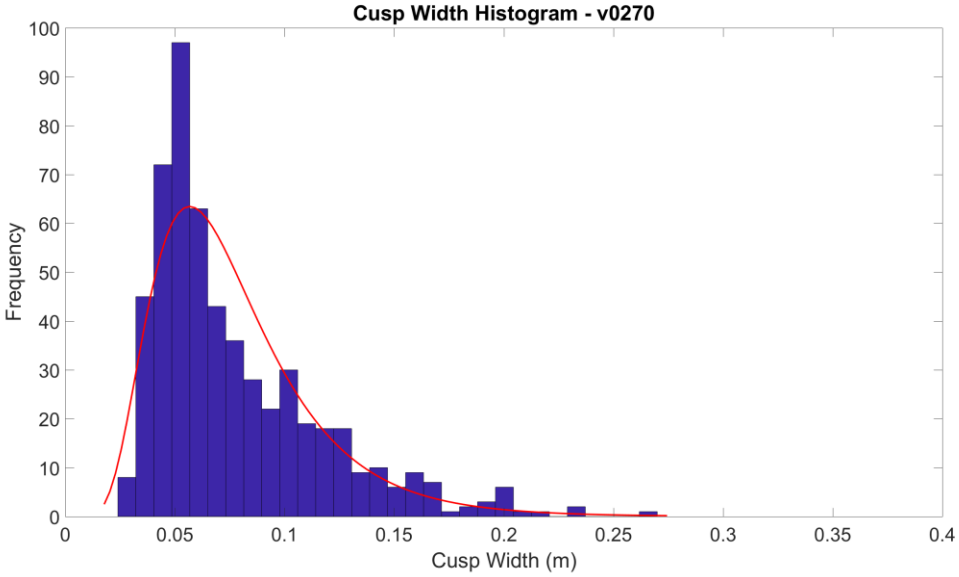
Cusp Width Histogram - v0270
Frequency
Cusp Width (m)
0
10
20
30
40
50
60
70
80
90
100
0
0.05
0.1
0.15
0.2
0.25
0.3
0.35
0.4

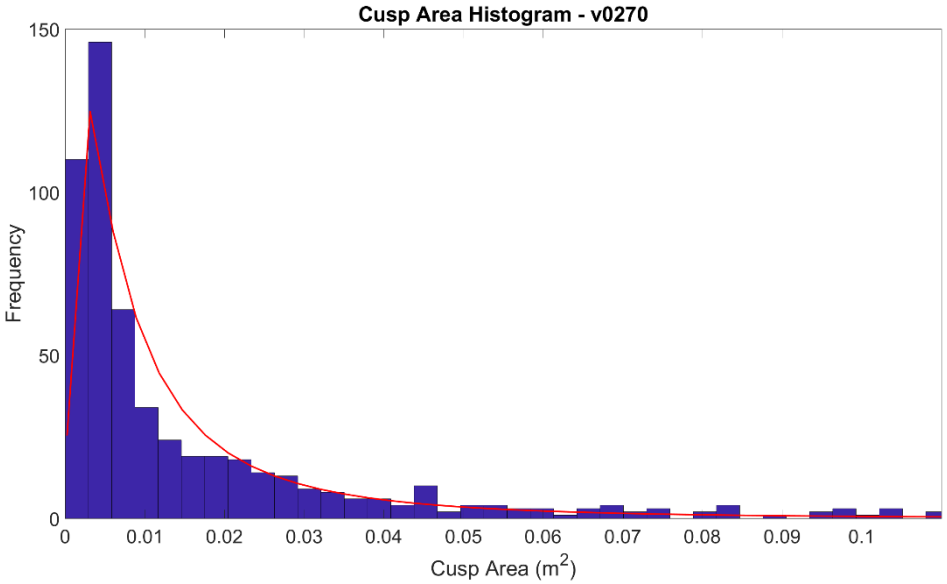
Cusp Area Histogram - v0270
Frequency
Cusp Area (m2)
0
50
100
150
0
0.01
0.02
0.03
0.04
0.05
0.06
0.07
0.08
0.09
0.1

Appendix C.4 V=0.270m/s Distributions

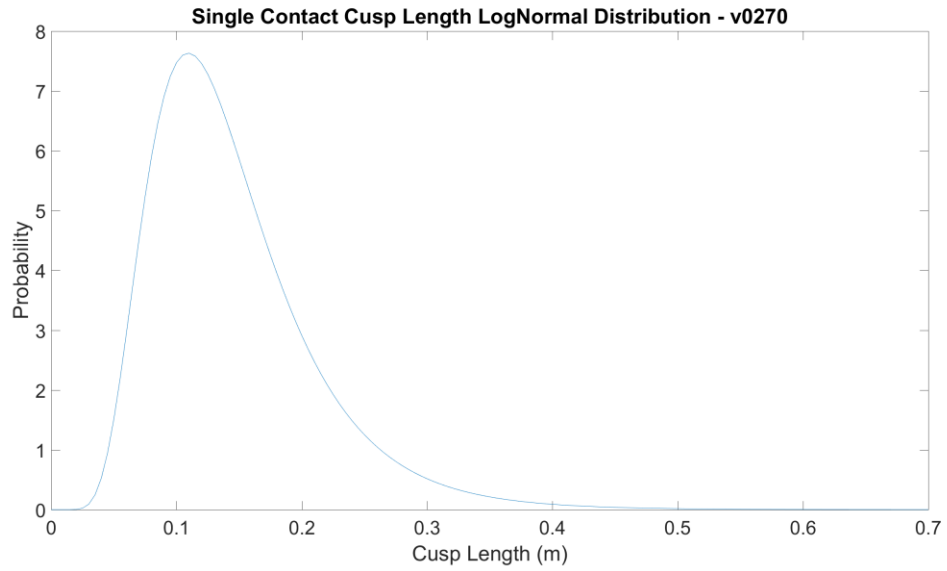
Single Contact Cusp Length LogNormal Distribution - v0270
Probability
Cusp Length (m)
0
1
2
3
4
5
6
7
8
0
0.1
0.2
0.3
0.4
0.5
0.6
0.7

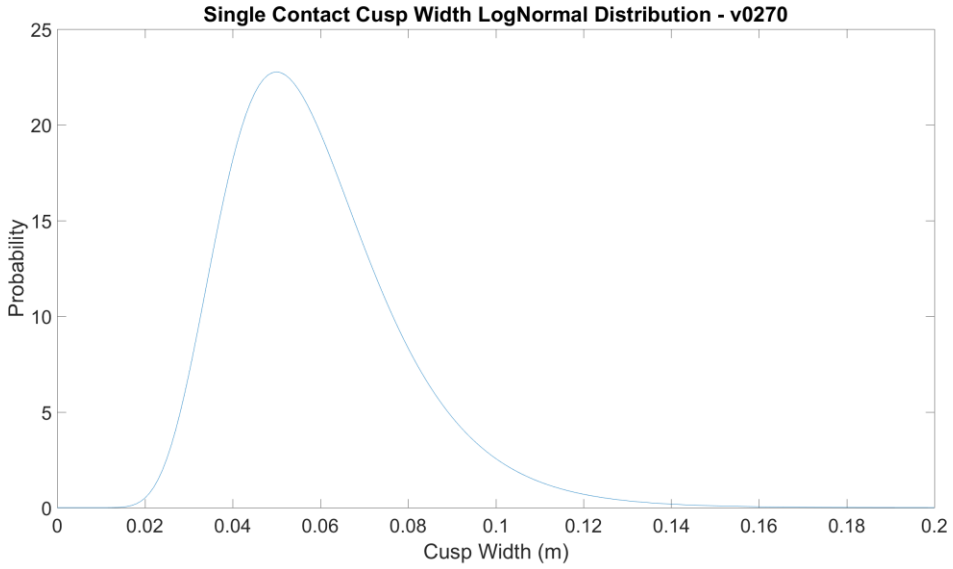
Single Contact Cusp Width LogNormal Distribution - v0270
Probability
Cusp Width (m)
0
5
10
15
20
25
0
0.02
0.04
0.06
0.08
0.1
0.12
0.14
0.16
0.18
0.2

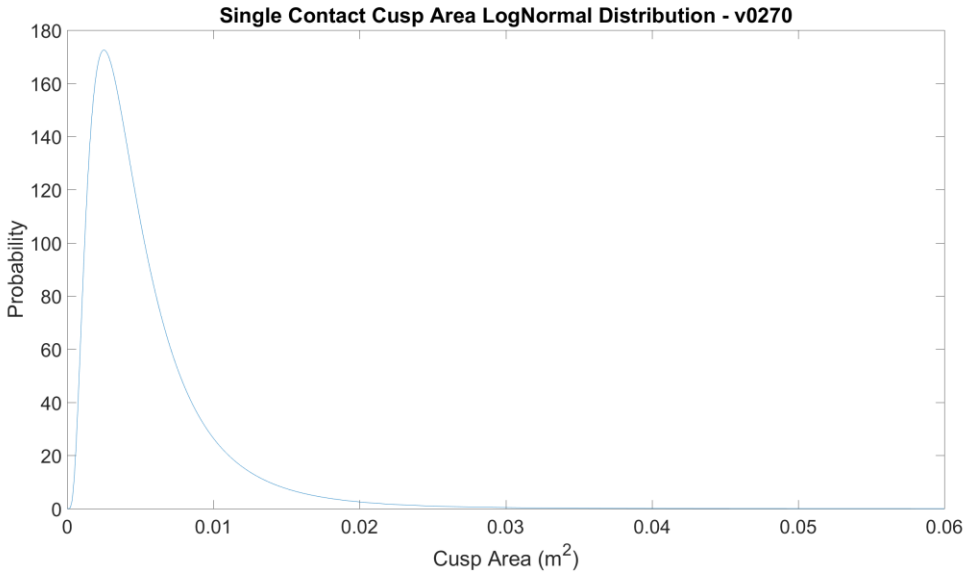
Single Contact Cusp Area LogNormal Distribution - v0270
Probability
Cusp Area (m2)
0
20
40
60
80
100
120
140
160
180
0
0.01
0.02
0.03
0.04
0.05
0.06

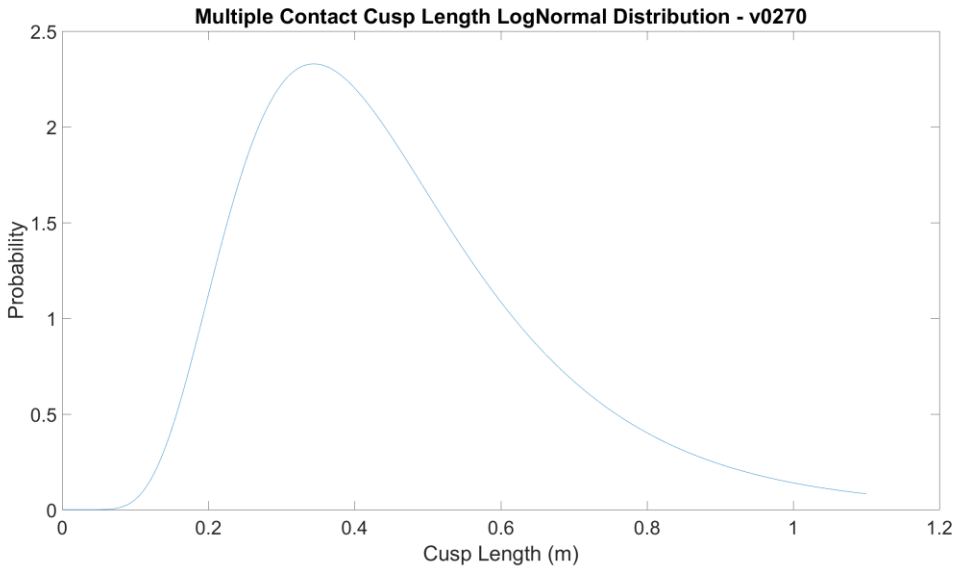
Multiple Contact Cusp Length LogNormal Distribution - v0270
Probability
Cusp Length (m)
0
0.5
1
1.5
2
2.5
0.2
0.4
0.6
0.8
1
1.2

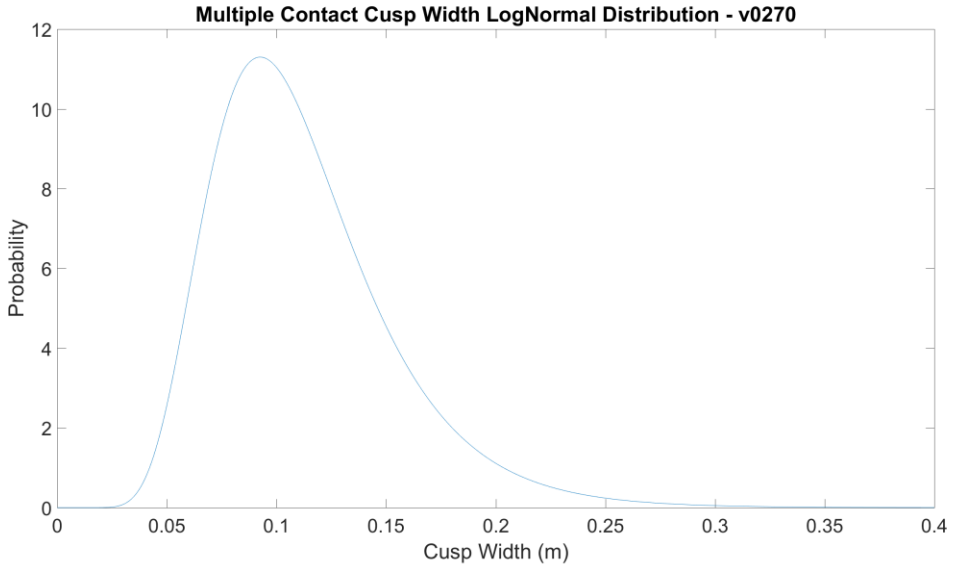
Multiple Contact Cusp Width LogNormal Distribution - v0270
Probability
Cusp Width (m)
0
2
4
6
8
10
12
0.05
0.1
0.15
0.2
0.25
0.3
0.35
0.4

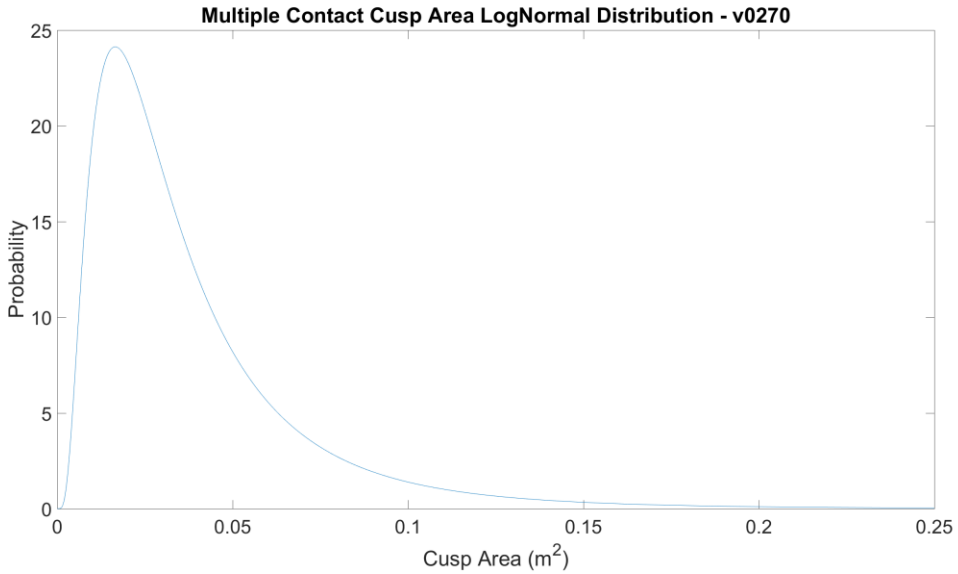
Multiple Contact Cusp Area LogNormal Distribution - v0270
Probability
Cusp Area (m2)
0
5
10
15
20
25
0.05
0.1
0.15
0.2
0.25

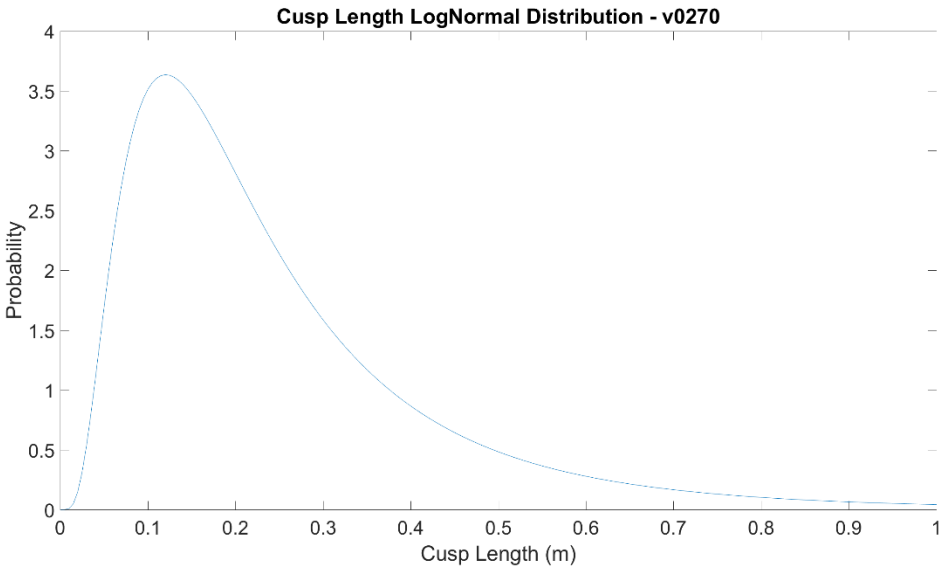
Cusp Length LogNormal Distribution - v0270
Probability
Cusp Length (m)
0
0.5
1
1.5
2
2.5
3
3.5
4
0.1
0.2
0.3
0.4
0.5
0.6
0.7
0.8
0.9
1

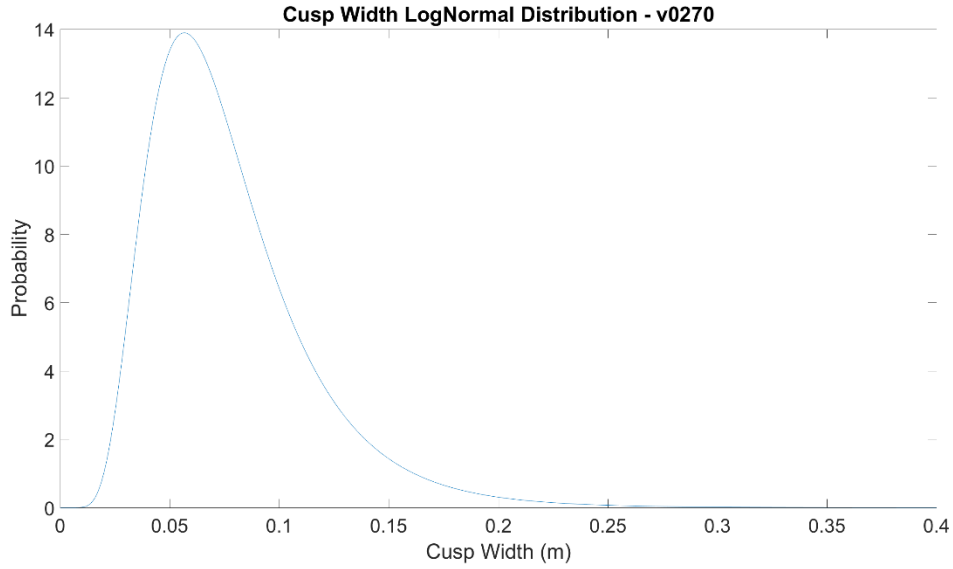
Cusp Width LogNormal Distribution - v0270
Probability
Cusp Width (m)
0
2
4
6
8
10
12
14
0.05
0.1
0.15
0.2
0.25
0.3
0.35
0.4

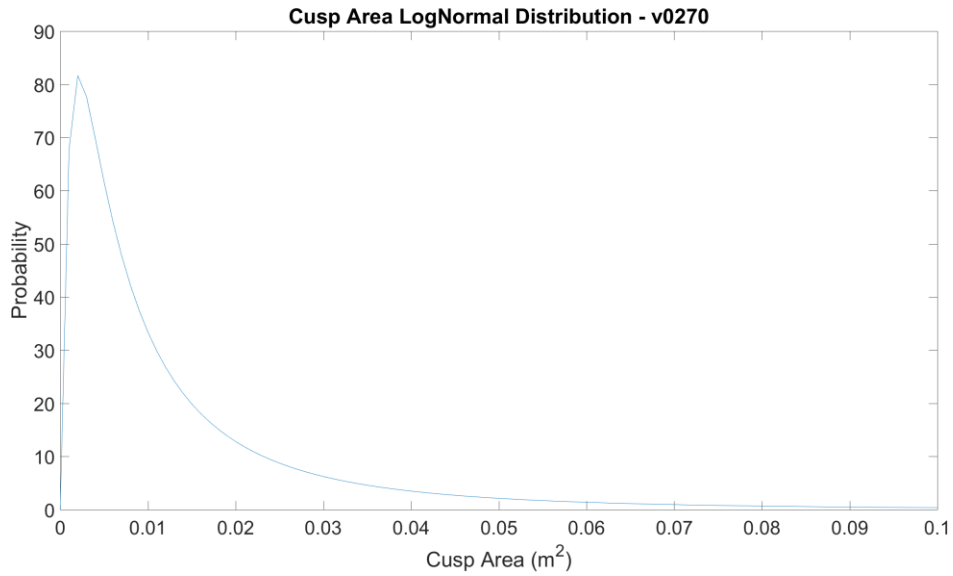
Cusp Area LogNormal Distribution - v0270
Probability
Cusp Area (m2)
0
10
20
30
40
50
60
70
80
90
0.01
0.02
0.03
0.04
0.05
0.06
0.07
0.08
0.09
0.1

Appendix C.5 Prediction Method Histogram Comparison

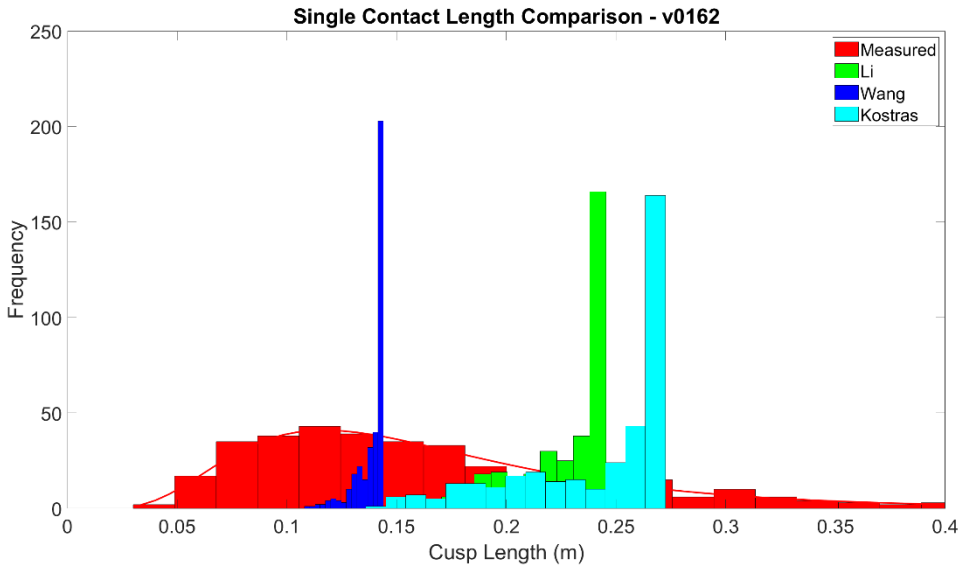
Single Contact Length Comparison - v0162
Measured
Li
Wang
Kostras
Frequency
Cusp Length (m)
0
50
100
150
200
250
0.05
0.1
0.15
0.2
0.25
0.3
0.35
0.4

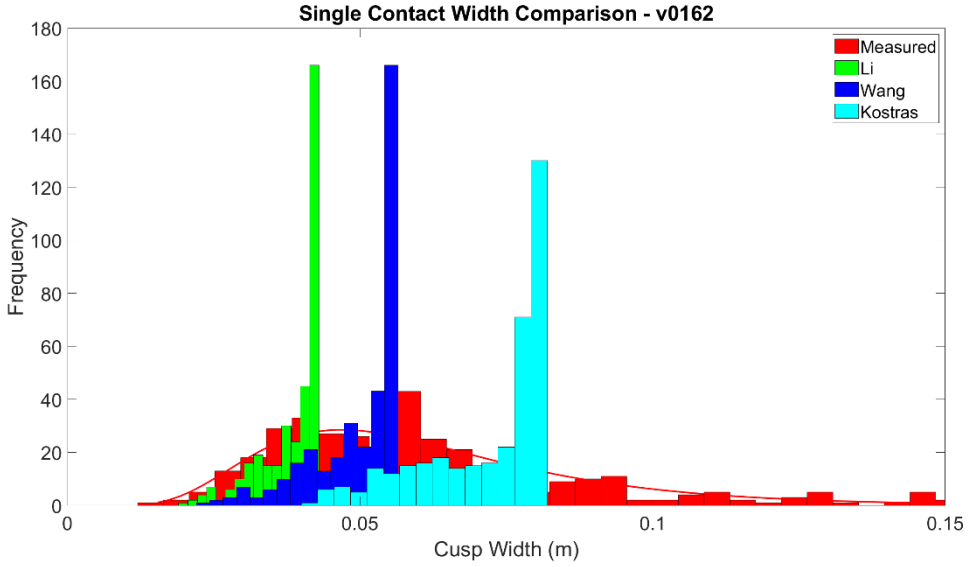
Single Contact Width Comparison - v0162
Measured
Li
Wang
Kostras
Frequency
Cusp Width (m)
0
20
40
60
80
100
120
140
160
180
0.05
0.1
0.15

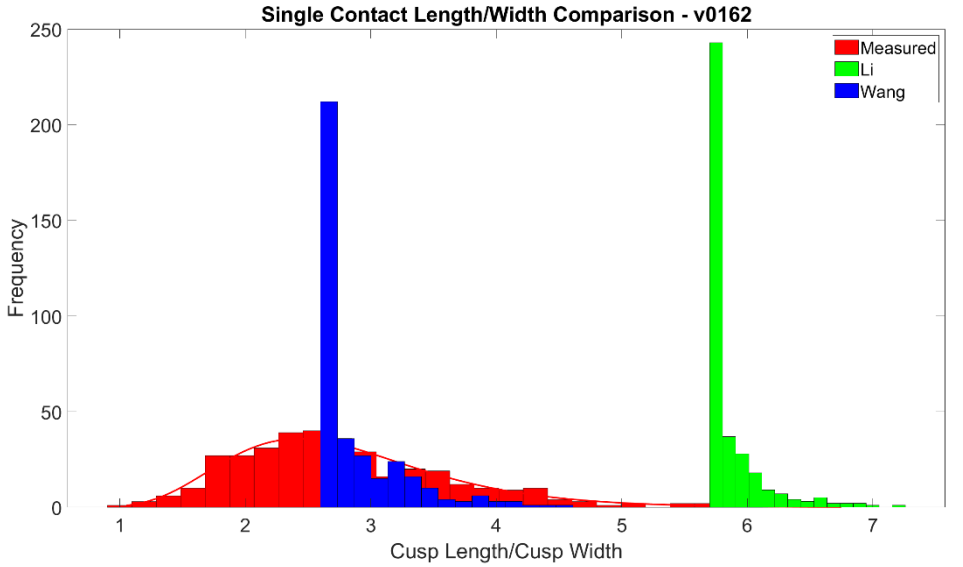
Single Contact Length/Width Comparison - v0162
Measured
Li
Wang
Frequency
Cusp Length/Cusp Width
0
50
100
150
200
250
1
2
3
4
5
6
7

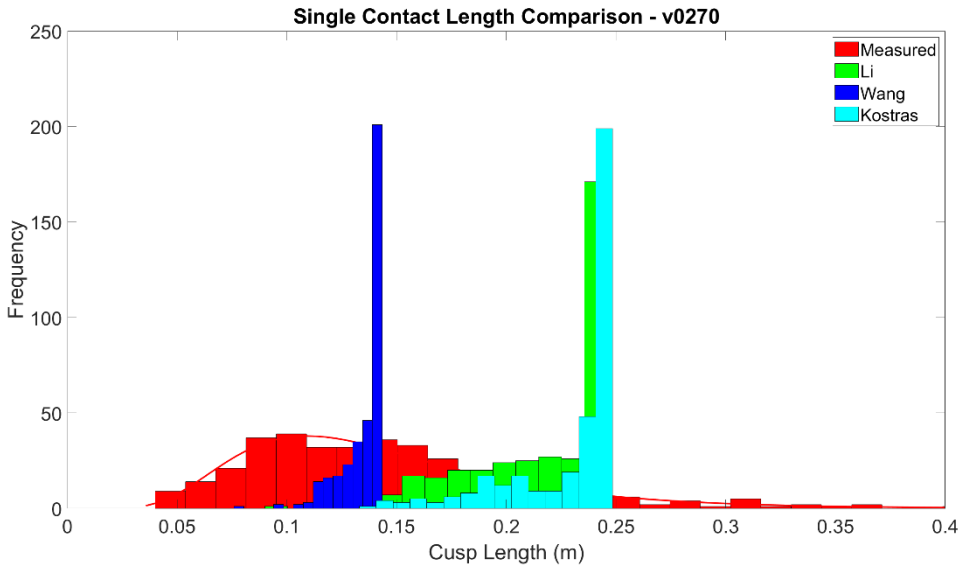
Single Contact Length Comparison - v0270
Measured
Li
Wang
Kostras
Frequency
Cusp Length (m)
0
50
100
150
200
250
0.05
0.1
0.15
0.2
0.25
0.3
0.35
0.4

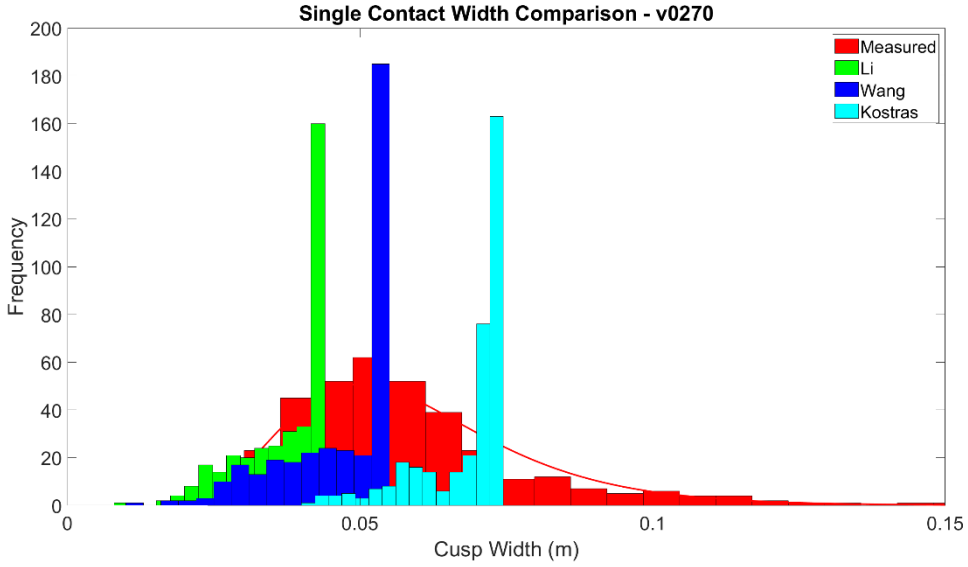
Single Contact Width Comparison - v0270
Measured
Li
Wang
Kostras
Frequency
Cusp Width (m)
0
20
40
60
80
100
120
140
160
180
200
0.05
0.1
0.15

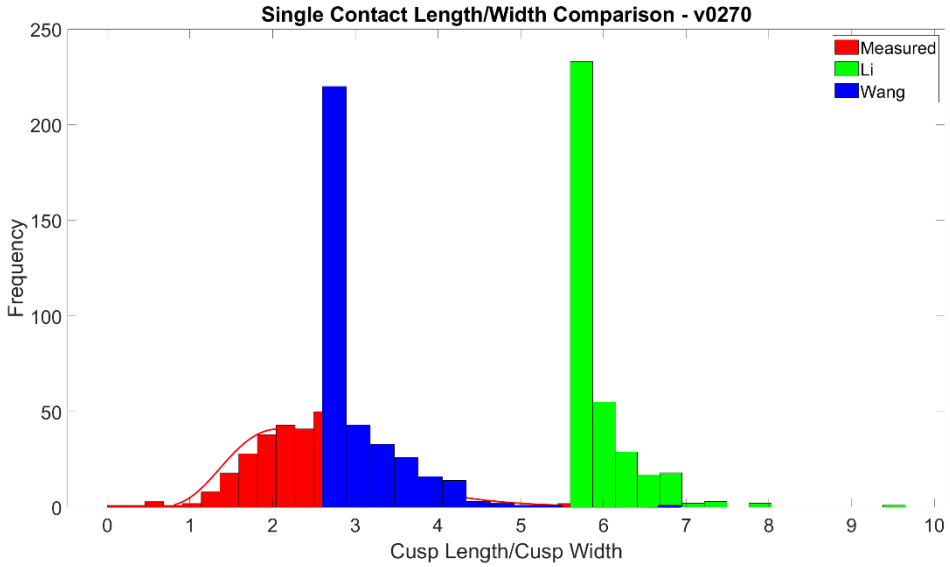
Single Contact Length/Width Comparison - v0270
Measured
Li
Wang
Frequency
Cusp Length/Cusp Width
0
50
100
150
200
250
1
2
3
4
5
6
7
8
9
10